

Stephen F. Austin State University

**SFA ScholarWorks**

---

Electronic Theses and Dissertations

---

12-2019

## 2D ELECTRICAL RESISTIVITY AND HYDROLOGICAL STUDY OF A SOLUTE PLUME'S MIGRATION PATHWAY THROUGH SANDY LOAM WITHIN NACOGDOCHES COUNTY, TEXAS, USA

Tyler Tandy  
tyleratandy@gmail.com

Wesley Brown  
Stephen F Austin State University, brownwa1@sfasu.edu

Kevin Stafford  
Stephen F Austin State University, staffordk@sfasu.edu

Follow this and additional works at: <https://scholarworks.sfasu.edu/etds>



Part of the [Geology Commons](#), [Geophysics and Seismology Commons](#), and the [Hydrology Commons](#)

[Tell us](#) how this article helped you.

---

### Repository Citation

Tandy, Tyler; Brown, Wesley; and Stafford, Kevin, "2D ELECTRICAL RESISTIVITY AND HYDROLOGICAL STUDY OF A SOLUTE PLUME'S MIGRATION PATHWAY THROUGH SANDY LOAM WITHIN NACOGDOCHES COUNTY, TEXAS, USA" (2019). *Electronic Theses and Dissertations*. 322.  
<https://scholarworks.sfasu.edu/etds/322>

This Thesis is brought to you for free and open access by SFA ScholarWorks. It has been accepted for inclusion in Electronic Theses and Dissertations by an authorized administrator of SFA ScholarWorks. For more information, please contact [cdsscholarworks@sfasu.edu](mailto:cdsscholarworks@sfasu.edu).

---

**2D ELECTRICAL RESISTIVITY AND HYDROLOGICAL STUDY OF A SOLUTE  
PLUME'S MIGRATION PATHWAY THROUGH SANDY LOAM WITHIN  
NACOGDOCHES COUNTY, TEXAS, USA**

**Creative Commons License**



This work is licensed under a [Creative Commons Attribution-Noncommercial-No Derivative Works 4.0 License](https://creativecommons.org/licenses/by-nc-nd/4.0/).

2D ELECTRICAL RESISTIVITY AND HYDROLOGICAL STUDY OF A SOLUTE  
PLUME'S MIGRATION PATHWAY THROUGH SANDY LOAM WITHIN  
NACOGDOCHES COUNTY, TEXAS, USA

By

Tyler Tandy, Bachelor of Science

Presented to the Faculty of the Graduate School of

Stephen F. Austin State University

In Partial Fulfillment

Of the Requirements

For the Degree of

Masters of Geology

STEPHEN F. AUSTIN STATE UNIVERSITY

December 2019

2D ELECTRICAL RESISTIVITY AND HYDROLOGICAL STUDY OF A SOLUTE  
PLUME'S MIGRATION PATHWAY THROUGH SANDY LOAM WITHIN  
NACOGDOCHES COUNTY, TEXAS, USA

By

Tyler A. Tandy, Bachelor of Science

Approved:

---

Dr. Wesley Brown, Thesis Director

---

Dr. Kevin Stafford, Committee Member

---

Dr. Melinda Faulkner, Committee Member

---

Dr. Walter Trikosko, Committee Member

---

Pauline M. Sampson Ph.D.  
Dean of Research and Graduate Studies

## ABSTRACT

A combined geophysical and hydrological study was conducted in a sandy loam near the campus of Stephen F. Austin State University in Nacogdoches, Texas. The study area contained three preinstalled piezometers which are located in the Sparta Sand of the Eocene Claiborne Group, a regressive tract of the Eocene sea.

Electrical DC resistivity surveys were conducted across one fifty-six-meter-long traverse using AGI's multi-electrode SuperSting R8 WIFI RES/IP/SP system, which allowed for rapid and reliable data collection. The resistivity line was surveyed using the dipole-dipole array configuration, which has been proven to produce high-quality horizontal resolution. Over the duration of fourteen days, a conductive solution composed of 88 ounces of NaCl combined with 24 liters of water were added into an infiltration pit daily and DC resistivity surveys were conducted every other day. DC resistivity data was processed and interpreted using AGI's EarthImager 2D inversion software. The electrical resistivity data acquired was paired with a hydrogeological survey of the area in order to better understand the migration of a solute plume through the sandy loam. The hydrogeologic survey consisted numerical modeling values obtained from a fine

grain analysis of three soil cores using the Bouyoucos hydrometer method. The data acquired provided useful information on the rate of infiltration as well as the migration pathway of any possible future contaminant spills that may occur in similar soils.

The principal objective of the study was to track the flow pattern and rate at which a known conductive aqueous solution flows through sandy loam. This geophysical study alongside a parallel hydrologic study will improve tracking of solute plume through sandy loam and allow researchers to monitor any interaction with groundwater.

## ACKNOWLEDGMENT

I would like to thank my thesis advisor, Dr. Wesley Brown, for the constant support of my thesis. Additionally, I am thankful to Dr. Kevin Stafford for taking the time to assist in data collection and the preparation of my manuscript, as well as my other committee members: Dr. Melinda Faulkner and Dr. Walter Trikosko.

Finally, I would like to thank my grandparents who have supported me throughout college. In particular, I would like to thank my grandpa (poppy) who first introduced me to geology.

## TABLE OF CONTENTS

ABSTRACT .....	i
ACKNOWLEDGMENT .....	iii
TABLE OF CONTENTS .....	iv
LIST OF FIGURES .....	vi
LIST OF EQUATIONS.....	viii
PREFACE.....	ix
2D ELECTRICAL RESISTIVITY AND HYDROLOGICAL STUDY OF A SOLUTE PLUME'S MIGRATION PATHWAY THROUGH SANDY LOAM WITHIN NACOGDOCHES COUNTY, TEXAS, USA.....	1
ABSTRACT .....	1
HYDROGEOLOGIC SETTING.....	7
ELECTRICAL RESISTIVITY METHODOLOGY .....	14
NUMERICAL MODELING .....	17
RESULTS.....	23
2-D ELECTRICAL RESISIVITY SURVEY.....	27
DISCUSSION AND CONCLUSION.....	38

REFERENCES.....	44
APPENDIX (A) LITERATURE REVIEW .....	49
APPENDIX (B) METHODOLOGY .....	82
APPENDIX (C) RESULTS.....	106

## LIST OF FIGURES

- Figure 1.** Image displaying the Sparta Formation in relation to the study site as well as the distribution of the formation throughout Nacogdoches County, Texas..... 6
- Figure 2.** Stratigraphic section showing relationship of the Claiborne Group with the transgressions and regressions of the Eocene Sea (Modified from Watkins, 2018; Fisher, 1964 and Forestar, 2011)..... 11
- Figure 3.** Image representing the approximate spacing of the three piezometers, survey line 1, and the infiltration pit positioned at the northwest end of survey line one on a contoured surface. .... 12
- Figure 4.** Temperature and precipitation for Nacogdoches County, Texas spanning from July 1, 2018 through September 30, 2018 (NOAA, 2019). Red line plot represents the daily maximum temperature, blue line plot represents the daily minimum temperature and bar graph represents the daily precipitation. The average high temperature was 31.7 °C, the average low temperature was 22. 8 °C, while receiving a total of 31.2 cm of rainfall during the study period. .... 13
- Figure 5.** Diagram representing the setup of the resistivity meter and the arrangement of each survey line. The low address is composed of two cables (1-14;15-28) connected to the low address switchbox, while the high address is composed of two cables (29-42; 43-56) connected to switch box 1-56. The switch box is then connected to the SuperSting R8 WIFI RES/IP/SP, which is powered by two deep cycle marine batteries. .... 16
- Figure 6.** A. Average grain size percentage across three 1.5-meter-deep cores. Blue represents % sand, orange % silt, gray % clay. B) Hydraulic conductivity averaged across three 1.5-meter-deep cores. .... 25

**Figure 7.** Vertical Hydraulic conductivity of the solute plume over 42 days, the time period from the addition of the first saline solution to the end of the final survey. The red line plot is representative of average hydraulic conductivity and average clay swelling, the blue line plot is representative of the average hydraulic conductivity negating clay swelling. The maximum rate of movement is 0.0874 meters per day, while the minimum rate of movement is 0.06 meters per day. .... 26

**Figure 8. (A)** Background resistivity analyses collected 7/20 (dipole-dipole array, 56 electrodes at a one-meter spacing). **(B)** Full 56 electrode inverted resistivity section with the presumed water table and the cut resistivity segment..... 28

**Figure 9.** Survey line one section between electrode 40 and electrode 56 (dipole-dipole array, 56 electrodes at a one-meter spacing). Iterations=8, scale 1:1, RMS range from 6-25%. **(A)** Background survey (7/20), **(B)** Inverted resistivity section day 2 (7/22), **(C)** Inverted resistivity section day 4 (7/24), **(D)** Inverted resistivity section day 6 (7/26) **(E)** Inverted resistivity section day 8 (7/28), **(F)** Inverted resistivity section day 10 (7/30), **(G)** Inverted resistivity section day 12 (8/1), **(H)** Inverted resistivity section day 14 (8/3) (Image was created in AGI's EarthImager 2D, 2016). .... 36

**Figure 10.** Survey line one interpreted section between electrode 40 and electrode 56 (dipole-dipole array, 56 electrodes at a one-meter spacing). Iterations=8, scale 1:1, RMS range from 12-18%. **(A)** Inverted resistivity section day 21 (8/10), **(B)** Inverted resistivity section day 28 (8/17), **(C)** Inverted resistivity section day 35 (8/24), **(D)** Inverted resistivity section day 42 (8/31) (Image was created in AGI's EarthImager 2D, 2016). .... 37

## LIST OF EQUATIONS

$K = Cd_{50}^j$ .....	19
$C_u = d_{60}/d_{10}$ .....	19
$K(rel) = \frac{K(j)}{K(ref)} = \left[ \frac{\epsilon(eff,j)}{\epsilon(eff,ref)} \right]^p$ .....	19
$x = (f)(3.6 \times 10^{-4})(ESP)(d^*)(\rho_b)$ .....	20
$ESP = \left[ \frac{Na}{CEC} \right] \times 100$ .....	20
$\epsilon (tot)-(f)(\rho_b)(10)(10^{-8})(8 \times 10^6)(0.9)(0.5)$ .....	21
$\epsilon (eff,ref) - x$ .....	21
$K(\theta) = k_r(\theta)k\rho_w g / \mu_w$ .....	21
$K = k_i \rho g / \mu$ .....	22

## PREFACE

The foundation of the research was to map the migration of a solute plume through a sandy loam in the subsurface. In the study, electrical resistivity and numerical modeling were the primary mechanisms utilized to achieve the goal. This study was conducted between July 2018 to January 2019.

The following manuscript was formatted to be submitted to the “Gulf Coast Association of Geological Societies” for publication. A literature review of the study site and surrounding region is presented in Appendix (A). Methodology for all work completed throughout the thesis research process is presented in Appendix (B) and all data acquired throughout the study is presented in Appendix (C).

2D ELECTRICAL RESISTIVITY AND HYDROLOGICAL STUDY OF A SOLUTE  
PLUME'S MIGRATION PATHWAY THROUGH SANDY LOAM WITHIN  
NACOGDOCHES COUNTY, TEXAS, USA

ABSTRACT

A combined geophysical and hydrological study was conducted in a sandy loam near the campus of Stephen F. Austin State University in Nacogdoches, Texas. The study area contained three preinstalled piezometers which are located in the Sparta Sand of the Eocene Claiborne Group, a regressive tract of the Eocene sea.

Electrical DC resistivity surveys were conducted across one fifty-six-meter-long traverse using AGI's multi-electrode SuperSting R8 WIFI RES/IP/SP system, which allowed for rapid and reliable data collection. The resistivity line was surveyed using the dipole-dipole array configuration, which has been proven to produce high-quality horizontal resolution. Over the duration of fourteen days, a conductive solution composed of 88 ounces of NaCl combined with 24 liters of water were added into an infiltration pit daily and DC resistivity surveys were conducted every other day. DC resistivity data was processed and interpreted using AGI's EarthImager 2D inversion software. The electrical resistivity data

acquired was paired with a hydrogeological survey of the area in order to better understand the migration of a solute plume through the sandy loam. The hydrogeologic survey consisted numerical modeling values obtained from a fine grain analysis of three soil cores using the Bouyoucos hydrometer method. The data acquired provided useful information on the rate of infiltration as well as the migration pathway of any possible future contaminant spills that may occur in similar soils.

The principal objective of the study was to track the flow pattern and rate at which a known conductive aqueous solution flows through sandy loam. This geophysical study alongside a parallel hydrologic study will improve tracking of solute plume through sandy loam and allow researchers to monitor any interaction with groundwater.

## INTRODUCTION

The Sparta Aquifer, a minor unconfined aquifer in East Texas contained within the Eocene Sparta Formation of the Claiborne Group, spans an area of 17,938 square kilometers, supplying  $1.2E7$  cubic meters of water for livestock and domestic use per year (George & Mace, 2011). The large sand packages composing the Sparta Formation leave the Sparta Aquifer highly vulnerable to near surface contaminants, due to their high hydraulic conductivities, roughly 21.3 m/day (Hosman and others, 1968), and their tendency to extend to the surface in multiple outcrops across East Texas. The Sparta Aquifer, not highly regarded for use in agriculture, is of importance as a source of fresh water for municipalities (McKee, 2002) across Texas, Arkansas, Louisiana, Mississippi and Tennessee. Assessment of the rate of contaminant infiltration into the groundwater system is significant in understanding the extent future contaminations may have on the aquifer.

Electrical resistivity surveys conducted using the AGI SuperSting R8 WIFI RES/IP/SP were employed in conjunction with numerical modeling to track induced solute migration potential of the aquifer. Electrical resistivity surveys characterized subsurface anomalies associated with geologic heterogeneity and introduced solute migration, allowing for resistivity variance to be displayed in 2-

D models; electrical resistivity imaging has been proven reliable in identifying saline and freshwater margins within shallow groundwater environments (Costall et al., 2018).

The study area lies in Nacogdoches County, Texas within the Gulf Coast Basin (**Figure 1**) composed of Claiborne Group strata; representing a regressive and transgressive Eocene sea (Ricoy & Brown, 1977). The formation exposed at the surface within the study site is that of the Sparta Formation. Deposited during a regressive track of the Eocene Sea, the formation is composed of fine to medium quartz sandstone packages with lagoon mud silt and clay lenses. The Sparta Formation and related Sparta Aquifer is bound by the Weches Formation's glauconitic shales below; the depth to the upper Weches Formation within the study site is approximately 6.7 meters based on cored sample penetration into abundant glauconite.

Direct Current (DC) resistivity surveys were conducted over one traverse in order to track solute migration pathways and infiltration rate of an introduced saline plume. Surveys were conducted prior to solute introduction and temporally after solute introduction over a six-week period, at two-day intervals for the first two weeks and weekly for the remaining four weeks for a total of 42 days. In addition to electrical resistivity survey characterizations, numerical modeling of vertical vadose migration was independently calculated based on hydrogeologic

characterization of the study site for comparison of modeled versus direct resistivity analyses of potential solute migration.

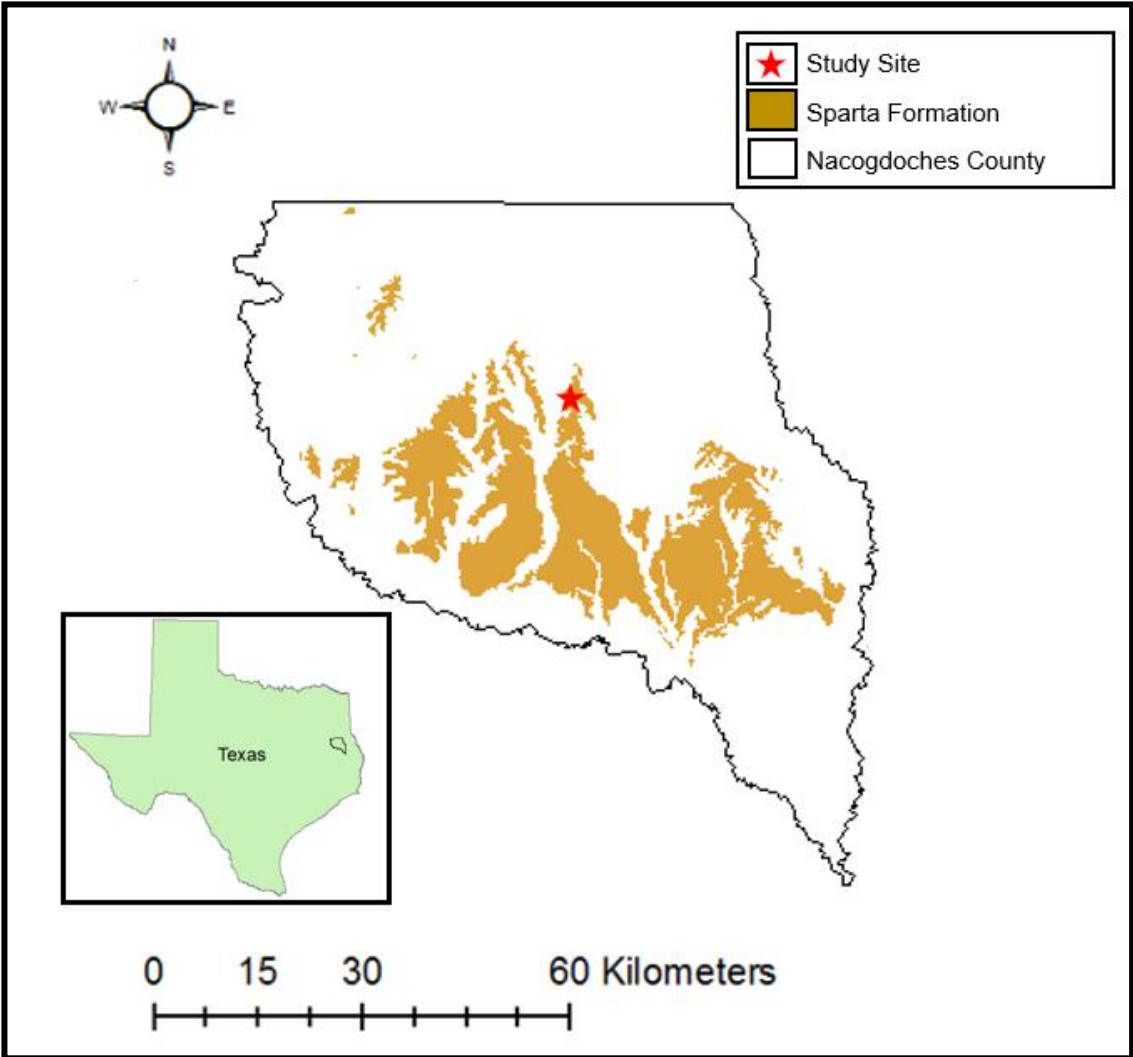


**Figure 1.** Image displaying the Sparta Formation in relation to the study site as well as the distribution of the formation throughout Nacogdoches County, Texas.

## HYDROGEOLOGIC SETTING

The East Texas and Gulf Coast basins were formed ~245 mya during the Mesozoic as the European and African plates drifted away from North America creating a belt of elongated rift basins. Sediments from adjacent uplifts were deposited in these basins and were later covered by marine salts as rifting continued (Bureau of Economic Geology, 1992). Construction of the Cenozoic Coastal Plain was due to progradation of sediments into the Gulf Basin and dominated by stages of marine regressions and transgressions. The Cenozoic transgressional coastlines were very similar to coastline conditions seen today, where salt marshes, bays and muddy lagoons are separated from the continental shelf by sandy barrier islands (Ferring, 2007). Stages of regression created large deltaic systems that prograded into the Gulf and associated fluvial environments. Tropical hard water swamps were commonly associated with fluvial environments where organic materials were deposited, buried and altered into lignite (Ferring, 2007).

Nacogdoches County lies within the Texas Eastern Coastal Plain (Ricoy & Brown, 1977). The Eocene units that dominate this area are predominantly from the Claiborne Group representing a period of transgressive and regressive

Eocene Seas (Jobe et al., 1993). The Claiborne Group is composed of seven formations, including, from youngest to oldest: Yegua, Cook Mountain, Sparta, Weches, Queen City, Reklaw and the Carrizo (**Figure 2**).

The Sparta Formation, deposited during a regressive tract of the Eocene Sea, is composed primarily of very fine to medium quartz sandstone with a maximum thickness of 304 meters. These sand units are beach and fluvial in origin and are generally cross-bedded or laminated with beds of clay and sandy clay intermixed (Hosman, 1991). In the lower portion of the unit, oxidation can occur causing outcrops to exhibit a red to orange tint. The Sparta Formation is bound by the lower Weches Formation and the upper Cook Mountain Formation both act as semi-confining strata for the Sparta Aquifer (Hosman, 1991). The upper Weches Formation signifies shallow marine deposition in which dark glauconitic marine shales were deposited (Berg, 1984). Due to low permeability and hydraulic conductivity of clay-sized grains, the shales of the upper Weches act as a lower confining layer for the Sparta Aquifer. The upper Cook Mountain Formation (formerly the Crocket Formation) is a transgressive system (Eargle, 1968) consisting primarily of gray fossiliferous marine shales, clays and sandy shales (Stenzel, 1935; Sellards & others, 1932). These stratigraphic units were deposited during the time of the Crockett Sea (Ricoy & Brown, 1977) and act as a semi-confining barrier above the Sparta Formation, similar to the Weches Formation below.

The Sparta Aquifer found within the large sand packages of the Sparta Formation is a minor source of groundwater for East Texas. The sand bodies that contain the aquifer are not seamlessly connected; therefore, in localized regions the sand bodies disconnect creating separate hydraulic systems (Payne, 1968). Recharge of the Sparta Aquifer is directly associated with infiltration from the outcropped sections where there is an absence of the Cook Mountain semi-confining layer.

The topography of the study site is defined by six agricultural terraces offset by gentle slopes (**Figure 3**), with an elevation change of roughly one meter between each terrace. The terraces within the study site have an east to west trend extending beyond the study site perimeter. The perimeter of the site is enveloped with heavy vegetation dominated by four tree species: American Beech (*Fagus grandifolia*), Water Oak (*Quercus nigra*), Eastern Red Cedar (*Juniperus virginiana var. virginiana*) and the Chinese Privet (*Ligustrum sinense*). Chinese Privet is the dominant vegetation within the study area, nearly surrounding the entire site on all sides. The interior is dominated by mixed native grasses.

Three preinstalled piezometers are located within the study site, allowing for investigation of the Sparta Formation beyond electrical resistivity and numerical modeling. The piezometers within the study site are identified as

piezometer 1, piezometer 2 and piezometer 3 (**Figure 3**). Hydraulic conductivity for each of the piezometers was calculated through replicate slug tests; Piezometer 1 located 139.1 meters above sea level (masl) exhibited average hydraulic conductivity of  $2.11\text{E-}02$  cm/s with a measured depth to the underlying Weches Formation at 6.7 meters; Piezometer 2 located 138.7 masl exhibited an average hydraulic conductivity of  $9.85\text{E-}03$ cm/s; Piezometer 3 located 136.67 masl exhibited average hydraulic conductivity of  $1.69\text{E-}02$  cm/s.

Average annual rainfall for Nacogdoches County, Texas is 122.8 cm/year (Texas Ecoregions, 2017). Thirty days prior to conducting the geophysical survey, the study site received 2.01 cm of rainfall. Over the duration of the initial 14-day survey spanning from July 20 to August 3, 2018, the survey site received a total of 0.08 cm of rainfall. The recorded average high in temperature for the duration of the survey was  $33.4$  °C with an average low temperature of  $22.9$  °C (NOAA, 2019) (**Figure 4**).

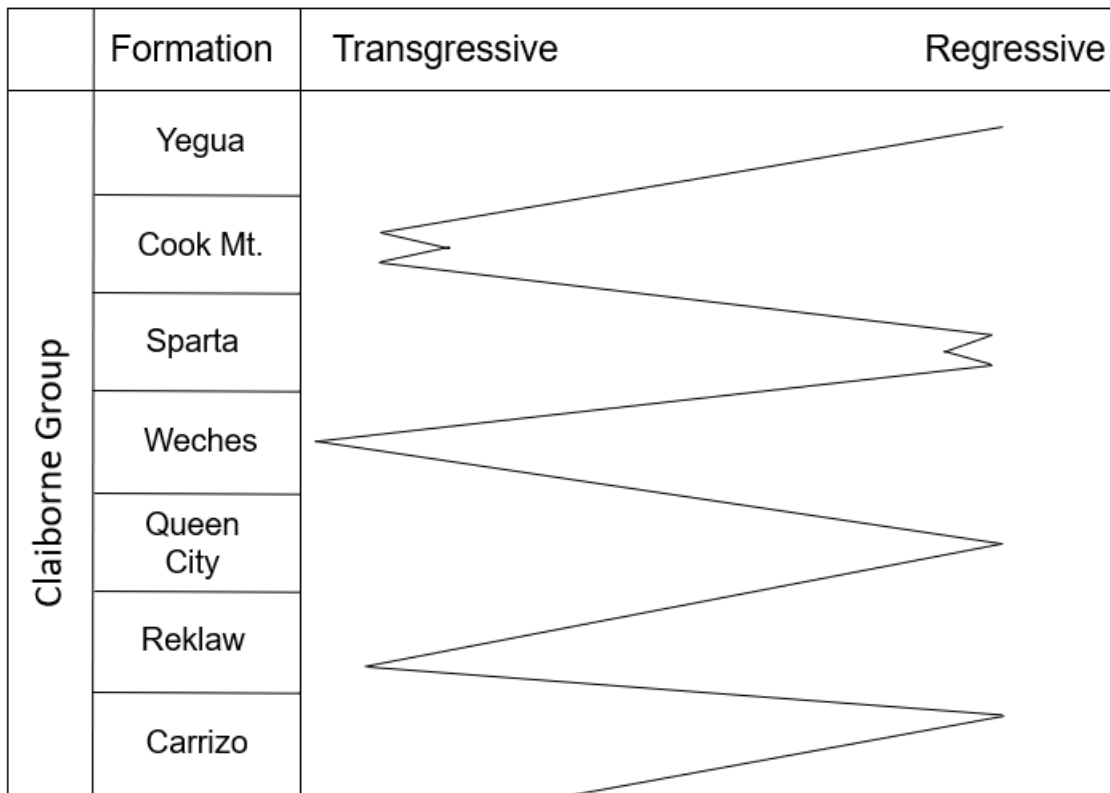


**Figure 2.** Stratigraphic section showing relationship of the Claiborne Group with the transgressions and regressions of the Eocene Sea (Modified from Watkins, 2018; Fisher, 1964 and Forestar, 2011).

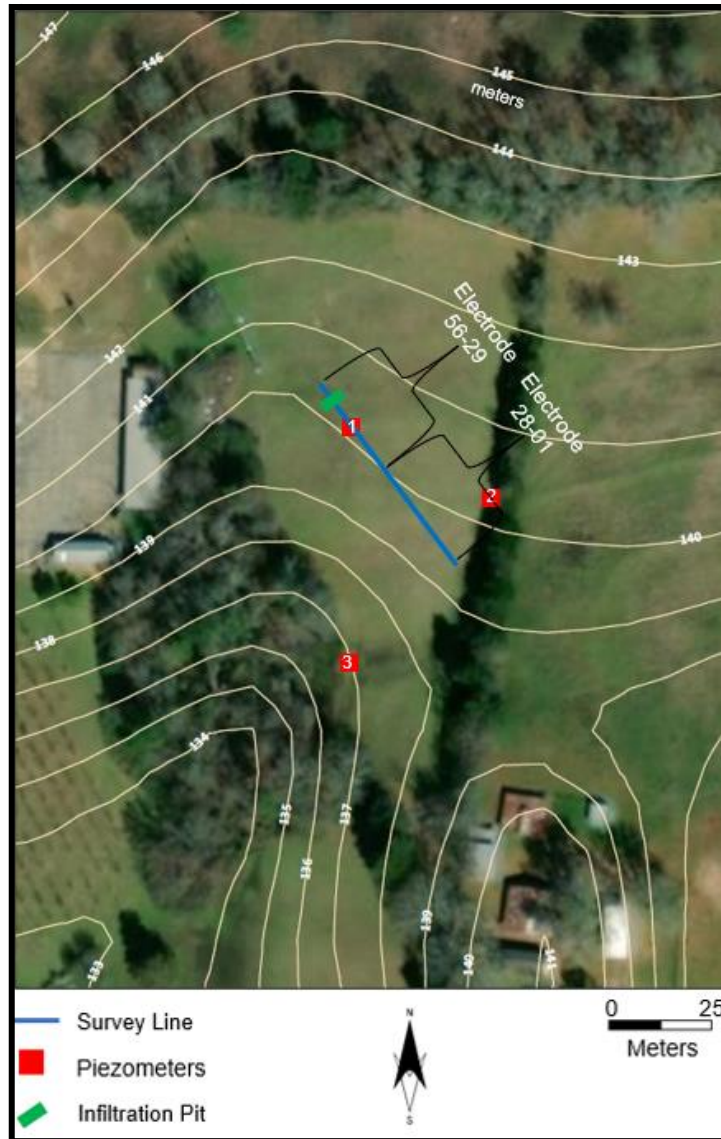


**Figure 3.** Image representing the approximate spacing of the three piezometers, survey line 1, and the infiltration pit positioned at the northwest end of survey line one on a contoured surface.

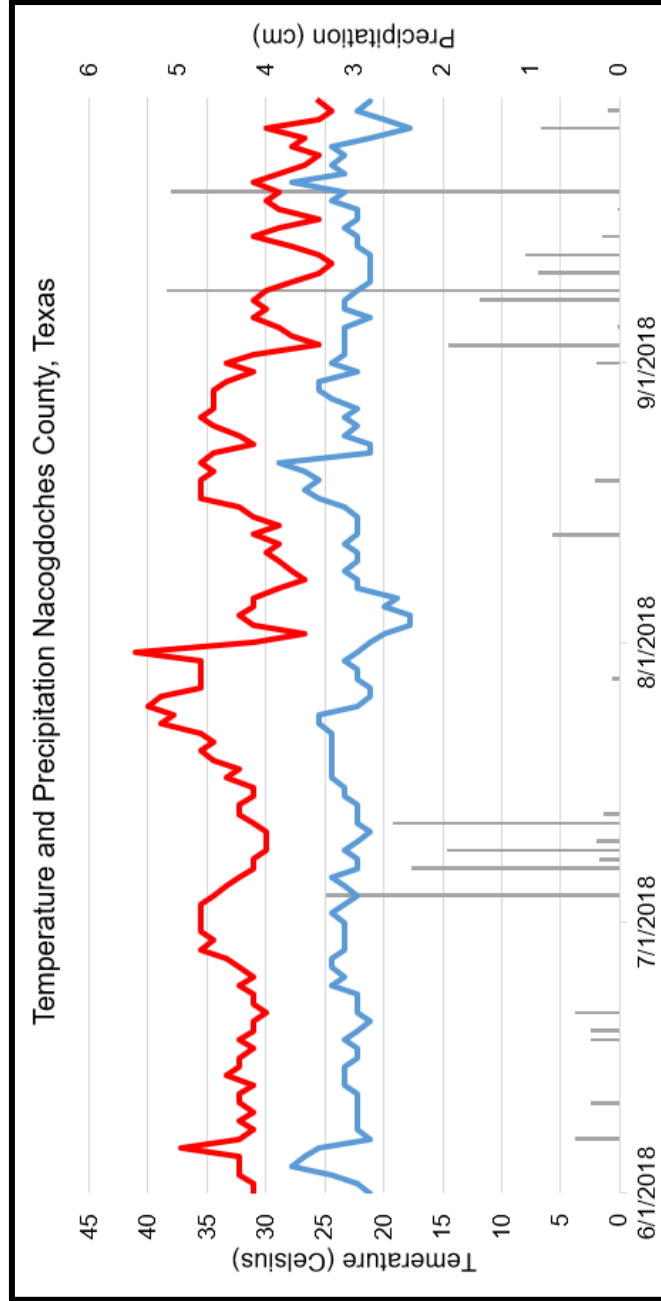


**Figure 4.** Temperature and precipitation for Nacogdoches County, Texas spanning from July 1, 2018 through September 30, 2018 (NOAA, 2019). Red line plot represents the daily maximum temperature, blue line plot represents the daily minimum temperature and bar graph represents the daily precipitation. The average high temperature was 31.7 °C, the average low temperature was 22.8 °C, while receiving a total of 31.2 cm of rainfall during the study period.

## ELECTRICAL RESISTIVITY METHODOLOGY

Two-dimensional direct current (DC) resistivity surveys were conducted across one, fifty-six-meter-long survey line using the SuperSting R8 WIFI RES/IP/SP produced by Advanced Geosciences Inc. (AGI) (**Figure 5**). The line was configured adjacent to three preinstalled piezometers with a solute infiltration site installed upgradient from Piezometer 1 (**Figure 3**).

The survey parameters were kept constant for each survey, those included; one-meter electrode spacing, dipole-dipole array as well as an injected current of 2000 mA. Measurement time was set at 800 milliseconds cycled twice at each electrode pair, the maximum error threshold per measurement was set to 2%. Electrodes were wetted with a dilute saline solution before each survey in order to reduce the contact resistance of the electrodes with the ground. Electrode contact resistance for each individual electrode on the fifty-six electrode lines were reduced to less than 5k ohms before the survey was conducted. To minimize the effects of evapotranspiration during data acquisition, all data were acquired between 1 AM and 9 AM on survey days in order to reduce evapotranspiration as a way to lower contact resistance.

Saline solution was introduced into the system daily for a fourteen-day period, from the start of the survey to the end of the initial survey, through an infiltration pit with a depth, length and width of 1.0, 0.75 and 0.33 meters, respectively. The infiltration pit was situated between electrodes 49 and 50, allowing for migration down gradient to be observed through the resistivity line as well as piezometer 1. The saline solution consisted of 88 grams table salt to 24 liters of fresh water, a solution of 104 ppt. Post initial 14-day survey, 24 liters of fresh water was introduced into the system through the infiltration for the duration of the survey time, 42 days.

Resistivity data was processed using *EarthImager 2D*, inversion software produced by Advanced Geosciences Inc. Resulting 2-D resistivity sections were inverted utilizing the surface setting with a robust inversion method. To ensure optimum data quality, Max RMS error and Error Reduction percentage were excluded from the software's stop criteria and the maximum number of iterations was set to eight. To lower the RMS error as well as to ensure for more accurate inverted resistivity sections, misfit data was removed utilizing the data misfit histogram. Terrain corrections were applied in order to accurately represent the topography of the terraces within the study area.

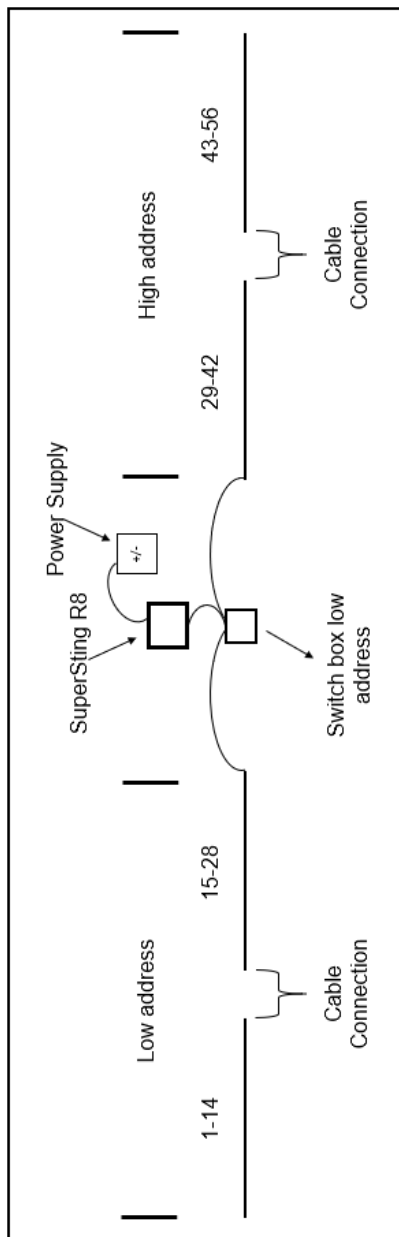


**Figure 5.** Diagram representing the setup of the resistivity meter and the arrangement of each survey line. The low address is composed of two cables (1-14; 15-28) connected to the low address switchbox, while the high address is composed of two cables (29-42; 43-56) connected to switch box 1-56. The switch box is then connected to the SuperSting R8 WIFI RES/IP/SP, which is powered by two deep cycle marine batteries.

## NUMERICAL MODELING

Numerical modeling was conducted to predict minimum and maximum rates of vertical solute migration in vadose conditions. Data for numerical modeling included slug tests, infiltration tests and soil core analysis.

Slug tests were conducted on each of the three piezometers within the survey site. Three slugs of non-saline water (0.5 liters, 1.0 liter and 2.0 liters) were introduced to each piezometer with an equilibrium time of two hours between each slug. Slug test data was attained using the Solinst Leveloggers which were introduced into each piezometer thirty minutes prior to the first slug. Hydraulic conductivity values were calculated using the Hvorslev method (Hvorslev, 1951) and averaged for each piezometer.

Infiltration tests were conducted along the survey line at electrodes 4, 28 and 52 using the falling head method (Head, 1982) to better understand surface infiltration rate of the study site. At each location, three Turf-Tec infiltration rings were deployed perpendicular to the survey line with the middle ring directly over the electrode with a one-meter spacing between all three rings. Rings were measured in fifteen-minute increments for an hour after an initial fifteen-minute settling period. The data collected at each fifteen-minute increment was averaged across the three rings at each electrode.

Soil analyses were conducted on six soil cores obtained throughout the study site. Three 1.5-meter-deep cores derived from electrodes 4, 28 and 52 divided into ten-centimeter increments, which were paired with cores obtained through the emplacement of the piezometers. The piezometer cores reached a much greater depth but were segregated based on lithologic change not vertical depth. All six cores were analyzed for fine grain distribution to calculate hydraulic conductivity. Fine grain distribution was calculated using the Bouyoucos hydrometer method (Bouyoucos, 1936). From the fine grain percentages hydraulic conductivities were deduced using a method created by Shepherd (1990) in which hydraulic conductivity was related to grain size. Hydraulic conductivities of each core segment were used to develop a solute transport model. The solute transport model obtained using the Shepherd method did not account for clay swelling. Due to the addition of NaCl to the system through the infiltration pit, other models were developed to account for changes in hydraulic conductivity values due to the inevitable clay swelling. The Lagerwerff (1969) relation considers the loss in hydraulic conductivity due the clay swelling and the tightening of the pores.

Hydraulic conductivity from sediment analyses for a non-saline solution were calculated based on work by Shepherd (1990) in which the hydraulic conductivity is related to grain size (1):

$$K = C d_{50}^j \quad (1)$$

where  $K$  is the hydraulic conductivity,  $C$  is the shape factor,  $d_{50}$  is the mean grain size and  $j$  is a constant 1.75, an exponent directly related to the deposition environment denoted by Shepherd (1990). The shape factor was derived based on Fetter (2004) for evaluating the uniformity coefficient (2):

$$C_u = d_{60}/d_{10} \quad (2)$$

where  $C_u$  is the uniformity coefficient,  $d_{60}$  is 60 percent finer by weight, and  $d_{10}$  ten percent finer by weight.

Hydraulic conductivity for a saline solution such as the one used in the study was computed using the Lagerwerff (1969) relation in which interlayer swelling amongst clay particles was considered (3):

$$K(rel) = \frac{K(j)}{K(ref)} = \left[ \frac{\epsilon (eff, j)}{\epsilon (eff, ref)} \right]^p \quad (3)$$

where  $K (rel)$  is the relative hydraulic conductivity,  $K (j)$  is the hydraulic conductivity of a saline solution,  $K (ref)$  is the hydraulic conductivity of the non-saline solution,  $\epsilon (eff, ref)$  is the effective porosity calculated in equation (6) and derived from Lagerwerff (1969),  $\epsilon (eff, j)$  is the effective porosity associated with a salt solution calculated in equation (7) and  $p$  is an exponent denoted by Lagerwerff (1969) ranging from zero to three.

Prior to calculation the reduction in hydraulic conductivity due to clay swelling, the interlayer swelling was calculated using a method similar to McNeal et al. (1968) and Dane (1978)(4):

$$x = (f)(3.6 \times 10^{-4})(ESP)(d^*)(\rho_b) \quad (4)$$

where  $x$  is the volumetric mineral interlayer swelling in  $\text{cm}^3/\text{cm}^3$ ,  $f$  grams of expansible soil per gram of soil estimated from Krutak and Kimbrells (1991) in which clay minerals from the Sparta Formation were identified, using SEM. For this study 25% of the clay content of each ten centimeter increment of soil was identified as potential swelling clays,  $3.6 \times 10^{-4}$  is a constant constructed by Dane (1978),  $ESP$  is the exchangeable sodium percentage calculated using equation (5) (Seilsepour et al, 2009),  $d^*$  adjusted interlayer spacing of 19 Å obtained from Yang et al., 2019,  $\rho_b$  is the average soil bulk density obtained from McKinzie et al. (2008) as  $1.55 \text{ g/cm}^3$

$ESP$  (Seilsepour et al., 2009) was calculated as:

$$ESP = \left[ \frac{Na}{CEC} \right] \times 100 \quad (5)$$

$Na$  is the measurable exchangeable sodium in mEq,  $CEC$  represents the cation exchange capacity in mEq.

Effective reference porosity of porous medium ( $\epsilon$  (eff, ref)) was calculated using:

$$\epsilon (tot) - (f)(\rho_b)(10)(10^{-8})(8 \times 10^6)(0.9)(0.5) \quad (6)$$

where  $\epsilon (tot)$  is total porosity of a porous medium,  $f$  is the grams of expansible soil per gram of soil, and  $\rho_b$  is bulk density. Constants for this equation (4): 10 is the minimum distance in Å between the expandable mineral platelets,  $10^{-8}$  cm/ Å,  $8 \times 10^6$  cm<sup>2</sup>/g, 0.9 fraction of surface involved in swelling (McNeal et al. 1968), 0.5 due to two surfaces per unit.

Effective porosity associated with salt solution ( $\epsilon (eff, j)$ ) equals:

$$\epsilon (eff, ref) - x \quad (7)$$

where  $\epsilon (eff, ref)$  comes from equation (6) and  $x$  from equation (1).

Using the hydraulic conductivity generated by both the saline and the non-saline solutions, the minimum and maximum vertical rate at which the solute plume would migrate through the vadose zone per day was predicted following the work of Fetter (2018). Hydraulic conductivity values were generated for each of the three 1.5-meter cores at ten-centimeter increments, based off the particle size analysis. Segments containing larger percentages of clay displayed a lower hydraulic conductivity due to clay swelling. (8):

$$K(\theta) = k_r(\theta)k\rho_w g / \mu_w \quad (8)$$

where,  $K(\theta)$  represents the unsaturated hydraulic conductivity,  $k_r(\theta)$  is the relative hydraulic conductivity of 1 cm/s,  $k$  is the intrinsic permeability gained from

equation (9),  $\rho_w$  is the density of water at 20 °C obtained from Weast (1972) as 0.9982 g/cm<sup>3</sup>,  $g$  is the acceleration due to gravity 9.8 m/s<sup>2</sup> and  $\mu_w$  is .01002 cm<sup>2</sup>/s the dynamic viscosity of soil water at 20 °C obtained from Hardy and Cottingham (1949).

The intrinsic permeability of the system was calculated based on Fetter (2018):

$$K = k_i \rho g / \mu \quad (9)$$

where  $K$  is the averaged hydraulic conductivity of the soil core nearest the infiltration pit,  $k_i$  is the intrinsic permeability,  $\rho$  is the fluid density of 0.9982 g/cm<sup>3</sup> (Weast, 1972),  $g$  is the gravitational constant and  $\mu$  is the fluid viscosity of 0.01002 cm<sup>2</sup>/s (Hardy and Cottingham, 1949)

## RESULTS

Several techniques were used over the duration of the study to monitor the migration of the solute plume through the vadose zone, including: electrical resistivity, numerical modeling and infiltration and slug tests. Soil cores collected at three locations along the survey line were used to calculate fine-grained particle size distribution for determination of hydraulic conductivity and percentage of swelling clay for each ten-centimeter increment of core (**Figure 6**). Hydraulic conductivity values of the solute plume, neglecting clay swelling, averaged to 0.087 meters per day or  $1.0\text{E-}4$  cm/s. When clay swelling within the system was accounted for, hydraulic conductivity dropped to 0.06 meters per day or  $7.4\text{E-}5$  cm/s (**Figure 7**).

Infiltration tests conducted at the 4-meter, 28-meter and 52-meter mark exhibited surface infiltration rates from  $2.5\text{E-}4$  cm/sec to  $6.47\text{E-}4$  cm/sec. Values similar to those calculated through numerical modeling, demonstrating the accuracy of the numerical modeling values. Lastly, slug tests were conducted on all three preinstalled piezometers. Piezometer 1 located closest in proximity to the infiltration pit along the survey line (**Figure 3**) exhibited an average hydraulic conductivity of  $2.1\text{E-}2$  cm/sec. Piezometer 2 and 3 exhibited average hydraulic

conductivities of  $4.8E-2$  cm/sec and  $1.7E-2$  cm/sec, respectively. These values were significantly higher than what was found in both the soil core analyses and the 2D electrical resistivity survey suggesting increased permeability near the base of the Sparta Formation. Infiltration values were comparable to values calculated through the soil core analysis, which averaged to  $2.3E-4$  cm/sec.

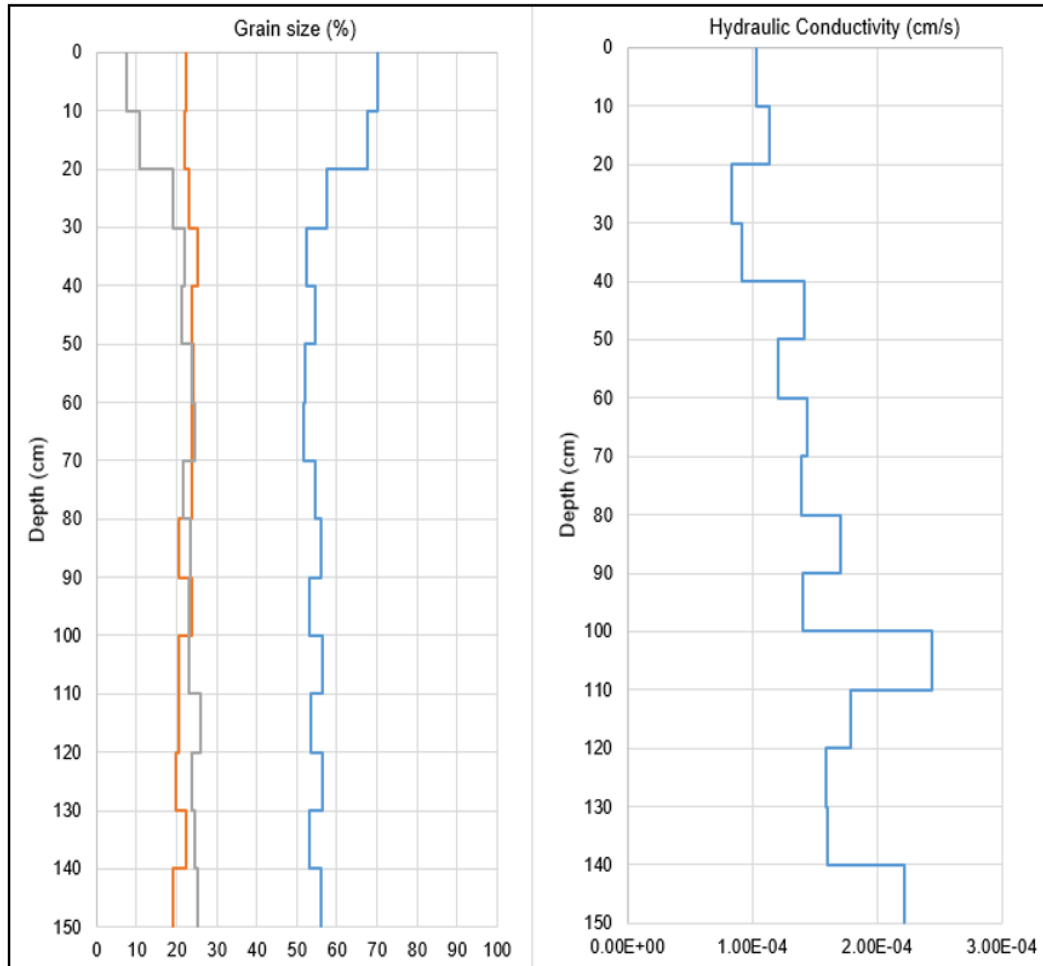


**Figure 6.** A. Average grain size percentage across three 1.5-meter-deep cores. Blue represents % sand, orange % silt, gray % clay. B) Hydraulic conductivity averaged across three 1.5-meter-deep cores.

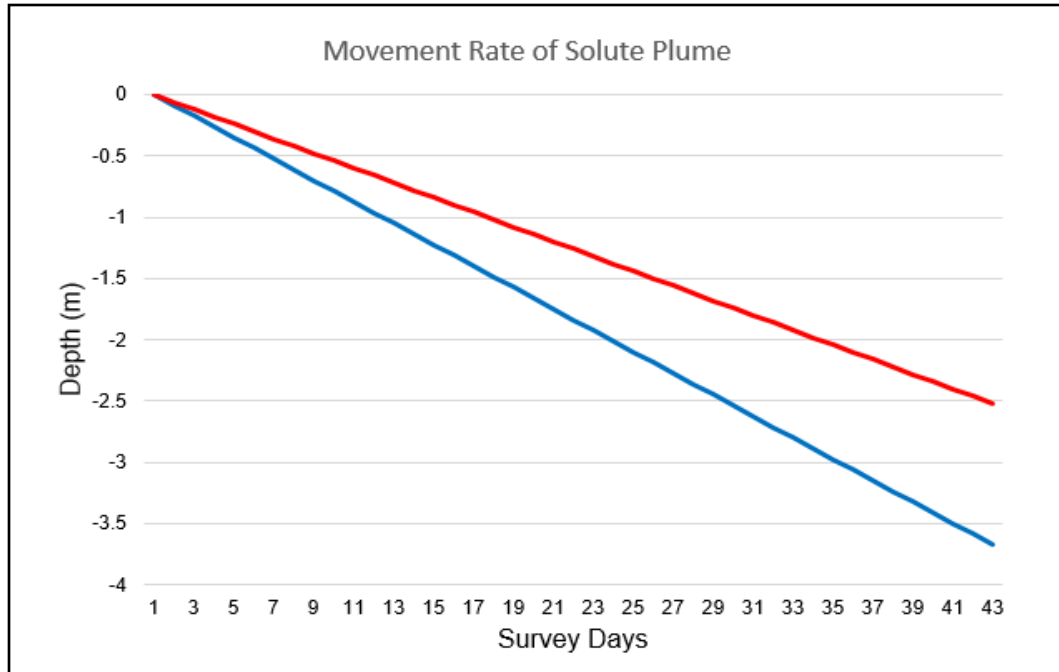


**Figure 7.** Vertical Hydraulic conductivity of the solute plume over 42 days, the time period from the addition of the first saline solution to the end of the final survey. The red line plot is representative of average hydraulic conductivity and average clay swelling, the blue line plot is representative of the average hydraulic conductivity negating clay swelling. The maximum rate of movement is 0.0874 meters per day, while the minimum rate of movement is 0.06 meters per day.

## 2-D ELECTRICAL RESISIVITY SURVEY

2-D electrical resistivity surveys were conducted using 56 electrodes at a one-meter spacing (**Figure 8 A**) configured in a dipole-dipole array. The survey line was positioned with a northwest to southeast trend through piezometer 1. Data collection was completed through two independent survey durations. Initially a fourteen-day survey was conducted in which data was collected every other day. An additional one-month survey was conducted directly after the completion of the fourteen-day survey. During the additional one-month survey data was collected weekly. Interpolated datasets were cut from the 56 electrodes of the survey to 16 electrodes (**Figure 8 B**) to better represent the subsurface near solute plume and avoid unnecessary noisy data. Only the 16 electrode cut segments were used for further analyses in this manuscript to focus on the site of solute migration. 172 ohm-m was used as the detectable boundary of the solute plume across all inverted resistivity sections throughout the duration of both survey durations.

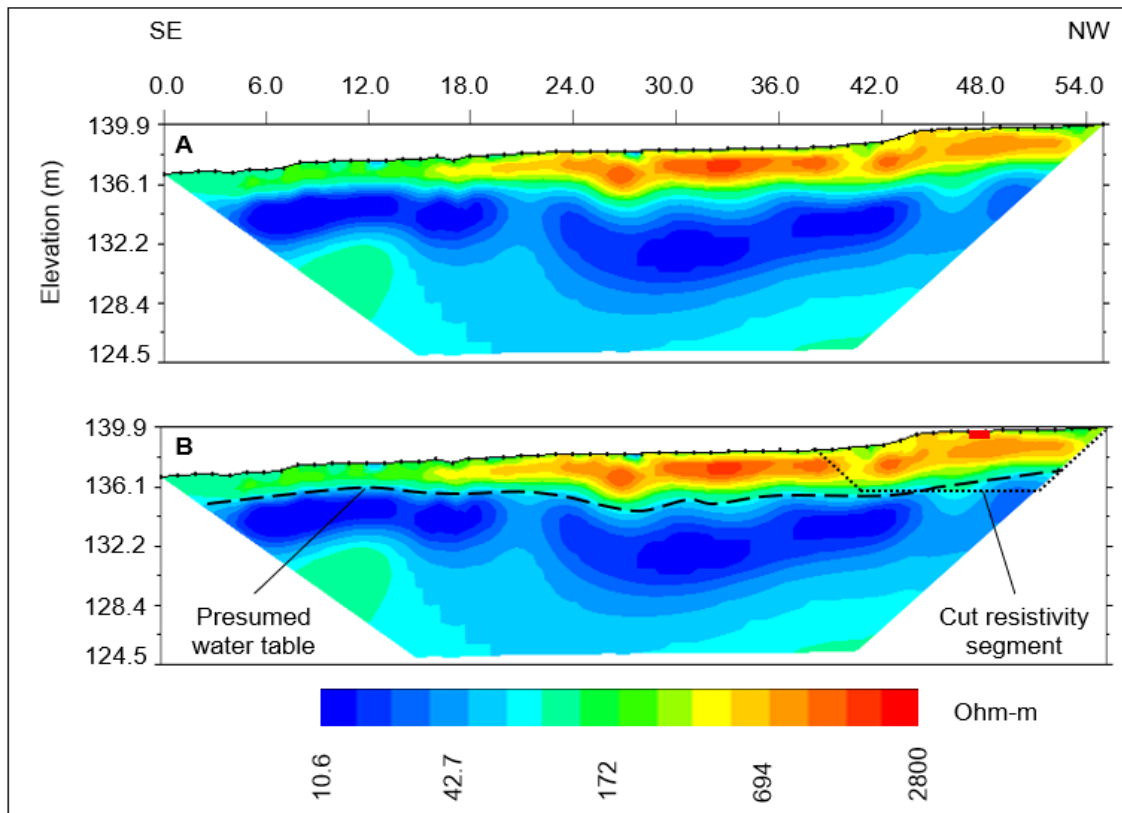


**Figure 8.** (A) Background resistivity analyses collected 7/20 (dipole-dipole array, 56 electrodes at a one-meter spacing). (B) Full 56 electrode inverted resistivity section with the presumed water table and the cut resistivity segment.

### Background Data Collection:

Background 2-D electrical resistivity data was acquired prior to saline introduction into the system, allowing for an undisturbed image of the subsurface in which future resistivity surveys could be correlated (**Figure 9 A**). High resistivities were present in the northwest portion of the survey line from electrode 15 to the end of the survey line at electrode 56. These higher areas of resistivity are attributed to low saturation in relation to the interpolated water table than the 14 electrodes in the southwest portion of the survey line. RMS and L2 error were significantly lower in the background survey (below 5%) than any other survey conducted, no data was removed in the data misfit histogram.

### Day 2:

Electrical resistivity data acquired two days subsequent to the injection of the solute solution through the infiltration pit did not detect the presence of any low resistivity characteristics of the saline solution (**Figure 9 B**). Resistivity section appeared identical to the background data collected two days prior. Vertical solute plume maximum and minimum migration based on numerical modeling values for day two were 0.17 and 0.12 meters, respectively (**Figure 7**).

### Day 4:

Electrical resistivity data acquired four days subsequent to the injection of the solute solution through the infiltration pit indicates the initial stage of a solute

plume migration through the vadose zone (**Figure 9 C**). Horizontal movement for the solute plume extending ~0.8 meters, with vertical movement ~0.6 meters. The water table on day four was observed at ~136.5 meters above sea level, ~2.4 meters below the solute plume. Vertical solute plume maximum and minimum migration based off numerical modeling values for day four were 0.35 and 0.24 meters, respectively (**Figure 7**).

Day 6:

Electrical resistivity data acquired six days subsequent to the injection of the solute solution through the infiltration pit indicates minimal vertical movement of the plume with a continued horizontal migration (**Figure 9 D**). Horizontal movement for the solute plume extended ~1.4 meters in the NW direction and ~0.5 meters to the SW. Vertical movement increased ~0.2 meters over the two-day period to ~0.8 meters. Vertical solute plume maximum and minimum migration based on numerical modeling values for day six were 0.52 and 0.36 meters, respectively (**Figure 7**).

Day 8:

Electrical resistivity data acquired eight days subsequent to the injection of the solute solution through the infiltration pit indicates an increase in conductivity of the solute plume represented by the low resistivity (~50 ohm-m) between the 48<sup>th</sup> and 49<sup>th</sup> electrode (**Figure 9 E**). Horizontal movement in the NW direction

was stagnant; however, horizontal movement to the SE increased to ~0.8 meters giving the plume a total horizontal migration of ~2.2 meters. Vertical migration through the vadose zone increased to ~1.3 meters. Vertical solute plume maximum and minimum migration based off numerical modeling values for day eight were 0.70 and 0.48 meters, respectively (**Figure 7**).

Day 10:

Electrical resistivity data acquired ten days subsequent to the injection of the solute solution through the infiltration pit indicates an increase in concentration of the solute plume represented by the low resistivity (~20 ohm-m) between the 48<sup>th</sup> and 49<sup>th</sup> electrode (**Figure 9 F**). Movement in the NW direction remained stagnant, again increasing to the SE to a full extent of ~2.2 meters. Vertical depth migration continued to increase to a total migration of ~2.3 meters. The area between the solute plume and the estimated water table in the inverted resistivity section displayed higher resistivity values (~2700 ohm-m) than prior surveys. Vertical solute plume maximum and minimum migration based off numerical modeling values for day ten were 0.87 and 0.60 meters, respectively (**Figure 7**).

Day 12:

Electrical resistivity data acquired twelve days subsequent to the injection of the solute solution through the infiltration pit indicates a steady low resistivity

(~20 ohm-m) solute plume (**Figure 9 G**). Horizontal and vertical movement remain constant at ~2.2 meters and ~2.3 meters, respectively. Survey results indicated a decrease in the high resistivity areas surround the plume from roughly ~2700 ohm-m to ~1400 ohm-m. Vertical solute plume maximum and minimum migration based off numerical modeling values for day twelve were 1.1 and 0.72 meters, respectively (**Figure 7**).

Day 14:

Electrical resistivity data acquired fourteen days subsequent to the injection of the solute solution through the infiltration pit indicates a significant migration of the solute plume through the vadose zone both vertically and horizontally (**Figure 9 H**). Horizontal movement increased in both NW and SE direction with a full extent of ~2.9 meters. Vertical migration through the vadose zone increased to ~2.5 meters, ~1.3 meters above the measured water table. Resistivity values surrounding the solute plume once again rose to high values (~2600 ohm-m) with the estimated water table falling ~1.4 meters since the start of the survey. Vertical solute plume maximum and minimum migration based off numerical modeling values for day fourteen were 1.2 and 0.84 meters, respectively (**Figure 7**).

Day 21:

Electrical resistivity data acquired twenty-one days subsequent to the injection of the solute solution through the infiltration pit and seven days after the addition of the saline solution concluded (**Figure 10 A**). Over the one-week period between surveys the solute plumes distinguishable boundaries decreased in both vertical depth and horizontal width. The low resistivity (~20 ohm-m) displayed in the inverted resistivity section indicating the solute plumes concentration is decreasing. Horizontal migration in the NW direction was ~1.4 meters, SE horizontal migration was ~0.4 meters. Soil surrounding the solute plume towards the water table displayed a significantly high resistivity ~2800 ohm-m. Vertical solute plume maximum and minimum migration based off numerical modeling values for day twenty-one were 1.8 and 1.3 meters, respectively (**Figure 7**).

Day 28:

Electrical resistivity data acquired twenty-eight days subsequent to the injection of the solute solution through the infiltration pit and fourteen days after the addition of the saline solution concluded (**Figure 10 B**). Inverted resistivity continued to display a diminishing distinguishable boundary of the solute plume with an increasing resistivity ~35 ohm-m. Total horizontal distinguishable migration had decreased to ~2.0 meters, ~1.1 meters of migration to the SE and ~0.9 meters of migration to the NW. Vertical migration was observed to be ~1.2

meters. Vertical solute plume maximum and minimum migration based off numerical modeling values for day twenty-eight were 2.4 and 1.7 meters, respectively (**Figure 7**).

Day 35:

Electrical resistivity data acquired thirty-five days subsequent to the injection of the solute solution through the infiltration pit through the infiltration pit and 21 days after the addition of the saline solution concluded (**Figure 10 C**). Inverted resistivity section displayed a transition from the diminishing distinguishable boundaries of the solute plume observed in the two surveys prior to an expanding yet diluted plume (~43 ohm-m). Horizontal migration increased in both the NW and SE direction to an extent of ~2.1 meters. Vertical migration yet again began to migrate towards the water table to a depth of ~1.6 meters. Soil surrounding the solute plume transitioned from resistivity values of ~2800 ohm-m to ~1747 ohm-m. Vertical solute plume maximum and minimum migration based off numerical modeling values for day thirty-five were 3.1 and 2.1 meters, respectively (**Figure 7**).

Day 42:

Electrical resistivity data acquired forty-two days subsequent to the initiation of solute solution into system (**Figure 10 D**) through the infiltration pit and 28 days after the addition of the saline solution concluded. Inverted resistivity

displayed a continued migration of the solute plume both vertically and horizontally. The concentration of the solute plume reached resistivity levels of ~43 ohm-m at its core closest to the injection site and up to ~200 ohm-m at its furthest limits. Horizontal migration totaled ~2.1 meters, ~1.1 in the NW direction and ~1.01 meters towards the SE. Vertical migration reached ~1.7 meters, ~2.1 meters above the measured water table. Vertical solute plume maximum and minimum migration based off numerical modeling values for day forty-two were 3.7 and 2.5 meters, respectively (**Figure 7**).

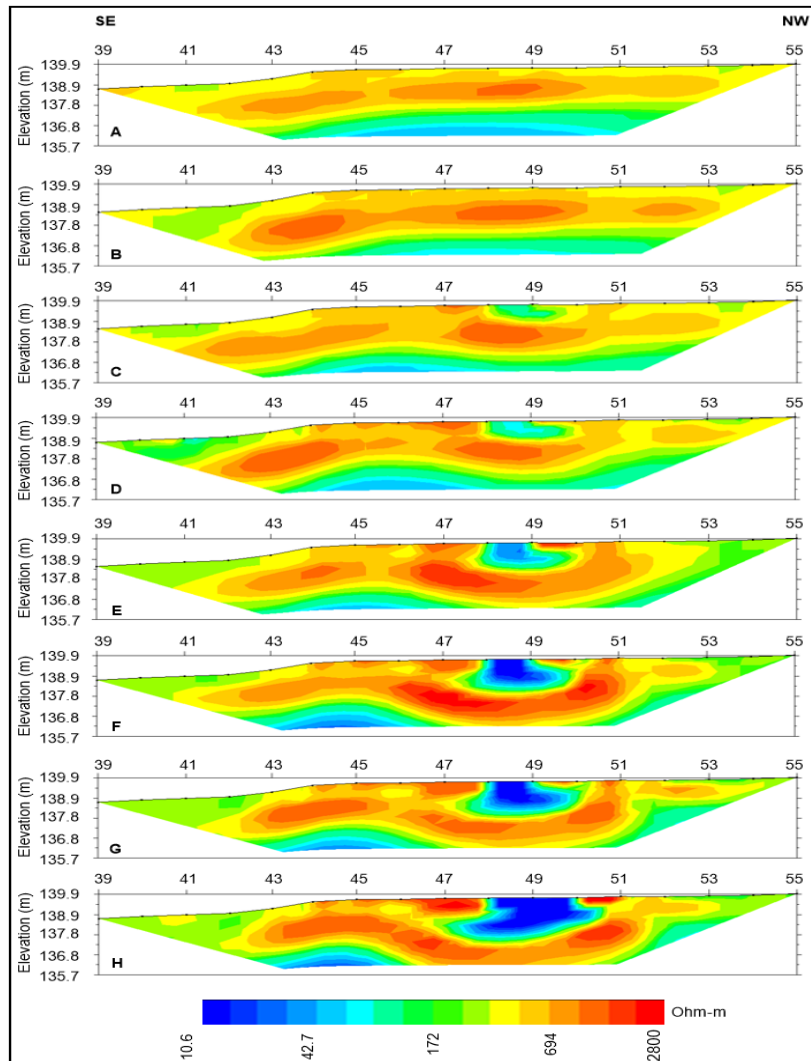


**Figure 9.** Survey line one section between electrode 40 and electrode 56 (dipole-dipole array, 56 electrodes at a one-meter spacing). Iterations=8, scale 1:1, RMS range from 6-25%. **(A)** Background survey (7/20), **(B)** Inverted resistivity section day 2 (7/22), **(C)** Inverted resistivity section day 4 (7/24), **(D)** Inverted resistivity section day 6 (7/26) **(E)** Inverted resistivity section day 8 (7/28), **(F)** Inverted resistivity section day 10 (7/30), **(G)** Inverted resistivity section day 12 (8/1), **(H)** Inverted resistivity section day 14 (8/3) (Image was created in AGI's EarthImager 2D, 2016).

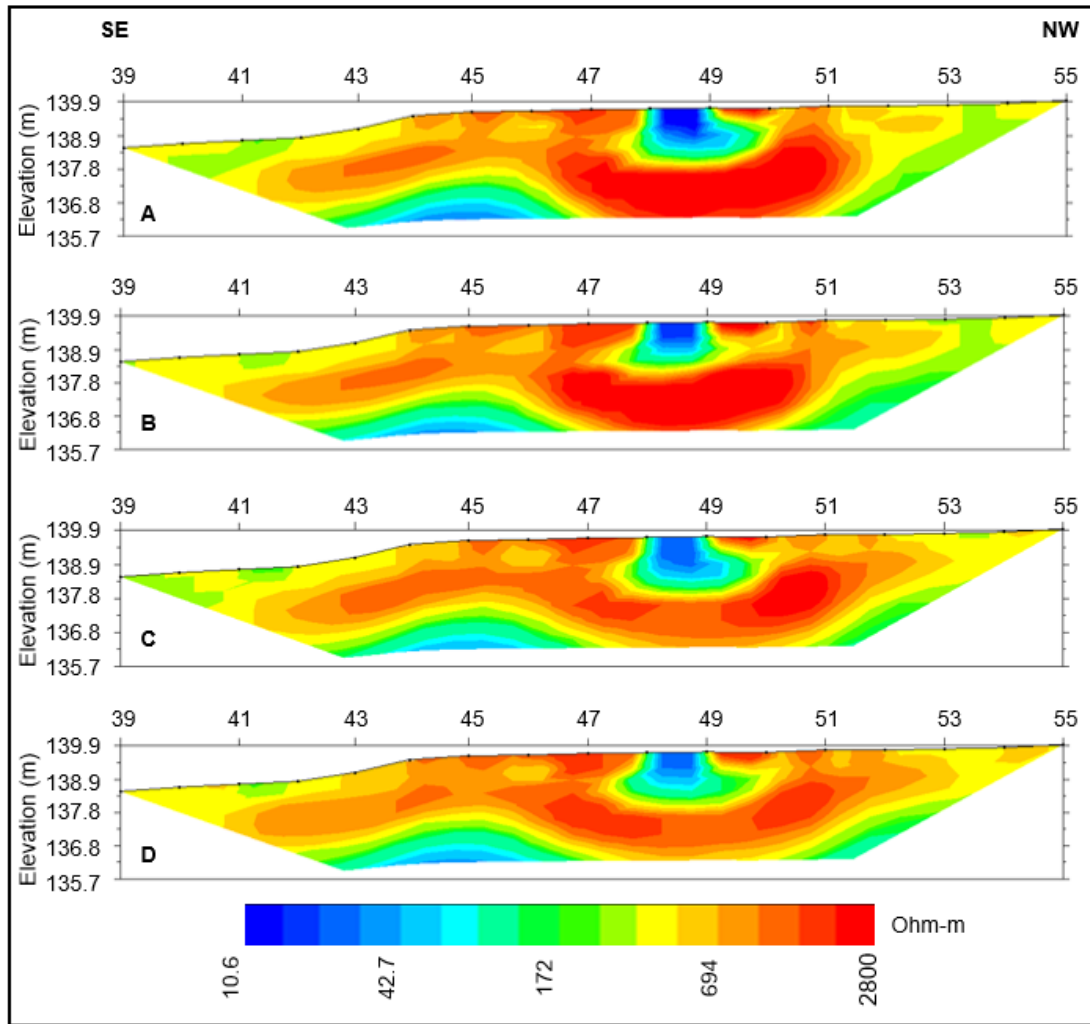


**Figure 10.** Survey line one interpreted section between electrode 40 and electrode 56 (dipole-dipole array, 56 electrodes at a one-meter spacing). Iterations=8, scale 1:1, RMS range from 12-18%. **(A)** Inverted resistivity section day 21 (8/10), **(B)** Inverted resistivity section day 28 (8/17), **(C)** Inverted resistivity section day 35 (8/24), **(D)** Inverted resistivity section day 42 (8/31) (Image was created in AGI's EarthImager 2D, 2016).

## DISCUSSION AND CONCLUSION

Electrical resistivity methods were used in conjunction with numerical modeling to track the migration pathway and tendencies of a solute plume through the subsurface within the Sparta Sandstone unit of the Claiborne Group to evaluate potential groundwater contamination migration into the unconfined portions of the Sparta Aquifer. The electrical resistivity surveys were conducted using the SuperSting R8 WIFI RES/IP/SP, over a period of 42 days. Surveys were conducted every two days for a two-week period and then weekly for an additional month. The purpose of the survey was to compare the effectiveness of the 2D electrical resistivity in tracking solute plume migration when compared with traditional numerical modeling.

According to 2D inverted resistivity at the conclusion of the 14<sup>th</sup> day survey the solute solution moved 1.5 meters laterally on either side of the infiltration pit. Horizontal movement migration tendencies can be attributed to dispersion. Vertical non-uniform migration tendencies through the vadose zone dominated the movement of the solute plume. Vertical migration as seen in inverted resistivity (**Figure 9**) reached 2.5 meters, 3.1 meters from the measured water table. Numerical modeling for the fourteen-day survey produced migration values between 1.2 and 0.8 meters, depths significantly shallower than those

indicated through 2D electrical resistivity. Discrepancies between the electrical resistivity and numerical modeling can be related to numerous factors applied to vadose zone migration. Values obtained through numerical modeling do not account for the heterogeneity of each ten-centimeter increment of soil due to the averaging of each cored section. Soils segments in the upper region of the cores reduced clay content and greater porosity, leading to the faster migration of the solute plume. Preferential flow of the plume along roots of grass and burrows factor into the increased migration through the upper segments of soil closer to the surface. Anisotropy within the soil potential generated a desirable flow path for the plume increasing the vertical migration to values greater than those calculated through numerical modeling.

Resistivity sections surveyed on the 21<sup>nd</sup>, 28<sup>th</sup>, 35<sup>th</sup> and 42<sup>nd</sup> day display a reduction of saline percentages and retardation of the solute plume within the system. Due to the addition of 24 liters of fresh water over a duration of 27 days (survey day 15 to 42) at the end of the initial study, the saline solution in the system became diluted, diminishing the detectable boundaries observed in the inverted resistivity sections. The dilution caused the conductivity of the plumes perimeter to gradually decrease in resistivity, as the fresh water diffused through the system, to levels undiscernible from the surrounding medium through the electrical resistivity survey. The final survey on the 42<sup>rd</sup> day displayed a solute plume that had migrated laterally 0.48 meters on either side of the infiltration pit

reaching a depth of 0.98 meters (**Figure 10**). Numerical modeling values did not account for the dilution of the solute plume therefore values for the 42<sup>nd</sup> day indicated a solute plume that should have migrated vertically between 3.7 and 2.5 meters.

Hydraulic conductivity values obtained through the Bouyoucos hydrometer method applied on the three 1.5-meter cores ranged from 1.1E-4 cm/sec to 9.9E-5 cm/sec with an average of 2.3E-4 cm/sec. These values are significantly lower than those obtained from the slug tests. However, rates calculated through the hydrometer method were similar to the rates obtained through the infiltration tests. Piezometer 1, the closest piezometer to the infiltration pit (**Figure 3**), had an average hydraulic conductivity of 2.11E-2 cm/s, significantly higher than laboratory calculations (**Figure 6**). Increased hydraulic conductivity values gained from the slug tests are attributed to an increase in grain size with depth, an attribute of the study site identified within the three cored sections. Slug tests were conducted at a depth greater than the cored sections leading to the increase in hydraulic conductivity values. Calculated averaged movement rates from the bottom of the infiltration pit at a depth of 0.2 meters to the bottom of the cored sections at 1.5-meters was 8.7 cm/day without consideration of clay swelling. When factoring in clay swelling, the solute plume migration rate would decrease to 6.4 cm/day. Clay swelling effects the hydraulic conductivity of the system through decreasing of pore space. As swelling clays are introduced to

moisture they expand, leading to the obstructing or partial obstruction of the pore space. Discrepancies in numerical modeling values can originate within the averaging of particle sizes through the ten-centimeter increments of the 1.5-meter-deep cores, as well as the estimation of percentages of swelling clays. Accounting for a higher percentage of clays prone to swelling would result in a decreased hydraulic conductivity throughout the system.

Sparta Sandstone and accompanying soil within the study site proved to have variances with depth based on the soil cores collected (**Figure 6 A**). Numerical modeling used throughout the study accounted solely for vertical migration with the intent to generate values comparable to the preconceived path of the solute plume towards the ground water table. The intent of the numerical modeling as presented in this study was to gain a better understanding of the vadose zone migration of the solute plume considering the hindering effects of clay swelling, thus leaving values for diffusion, advection and lateral transport absent from the final models. The absence of these values leaves the numerical modeling data deficient in its ability to track the horizontal migration of the solute plume yet strengthens its ability to track the vertical migration of the solute plume.

Vertical solute plume migration patterns shown in 2D electrical resistivity were outside the parameters calculated through numerical modeling for the initial

fourteen-day survey. 2D electrical resistivity displayed a solute plume migrating faster than what was calculated through numerical modeling likely due to the averaging that was applied to the vertical numerical modeling. Inverted resistivity for the additional one-month survey displayed a diluted solute plume. Dilution occurred to such an extent that the plumes outer boundaries were no longer distinguishable from the surrounding strata leaving the full vertical migration of the solute plume undetectable through 2D electrical resistivity.

Numerical modeling employed in this survey was simplified to account for variables effecting vertical migration through the vadose zone such as clay swelling and hydraulic conductivity. Lateral migration caused by advection and diffusion and anisotropy are factors of the solute plume as it migrates through the strata, however, they are absent from the numerical modeling. Additionally, hysteresis a force prevalent in vadose zone migration was not calculated.

This study is beneficial for future potential near surface contaminants spill delineation and clearly shows the limitations of both resistivity and numerical modeling approaches. However, data collected from this survey cannot be applied to the entirety of Eocene Sparta Sandstone unit. Low hydraulic conductivity values paired with low permeability demonstrates a highly varied lithology of the Sparta Sandstone. The study site characteristics differ from what is typically observed, in Sparta Sandstone outcrops. Within the study site the

Sparta is characterized by higher percentages of clays and smaller grain sizes. Leading the Sparta Sandstone unit within the study site based of the three, 1.5-meter-deep soil cores to be classified as a sandy clay loam, representative of a lagoonal mudstone interface. Data gained throughout this survey is beneficial in tracking future contaminant migration within sandy clay loams, displaying the ability of clay lenses throughout the Sparta Formation to act as permeability boundaries in the transport of contaminants in the subsurface.

2-D electrical resistivity methods proved viable in tracking the migration and tendencies of the solute plume through the vadose zone in strata that display characteristics of heterogeneity and anisotropic soils. Solute plume migration through soils with these characteristics is dictated by the electrostatic double layer. Future solute studies should employ multiple closely spaced resistivity lines in order to more accurately track the horizontal movement of the plume.

## REFERENCES

- Berg, R. R. (1984). The Cretaceous-Tertiary Boundary and Lower Tertiary of the Brazos River Valley. *Stratigraphy of the Claiborne Group*, 10-16.
- Bouyoucos, G. J. (1936). Directions For Making Mechanical Analyses Of Soils By The Hydrometer Method. *Soil Science*, 42(3), 225-230.
- Bureau of Economic Geology. (1992). Geology of Texas. Retrieved October 7, 2018, from <http://www.beg.utexas.edu/UTopia/images/pagesizemaps/geologic.pdf>
- Costall, A., Harris, B., & Pigois, J. P. (2018). Electrical Resistivity Imaging and the Saline Water Interface in High-Quality Coastal Aquifers. *Surveys in Geophysics*, 39(4), 753-816. doi:10.1007/s10712-018-9468-0
- Dane, J. H. & Klute, A. 1971. Effects of salts on the hydraulic properties of a swelling soil. *Soil Sci. Soc. Amer. J.* (in press)
- Eargle, H. (1968). Nomenclature of formations of Claiborne Group, middle Eocene, Coastal Plain of Texas. *Geological Survey Bulletin*, 1251(D), 1-25.
- Ferring, C. R. (2007). Geology of Texas. Denton, TX: Thomson Brooks/Cole.

Fetter, C. W. (2004). Applied hydrogeology (Fourth ed.). Long Grove, IL:  
Waveland Press.

Fetter C.W. (2018) Contaminant Hydrogeology. 500 pp. Upper Saddle River, NJ:  
Prentice-Hall.

Fisher, W.L., 1964, Sedimentary Patterns in Eocene Cyclic Deposits, Northern  
Gulf Coast Region, Bureau of Economic Geology, Austin, Texas,  
<http://www.kgs.ku.edu/Publications/Bulletins/169/Fisher>.

Forestar, 2011, Map, East Texas Basin,  
[http://www.forestargroup.com/assets/minerals/FORE\\_EastTx.pdf](http://www.forestargroup.com/assets/minerals/FORE_EastTx.pdf)

George, P. G., & Mace, R. E. (2011). Aquifers of Texas. *Texas Water  
Development Board*,380, 15-149.

Hardy, R. C., & Cottington, R. L. (1949). Viscosity of Deuterium Oxide and Water  
from 5° to 125°C. *The Journal of Chemical Physics*, 17(5), 509-510.

Head, K. H., 1982, Manual of soil laboratory testing, Vol 2, Pentech Press, ISBN  
0-7273-1305-3

Hosman, R. L. (1991). Regional Stratigraphy and Subsurface Geology of  
Cenozoic Deposits, Gulf Coastal Plain, South-central United States. *U.S  
Department of Interior*,1-43.

- Hosman, R.L., Long, A.T., Lambert, T.W., and others, 1968, Tertiary aquifers in the Mississippi embayment, with discussions of quality of the water, by Jeffery, H.G.: U.S. Geological Survey Professional Paper 448-D, 29 p.
- Hvorslev M.J. 1951. Time Lag and Soil Permeability in Ground-Water Observations. Bull. No.36, Waterways Experiment Station, Corps. Of Engineers, U.S. Army, pp. 50.
- Jobe, K., Ledger, E., Sharp, P., & Crocker, M. (1993). Radiostratigraphy and Heavy Mineral Content of the Weches Formation (Eocene), Nacogdoches County, Texas. *AAPG Bulletin*,77.
- Krutak, P., & Kimbrell, C. (1991). Sparta B Sandstones (Eocene), Fordoche Field, Pointe Coupee Parish, Louisiana-A Compartmentalized, Barrier-Island Oil and Gas Reservoir. *AAPG Bulletin*,75, 383-404.
- Lagerwerff, J. V., Nakayama, F. S. and Frere, H. M. 1969. Hydraulic conductivity related to porosity and swelling of soil. *Soil Sci. Soc. Amer. Proc.* 33:3-12.
- Mckee, P. W., & Hays, P. D. (2002). The Sparta Aquifer: A Sustainable Water Resource? *Fact Sheet*,1-4.
- McKenzie, N., Coughlan, K., & Cresswell, H. (2008). *Soil physical measurement and interpretation for land evaluation*. New Delhi.

McNeal, B. L., Layfield, D. A., Norvell, W. A. & Rhoades, J. D. 1968. Factors influencing hydraulic conductivity of soils in the presence of mixed-salt solutions. *Soil Sci. Soc. Amer. Proc.* 32:187-190.

National Centers for Environmental information, Climate at a Glance: County Time Series, published April 2019, retrieved on April 22, 2019 from <https://www.ncdc.noaa.gov/cag/>

Payne, J. (1968). Hydrologic significance of the lithofacies of the Sparta Sand in Arkansas, Louisiana, Mississippi, and Texas. *U.S. Geological Survey*,5-7.

Ricoy, J. U., & Brown, L., Jr. (1977). Depositional Systems in Sparta Formation (Eocene), Gulf Coast Basin of Texas: ABSTRACT. *AAPG Bulletin*, 61, 139-154.

Seilsepour, M., Rashidi, M., & Khabbaz, G. (2009). Prediction of Soil Exchangeable Sodium Percentage Based on Soil Sodium Adsorption Ratio. *American-Eurasian J. Agric. & Environ. Sci*,1-4.

Shepherd, R. G. (1990). "Correlations of Permeability and Grain Size". *Ground Water*,28(1), 116-116.

Sellards, E. H., Adkins, W. S., & Plume mer, F. B., 1932a, Geology of Texas, University of Texas Bulletin, v. 1, p. 635-651., 1932b, Geology of Texas: University of Texas Bulletin 3232, v. 1, p. 528.

Stenzel, H. B., 1935, A New Formation in the Claiborne Group: Univ. Texas Bull. 3501, p. 267—279.

Texas Ecoregions. (2017, July 31). Retrieved from <https://tpwd.texas.gov/education/hunter-education/online-course/wildlife-conservation/texas-ecoregions>

Watkins, J. (2018) Mercury in Big Cypress Bayou and Caddo Lake watersheds in Marion and Harrison Counties Texas (unpublished master's thesis). Stephen F. Austin State University, Nacogdoches, Texas.

Weast, R. C. (1972). *Handbook of Chemistry and Physics 53rd Edition*. Cleveland: Chemical Rubber Pub.

Yang, Y., Mu, L., Chen, L., Shi, G., & Fang, H. (2019). Precise control of the interlayer spacing between graphene sheets by hydrated cations. *Physical Chemistry Chemical Physics*, 21 (14), 7623-7629

## APPENDIX (A) LITERATURE REVIEW

## Introduction

The study area is located ninety meters to the east of the Stephen F. Austin Scientific Research Center at the corner of Highway 59 and Ernest McLain road. Roughly six kilometers northwest of the Stephen F. Austin State University campus, Nacogdoches County, Texas (**Figure A 1**). The purpose of the study is to temporally analyze the flow behavior of a conductive solution when it is introduced into a system (sandy clay loam) and tracked as it migrates towards the water table. The study will be looking at three fifty-six-meter-long resistivity survey lines placed strategically around three piezometers. An AGI SuperSting R8 WIFI RES/IP/SP will be used to conduct dipole-dipole resistivity surveys along the three predetermined traverses. Once data is acquired and processed, 2D images of the subsurface will be produced that allows for the flow path of the conductive solution to be mapped.

Different sediment types yield different resistivity values, depending on many different variables such as permeability, porosity and water content within the matrix of the grains. The heterogeneity of the media will allow for the migration of the conductive solution to be mapped in the subsurface. Data will be collected every other day for a two-week period, allowing for temporal modelling to be conducted.

The study site lies within the Gulf Coast basin. Sediments surrounding the area are of those related to the Eocene regressive and transgressive seas. A study conducted by Jobe and others (1993) identified significant heavy mineral proportion within these sediments. Thorium and Uranium are two heavy minerals that closely correlate in vertical sequences throughout the Queen City, Sparta and Weches formations. Within the study sites boundary, Sparta sandstone can be observed at the surface and is a representation of a regression of the Eocene sea.

Conducting a resistivity survey can be completed using a variety of electrical resistivity arrays. The dipole-dipole array will be used to conduct this electrical resistivity survey. This setup is appealing for a few reasons. The array allows for great horizontal resolution as well as fast data accumulation; the SuperSting's eight-channel capability allows eight readings to be acquired simultaneously. The dipole-dipole array consists of two current electrodes paired together with two potential electrodes. The instrument runs current through the two current electrodes at position one and two, labeled A and B and measures the potential difference of the ground through the potential electrodes at position three and four, labeled M and N. Once the readings for the two dipoles are complete, the instrument moves the potential electrodes, previously in position three and four, to position four and five while the current electrodes stay stationary. This process of changing the potential electrode is repeated until the

whole line has been surveyed and all the data collected. After the readings are accumulated the electrodes physically stay in the same place but the current and potential electrodes move out from the center. The results are plotted in a pseudo-section, at the approximate midpoint between the two dipoles and at a depth estimated by half the distance between the dipoles ("Dipole-Dipole Array," 2018). After processing the data through the EarthImager 2D inversion software, true resistivity values are contoured to give approximate values of the resistivity of the subsurface. This process allows for the ability to trace the highly conductive plume through the subsurface.

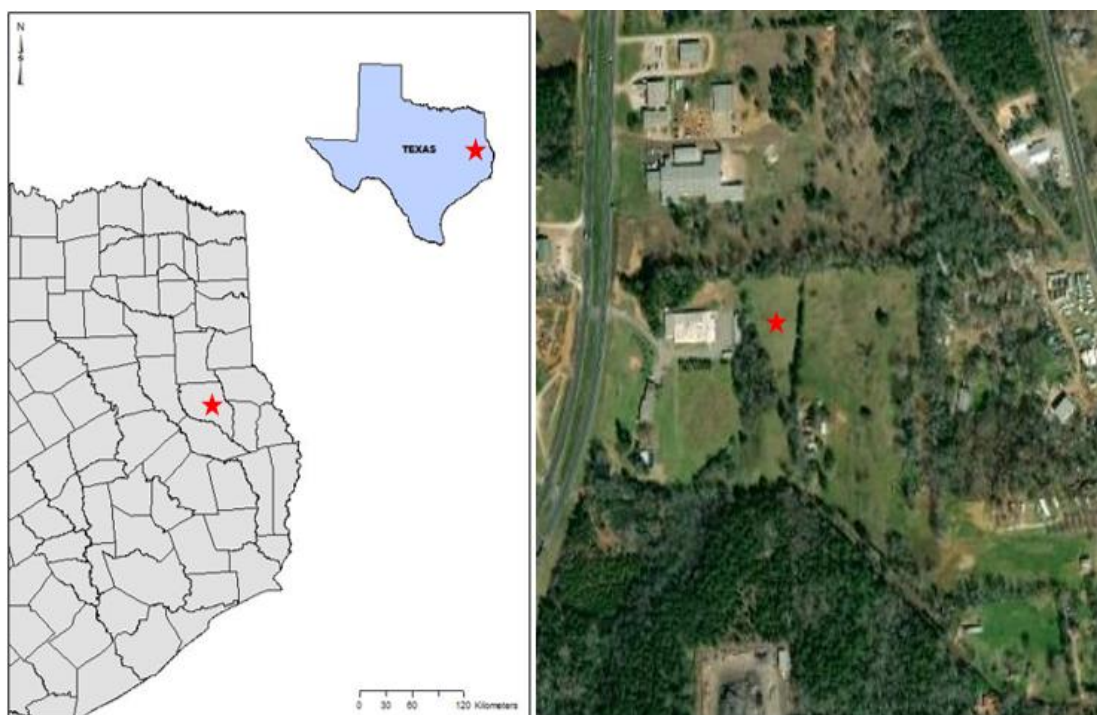


**Figure A 1.** (Left) Map of the study area showing geographic relationship to Texas with relationship to the counties of East Texas. (Right) Zoomed in satellite image of the study area within Nacogdoches County, Texas.

## EOCENE STRATIGRAPHY

Nacogdoches County lies within the Texas Eastern Coastal Plain (Ricoy and Brown, 1977). The units that dominate this area are Eocene in age predominantly from the Claiborne Group representing a period of transgressive and regressive Eocene Seas (**Figure A 2**). The units that compose the Claiborne Group were deposited roughly 40 mya as overlapping, terrigenous clastic wedge sequences (Ricoy and Brown, 1977). In East Texas, the Claiborne Group was originally divided up by Dumble (1924) into four divisions: Yegua, Nacogdoches, Cook Mountain and Mount Selman. Two years later, through observation of outcrops and subsurface analysis, the Claiborne Group of East Texas was further subdivided. Wenlandt and Knebel (1926) subdivided the Cook Mountain into the Crockett and Sparta formations as well as subdividing the Mount Selman into the Weches, Queen City, Reklaw and Carrizo formations. After these subdivisions were made, the Nacogdoches Formation was removed from literature. This section will cover the units in the Claiborne Group which are important to regional geology; however, the primary focus will be on the Sparta Formation.

Claiborne Group

Yegua Formation

The Yegua is an upper member of the Caliborne Group roughly 335 meters thick and is associated with transgressive and regressive cycles as first described by Kennedy in (1892). The basal Yegua is composed of interbedded sandstones and marine shales; while the upper portion consists of deltaic, fluvial and non-marine deposits (Fisher, 1969) (Berg, 1984).

### Cook Mountain

The Cook Mountain Formation (formerly the Crocket Formation) is a transgressive system (Figure A3) consisting primarily of gray fossiliferous marine shales, clays and sandy shales (H. B. Stenzel in Sellards and others, 1932). These stratigraphic units were deposited during the time of the Crockett Sea (Ricoy and Brown, 1977). Due to the depositional environment, marine fossils are very prevalent throughout the formation. Prominent fossils include: *Corbula*, *Phos texanus* Gabb, and *Dentalium* (Deussen, 1924). Segments of the Cook Mountain Formation exposed in road cuts along the Little Brazos River in Brazos County, Texas illustrates a seven-meter segment of the described fossiliferous marine shales. The observed stratigraphy was six meters of shale, thirty centimeters of glauconite and one meter of marl and shale (Stenzel, 1935).

### Sparta

The Sparta Formation is composed primarily of very fine to medium quartz sandstone with a maximum thickness of 304 meters. These sand units are beach

and fluvial in origin and are generally cross-bedded or laminated with beds of clay and sandy clay intermixed. These clays are light gray and chocolate colored (Hosman, 1991). In the lower portion of the unit, oxidation can occur causing outcrops to exhibit a red to orange tint. Within the study area, the oxidized sandy clays of the Sparta can be seen at the surface.

### Weches

Represented as the Weches Sea, the Weches Formation is a transgressional depositional period of shallow marine water laid down before the Sparta Sandstone (Sellards and others, 1932). The Weches consists of two shale units separated by a thick sandstone layer. Both of the shale layers contain glauconite, the lower layer is composed of dark grey clay with greenish brown marl. While the upper shale is a dark gray claystone with lenses of glauconitic sands (Berg, 1984). The middle sandstone unit that makes up the majority of the formation consists of primarily glauconitic sands. These dark green sands are highly cross-bedded, lenticular and interbedded with thin beds of clays and shales and give the Weches Formation its “greensand” name (Hosman, 1991).

### Queen City

The Queen City Sandstone overlies the Reklaw Formation and is commonly exposed in outcrop. Dispersed outcrops across Arkansas show the Queen City to be a fine-grained, cross-bedded sandstone with interbedded

shales (Berg, 1984). The sands are generally light gray to grayish brown and are composed of fine to medium-grained quartz. Within the observed outcrops, interbeds of carbonaceous shale, silt and impure lignite can be found (Hosman, 1991).

#### Reklaw

The Reklaw Formation overlies the Carrizo sands and is composed primarily of dark, stratified sands and shales (Hosman, 1991). The lowermost sandy unit contains medium to coarse glauconitic sand-sized grains and dark reddish gray shales, while the upper unit is predominantly a dark gray to brown claystone. However, the Reklaw Formation is simply known as a sandy unit since distinguishing the two units cannot always be accomplished (Berg, 1984).

#### Carrizo

Representing a regression succession of barrier island deposits, the Carrizo is the basal unit within the Claiborne Group of East Texas underlying the Reklaw Formation (Owen, 1889). With a maximum thickness of up to 365 meters in South Texas the Carrizo is a very coarse, light gray to brownish gray sand containing little to no lignite. The upper most strata contain small amounts of thin, light gray to yellowish lentils (Hosman, 1991). Upon weathering, the Carrizo gives off a bright color which makes it very distinctive in outcrop allowing for it to be easily distinguished as the base of the Claiborne Group.

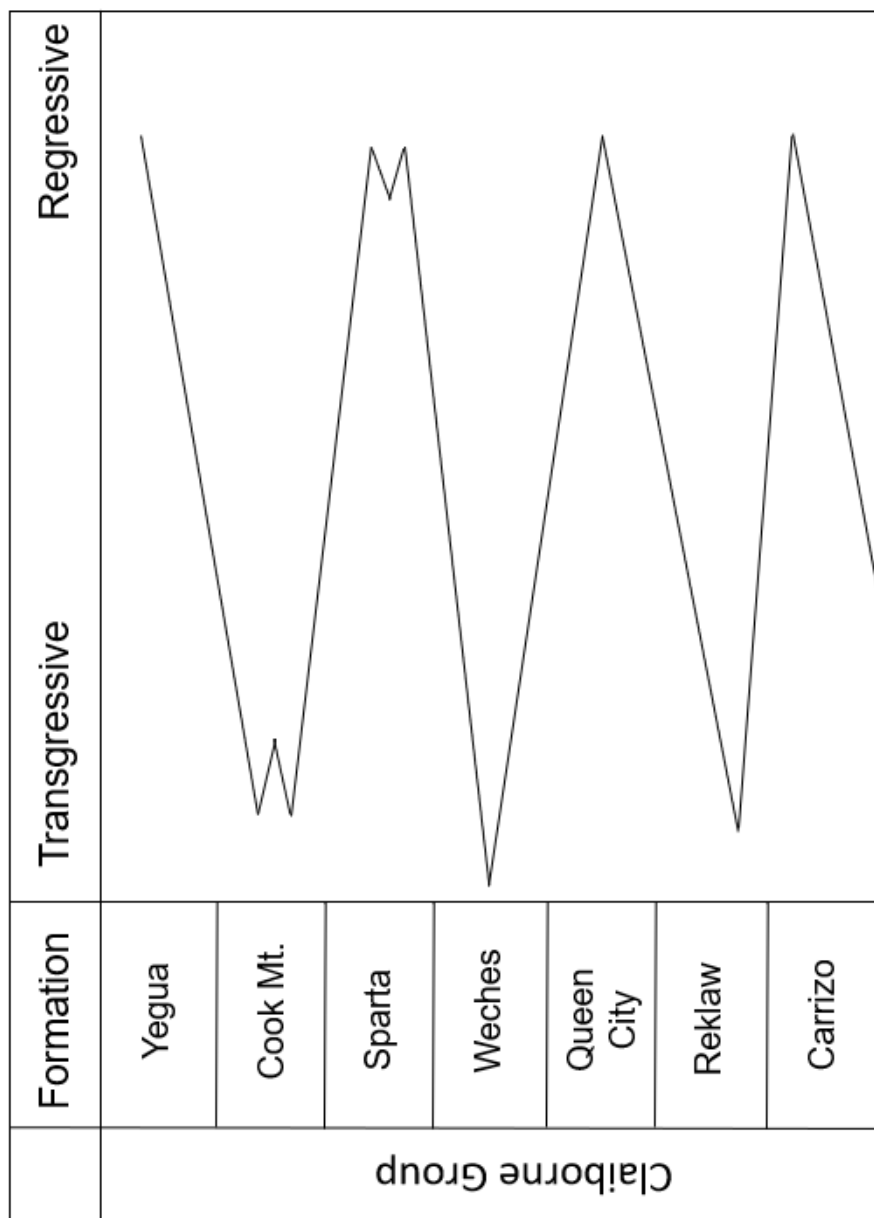


**Figure A 2.** Stratigraphic section showing relationship of the Claiborne Group with the transgressions and regressions of the Eocene Sea (Modified from Watkins, 2018; Fisher, 1964 and Forestar, 2011).

## STRUCTURE

The up dip structural control of the Texas Coastal Plain is the Balcones fault system, a 300-million-year old fault system associated with continental collision between the North American, African and European plates. The Balcones fault separates the Edwards Plateau from the Gulf Coast Plain (Ferrill & Morris, 2008) (**Figure A 3**). The predominate structure associated the Texas Gulf Coast basin is a broad homocline that dips towards the Gulf of Mexico (creates the base for future sediments to be deposited). Regional features include the Sabine Uplift, San Marcos Arch and the Rio Grande Embayment (Waters, McFarland and Lea, 1955).

The Sabine Uplift is a structural high, Jurassic in age that covers an area of easternmost Texas and northwest Louisiana showing little Cretaceous igneous activity (Ewing, 2009) (**Figure A 3**). The uplift was submerged during the early part of the Tertiary, as evident by the presence of marine clays belonging to the Midway Group. Wilcox Group deposits ringed by outcropping Claiborne Group deposits compose the upper most portion of the uplift (Hosman and Weiss, 1991).

San Marcos Arch is marked by unconformities beginning in the late Albanian (105 mya) through the basal Cenozoic (65 mya), extending 161

kilometers long and 241 kilometers wide form Hayes County to Jackson County, Texas with a trend to the southeast (Ewing, 2003) (**Figure A 3**). The San Marcos Arch acted as gentle positive structure that affected the deposition of upper Cretaceous and Paleogene strata (Rose, 2016). As well as separating the Rio Grande Embayment in southern Texas from the Houston embayment (Hosman and Weiss, 1991).

Salt domes are in abundance throughout the Gulf Coast Plain. The salt domes are concentrated predominantly in two bands. The larger of the two bands extends from the southeastern coast of Texas to north Louisiana. The second band lies inland, extending from northeastern Texas across Louisiana into southern Mississippi. The origin of both bands is the Louann Salt; the depositional timeframe is somewhere between Permian to late Jurassic in age (Hosman, 1991). Overburden pressures and density differences created by sedimentary deposits caused the once horizontal salt deposits to flow into salt structures (salt domes) (Beckman and Williamson, 1990). Structural features such as synclines and faulting can be associated with salt domes. However, these structures do not play a role in the regional geology, instead salt structures are extremely localized.

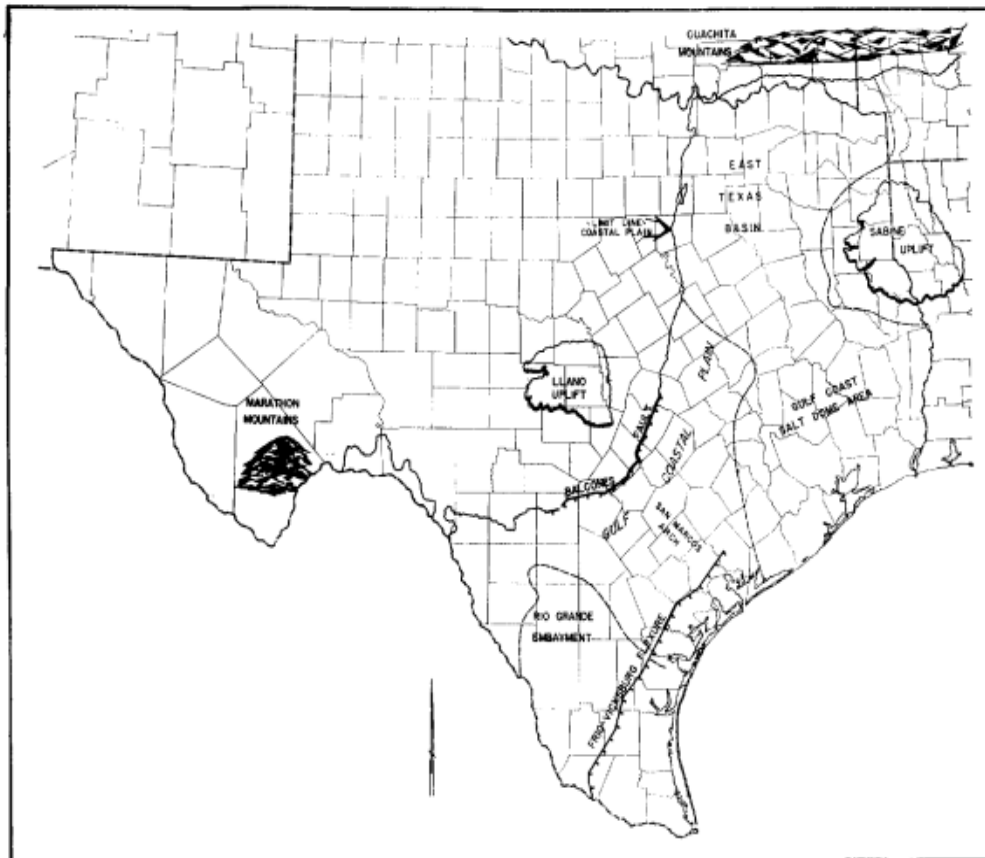


**Figure A 3.** Structural map of the Gulf Coast Basin. Many of the structural features associated with East Texas can be observed in the image above. To the South there is the San Marcos Arch, the interior is controlled by numerous salt domes and in northern East Texas the Sabine Uplift. All of the features present within East Texas played a vital role in the geology present today (Waters and McFarland, 1955).

## HYDROGEOLOGY

The Carrizo-Wilcox Aquifer is a productive groundwater source for East Texas, extending from the Louisiana border to the border of Mexico and covering an area of 65,809 square kilometers within the subsurface. Sixty counties between the Rio Grande and the Red River rely on the aquifer in some extent for purposes such as irrigation, industrial use and for the public supply pumping nearly 5.5E8 cubic meters in 2003 (Boghici, 2009). Thirty-five percent of the aquifers production was for irrigation pumping for Zavala, Frio, Atascosa, Wilson and Dimmit counties. While major towns that rely on groundwater from the aquifer are Bryan-College Station, Lufkin, Nacogdoches and Tyler (Boghici, 2009).

The water-bearing units of the aquifer are the Wilcox Group and the Carrizo Formation; both are Eocene in age and belong to the greater Claiborne Group (Boghici, 2009). The Wilcox Group can then be divided into the Calvert Bluff, Simsboro and the Hooper formations. The Carrizo and Simsboro formation contain the largest volume of water regionally for the aquifer (Thorkildsen and Price, 1991). Between the Colorado and Trinity rivers, the three previously mentioned formations of the Wilcox Group exist as large sand reservoirs for fresh and slightly saline water. North of the Trinity River, however,

these three formations of the Wilcox are no longer distinguishable. The once large sandstone formations are interbedded and cross stratified with clay and lignite in this region (Thorkildsen and Price, 1991). The most permeable formation within the Carrizo-Wilcox Aquifer belongs to the Carrizo Sand. The majority of the water is stored within these massive sand units. The high permeability and latterly connected sand bodies of the Carrizo makes the Carrizo-Wilcox Aquifer one of the most productive aquifers in Texas (Boghici, 2009).

Recharge of the Carrizo-Wilcox Aquifer is predominantly by natural means. The main source of natural recharge for the aquifer is precipitation (Thorkildsen and Price, 1991). Other sources can be attributed to recharge of the aquifer such as the topography of the region, vegetation and infiltration characteristics of the soil. These other sources, however, play a minute role when compared to precipitation. The current rate of recharge for the Carrizo-Wilcox Aquifer is estimated to be 2.5 centimeters per year (Thorkildsen and Price, 1991). Boghici (2009) conducted a survey in which 331 wells from the aquifer were sampled. The results concluded that the groundwater was predominantly fresh to slightly saline and contained dissolved solids below 3,000 milligrams per liter. The salinity of the groundwater increases down gradient due to the precipitation recharge dissolving minerals as it travels through the

subsurface until finally mixing with deep, high salinity ground water (Kreitler, 1979).

## FORESTRY

Plants enact a significant influence on the movement of groundwater primarily within the vadose zone, constantly pumping water through their root systems in order to supply the plant with nutrients. The vadose zone is situated directly below the land surface and is described as an area containing both air and water (Fetter, 2018). As the water derived from the vadose zone is used by the plant, transpiration occurs. Transpiration is the process by which the water within the plant turns to water vapor and is then released back into the atmosphere (“Transpiration- The Water Cycle,” 2016). Plant species vary from region to region, with the differences in species come a difference in the effects on the hydrogeology. Understanding these effects caused by plants can additionally assist in the understanding of the groundwater flow.

Texas is the second largest state in the United States of America in terms of land area, covering nearly 691,027 square kilometers. Due to its vast extent, Texas has many different climates and landscapes that create a wide array of habitat diversity. Throughout the entirety of the state there are ten ecoregions; those being: Piney Woods, Gulf Prairies and marsh, the Post Oak Savannah, the Blackland Prairies, the Cross Timbers, the South Texas Plains, the Edward Plateau, the rolling Plains, the High Plains and the Trans Pecos (“Texas

Ecoregions,” 2017). Since the study site lies within Nacogdoches County, the ecoregion for this area is the Pineywoods. The Pineywoods ecoregion is characterized by minty one to one hundred and twenty-seven centimeters of rainfall annually, with humidity and temperatures are characteristically high. Elevated anywhere from 60-150 meters above sea level the region is described as pine-hardwood forests with scattered areas of cropland, planted pastures and native pastures (“Texas Ecoregions”, 2017). Within the study are four different tree species, those being: American Beech, Water Oak, Eastern Red Cedar and the Chinese privet. The Chinese privet is the most dominate vegetation within the study area, nearly surrounding the entire site on all sides.

American Beech (*Fagus grabdifolia*) is a large tree native to east Texas, growing up to thirty meters in height with a large trunk that can have a trunk one meter in diameter (“Trees of Texas,” 2018). The canopy of this species are dense and provide dense amounts of shade, with elliptical and green leaves that form parallel veins and saw-tooth edges (“American Beech,” 2002). The distinguishable feature of *Fagus grabdifolia* is its smooth textured light gray bark that persists through the mature years of the tree. In shaded forest conditions, the trunks grow long and straight, eventually giving way to a crown of foliage (“American Beech,” 2002).

Water Oak (*Quercus nigra*), also known as the Pin Oak, grows to have height of twenty-seven meters with a maximum trunk diameter of one meter. This species of tree has a large dense crown of dark green foliage (“Trees of Texas,” 2018). The elevation at which *Quercus nigra* flourishes ranges from the lowlands up to 450 meters. When the right conditions are met, *Quercus nigra* can grow at rates of up to sixty centimeters per year and live on average anywhere from thirty to fifty years in age (Grant, 2018). The soil profile to which the tree is keen is that of heavy, compacted, wet soils (“Water Oak,” n.d.). The water oak is an important tree to the wildlife in the ecoregions in which it thrives producing numerous acorns, the food for many animals such as deer, squirrels, pigs, turkeys, ducks and quail. While the hollow stems of the tree act as a nest for both insects and small animals (Grant, 2018).

Eastern Red Cedar (*Juniperus virginiana*), a native tree to Texas, can be found throughout East Texas as well as eastern North America along fence lines, gravel ridges, sandstone plateaus and dry and rocky hillsides. *Juniperus virginiana* grow to heights of fifteen meters tall with a trunk diameter anywhere from thirty to seventy centimeters (“Trees of Texas,” 2018). This species population grows due to the abandonment of farmland and due to fire control at elevations ranging from 1 to 1000 meters (Farjon, 2013). The Eastern Red Cedar can be identified by a dark green minute leaf, grasping the twig so that the twig appears square. The fruit associated with this species are dark blue, .25

centimeters in diameter with a waxy coating which encloses one to two seeds (“Trees of Texas,” 2018).

Chinese Privet (*Ligustrum sinense*) is an invasive species of shrub that has been introduced to the eastern United States, including eastern Texas, through ornamental planting (Urbatsch, n.d.). The shrub ranges in size from two to four meters, reproducing rapidly allowing the shrub to spread swiftly. The root system of *Ligustrum sinense* is shallow but extensive with trunks that occur as multiple stems; these trunks support multiple long leafy branches that arch down towards the ground. The leaves of *Ligustrum sinense* are semi-evergreen to semi-deciduous with flowers that occur in numerous branch clusters, two to ten centimeters long, that cover the shrub when it is flowering (Urbatsch, n.d.). Able to survive in a wide variety of soils, the Chinese privet flourishes when it is exposed to abundant sunlight and soils that are plentiful in both moisture and nutrient levels (Thomas, 1980).

## FLUID PROPERTIES

Permeability and porosity are two characteristics that control how well a geological unit behaves as an aquifer. Porosity is a measure of how much of the rock is open space while permeability is the measure of the ease it which fluids can flow through the open spaces (“How Does Water Move through the Ground,” n.d.). These two characteristics of a rock unit or sedimentary layer will greatly affect not only the water table but also how fast fluid runoff / infiltration occurs. Furthermore, both properties can help measure the time it will take a fluid to be transported from the surface to the ground water table.

### Sparta

An investigation conducted by Krutak and Kimbrell in 1991 observed a cored section of the Sparta Sandstone unit utilizing petrographic, SEM, and EDX studies in order to gain a better understanding of the permeability and porosity. Their investigation observed twelve meters of the Sparta within the Dreyfus #1 well. Within the Dreyfus #1 well, the Sparta is divided into two sections, the lower section is representative of an upper shoreline sandstone, while the second section is composed of storm wash over sandstones and lagoon muds which caps the lower section. The upper section that is comprised of storm wash over lagoonal muds has an average porosity of (20-25 %), with a high permeability of

(250-500 Md). The lower section of the upper shoreline facies has an average porosity of (3.3-21.8%), with an average permeability of (0.01-42.00 Md) (Krutak and Kimbrell, 1991). The permeability and the porosity decrease substantially from the storm wash over lagoonal muds to the upper shoreline sandstones.

## Weches

Minuscule amounts of data have been reported over the permeability and porosity of the Weches Formation, primarily due to the Weches lying amongst the two large producing formations of the Sparta Sandstone and the Queen City Sand. The Weches itself however is not known as a producing formation.

However, the Weches has been identified through outcrop observations as a thin marine formation consisting of fossiliferous glauconitic clay with some marl and limestone (Stenzel, 1938). Due to the high clay content of the Weches Formation, a rudimentary understanding of a clay formation can be used. C.W. Fetter's book "Applied Hydrogeology" (2018) defines clays to have porosity of 33-60% with a low permeability.

## SOLUTE TRANSPORT

Pollutants enter the subsurface in two forms, point source pollution and diffuse source. Point source pollution is usually caused by accident and covers a limited area, while diffuse source pollution generally covers a large area and is caused by large scale operations (Van Der Zee and Leijnse, 2013). When a contaminant (solute plume) enters the subsurface, four transportation mechanisms can have an effect on the transported substance as well as the subsurface. The four transportation mechanisms are as follows: advection, dispersion, diffusion and adsorption. The results of the transportation mechanisms on the contaminant result in a multifaceted circulation of the contaminant within the ground water system (Schulze-Makuch, 2009).

Advection refers to the transport of a solute dissolved within the groundwater by bulk movement and can be defined by the following equation:

$$F_x = q_x C \quad (1)$$

where  $F_x$  is the mass flux of the contaminant in the x direction,  $q_x$  is the specific discharge of the water in the x direction and  $C$  is the concentration of the

contaminate within the water (Van Der Zee and Leijnse, 2013). The assumption that coincides with this equation is that the dissolved substances move at the same rate as the groundwater (Schulze-Makuch, 2009). In most instances where the size of the dissolved solids are small, this generalization is acceptable. However, there are instances where the dissolved particles are larger and different variable need to be considered (Van Der Zee and Leijnse, 2013).

Dispersion is the spreading of a dissolved solute due to differences in the flow velocity of the groundwater and tortuosity of flow paths. Differences in flow velocities can be attributed to the flow of water through pores. The flow of the groundwater will be faster through the center of pores while reduced along the edges (Fetter, 1999). Dispersion can occur on a single pore scale (mechanical dispersion) or on a multiple pore scale (hydrodynamic dispersion) (Van Der Zee and Leijnse, 2013). Mechanical dispersion occurs when the solute solution enters the subsurface and mixing with the ground water ensues. The mixing of the solute with the groundwater occurs because of the varying flow velocities of the solute solution due to the friction caused by the pore space, the result is a diluted solute solution at the edge of the flow path (Fetter, 1999). Hydrodynamic dispersion refers to the combination of molecular diffusion and mechanical dispersion (Fetter, 1999). Occurring over a larger scale hydrodynamic dispersion accounts for all the factors not accounted for by mechanical diffusion alone, primarily diffusion (Van Der Zee and Leijnse, 2013).

Diffusion refers to solute migration from an area of greater concentration to an area of lower concentration. As long as a concentration gradient is present between two fluids, diffusion can occur; if the gradient is absent, then diffusion ceases (Fetter, 1999). Diffusion can be described by Fick's First Law:

$$F = -D_d \frac{dC}{dx} \quad (2)$$

where  $F$  is the mass flux of solute per unit area per time,  $D_d$  is the diffusion coefficient,  $C$  is the solute concentration and  $dC/dx$  is the concentration gradient. The diffusion coefficient can range from  $1 \times 10^{-9}$  to  $2 \times 10^{-9}$  m<sup>2</sup>/s; the coefficient is smaller in porous media due to the adsorption on the solids as well as the presence of particles within the solid matrix (Freeze and Cherry, 1979).

Adsorption and desorption are found in tandem within the ground water system, molecules in suspension will attach to solid material while readily capable of being released into the water phase (Van Der Zee and Leijnse, 2013). A homogeneous saturated media with steady state flow can be expressed by the one dimensional form of the adsorption equation:

$$D_l \frac{\partial^2 C}{\partial t^2} - \bar{v}_l \frac{\partial C}{\partial l} + \frac{\rho_b}{n} \frac{\partial S}{\partial t} = \frac{\partial C}{\partial t} \quad (3)$$

where  $\rho_b$  is the bulk mass density of the porous medium,  $n$  is the porosity, and  $S$  is the mass of the chemical constituent adsorbed on the solid portion of the porous medium per unit mass of solid.  $\partial S/\partial t$  represents the rate at which the constituent is adsorbed and  $(\rho_b/n) (\partial S/\partial t)$  represents the change in concentration of the fluid by adsorption or desorption (Freeze and Cherry, 1979). Adsorption reactions for contaminant groundwater are thought to be rapid relative to the flow velocity of the groundwater. Interactions of the solute in the subsurface can occur between the solute and solid material as well as the solute and colloidal particles. An opposition can occur between adsorption of the solid matrix and adsorption on the colloidal particles which leads to enhanced transportation (Van Der Zee and Leijnse, 2013).

## REFERENCES

- American Beech. (2002). Retrieved from  
<https://www.psu.edu/dept/nkbiology/naturetrail/speciespages/beechn.htm>
- Beckman, J. D., & Williamson, A. K. (1990). Salt-dome locations in the Gulf Coastal Plain, South-Central United States. *U.S. Geological Survey*,1-44.  
doi:10.3133/wri904060
- Berg, R. R. (1984). The Cretaceous-Tertiary Boundary and Lower Tertiary of the Brazos River Valley. *Stratigraphy of the Claiborne Group*,10-16.
- Boghici, R. (2009). Water Quality in the Carrizo-Wilcox Aquifer, 1990–2006. *Texas Water Development Board*,1-33.
- Deussen, A., 1924, Geology of the Coastal Plain of Texas west of Brazos River: U.S. Geol. Survey Prof. Paper 126, p. 145.
- Dipole-Dipole Array: Electrical Resistivity Methods, Part 3. (2018, August 02). Retrieved from <https://www.agiusa.com/dipole-dipole-array>
- Dumble, E. T., 1918, The Geology of East Texas: Univ. Texas Bull. 1869, p. 388.  
1924, A revision of the Texas Tertiary section with special reference to the oil-well geology of the coast region: Am. Assoc. Petroleum Geologists Bull., v. 8, p. 424—444

- Eargle, H. (1968). Nomenclature of formations of Claiborne Group, middle Eocene, Coastal Plain of Texas. *Geological Survey Bulletin*, 1251(D), 1-25.
- Ewing, T. E., 2003, Upper Cretaceous (post-Edwards) stratigraphic framework of the Maverick / Rio Escondido Basin, Southwest Texas and Coahuila—A progress report, in Structure and stratigraphy of South Texas and northeast Ewing 266 Mexico: Applications to exploration: Gulf Coast Section of the Society of Economic Paleontologists and Mineralogists Foundation (Houston, Texas) and South Texas Geological Society (San Antonio), p. 122-141.
- Ewing, T. E., 2009, The Ups and Downs of the Sabine Uplift and the Northern Gulf of Mexico Basin: Jurassic basement blocks, Cretaceous thermal uplifts, and Cenozoic flexure: Gulf Coast Association of Geological Societies Transactions, v. 59, p. 253-269.
- Farjon, A. 2013. *Juniperus virginiana*. The IUCN Red List of Threatened Species 2013: e.T42257A2967510. <http://dx.doi.org/10.2305/IUCN.UK.2013-1.RLTS.T42257A2967510.en>. Downloaded on 19 December 2018.
- Ferrill, D.A., and Morris, A.P., 2008, Fault Zone Deformation Controlled by Carbonate Mechanical Stratigraphy, Balcones Fault System, Texas: American Association of Petroleum Geologists Bulletin, v. 92, no. 3, pp. 359-380

Fetter, C. W. (2004). Applied hydrogeology (Fourth ed.). Long Grove, IL:  
Waveland Press.

Fetter C.W. (2018) Contaminant Hydrogeology. 500 pp. Upper Saddle River, NJ:  
Prentice-Hall.

Freeze R.A. and Cherry J.A. (1979) Groundwater. 604 pp. Englewood Cliffs, NJ:  
Prentice-Hall.

Fisher, W.L., 1964, Sedimentary Patterns in Eocene Cyclic Deposits, Northern  
Gulf Coast Region, Bureau of Economic Geology, Austin, Texas,  
<http://www.kgs.ku.edu/Publications/Bulletins/169/Fisher>.

Fisher, W. L., 1969, Facies Characterization of Gulf Coast Basin Delta Systems,  
with some Holocene Analogues: Gulf Coast Assoc. Geol. Socs., Trans., v.  
19, p. 239— 261.

Forestar, 2011, Map, East Texas Basin,  
[http://www.forestargroup.com/assets/minerals/FORE\\_EastTx.pdf](http://www.forestargroup.com/assets/minerals/FORE_EastTx.pdf)

Grant, B. (2018). Water Oak Tree Care: Growing Water Oak Trees In The  
Landscape. Retrieved from  
<https://www.gardeningknowhow.com/ornamental/trees/oak/water-oak-tree-care.htm>

Hosman, R. L. (1991). Regional Stratigraphy and Subsurface Geology of Cenozoic Deposits, Gulf Coastal Plain, South-central United States. *U.S Department of Interior*,1-43.

Hosman, R.L. and Weiss, J.S., 1991, Geohydrologic units of the Mississippi Embayment and Texas Coastal Uplands Aquifer Systems, South-Central United States –Regional aquifer system analysis-G

How Does Water Move through the Ground? (n.d.). Retrieved from [https://www.classzone.com/books/earth\\_science/terc/content/investigations/es1401/es1401page04.cfm](https://www.classzone.com/books/earth_science/terc/content/investigations/es1401/es1401page04.cfm)

Jobe, K., Ledger, E., Sharp, P., & Crocker, M. (1993). Radiostratigraphy and Heavy Mineral Content of the Weches Formation (Eocene), Nacogdoches County, Texas. *AAPG Bulletin*,77.

Kennedy, W., 1892, Geol. Survey of Texas, 3rd Ann. Rept. p. 52 and 105.

Kreitler, C.W., 1979, Ground water hydrology of depositional systems, in Galloway, W.E., and others, Depositional and ground water flow systems in the exploration for uranium, a research colloquium: The University of Texas at Austin, Bureau of Economic Geology, p. 118–176.

- Krutak, P. R., & Kimbrell, W. C. (1991). Sparta B Sandstones (Eocene), Fordoche Field, Pointe Coupee Parish, Louisiana-A Compartmentalized, Barrier-Island Oil and Gas Reservoir. *AAPG Bulletin*, 75, 383-404.
- Owen, John, 1889, Report of geologists for southern Texas: Texas Geological Survey Progress Report 1, p. 69-74.
- Ricoy, J. U., & Brown, L., Jr. (1977). Depositional Systems in Sparta Formation (Eocene), Gulf Coast Basin of Texas: ABSTRACT. *AAPG Bulletin*, 61, 139-154. doi:10.1306/c1ea4667-16c9-11d7-8645000102c1865d
- Rose, P. R. (2016). *Late Cretaceous and Tertiary Burial History, Central Texas* Gulf Coast Association of Geological Societies, 5, 141-179.
- Schulze-Makuch, D. (2009). Advection, Dispersion, Sorption, Degradation, Attenuation. In *Groundwater* (Vol. II). Oxford: Eolss.
- Sellards, E. H., Adkins, W. S., and Plume mer, F. B., 1932a, Geology of Texas, University of Texas Bulletin, v. 1, p. 635-651., 1932b, Geology of Texas: University of Texas Bulletin 3232, v. 1, p. 528.
- Stenzel, H. B., 1935, A New Formation in the Claiborne Group: Univ. Texas Bull. 3501, p. 267—279.

Stenzel, H. B., 1938, The geology of Leon County, Texas: Texas Univ. Pub.

3818, 295 p. 1940, The Yegua problem: Texas Univ. Pub. 3945, p. 847-910.

Texas Ecoregions. (2017, July 31). Retrieved from

<https://tpwd.texas.gov/education/hunter-education/online-course/wildlife-conservation/texas-ecoregions>

Thomas, E. H. 1980. The New York Botanical Garden illustrated encyclopedia of horticulture. Garland STPM Press, New York, New York.

Thorkildsen, D. and Price, R.D. (1991). Ground-water resources of the Carrizo-Wilcox Aquifer in the Central Texas Region. Austin: Texas Water Development Board, Report #332.

Transpiration - The Water Cycle. (2016, December 02). Retrieved from

<https://water.usgs.gov/edu/watercycletranspiration.html>

Trees of Texas. (2018). Retrieved from

<http://texastreeid.tamu.edu/content/TreeDetails/?id=60&t=R>

TWDB Water Use Survey,

<http://www.twdb.state.tx.us/wushistorical/DesktopDefault.aspx?PageID=2>.

Urbatsch, L. (n.d.). CHINESE PRIVET. *United States Department of Agriculture*, 1-5.

Van Der Zee, S., & Leijnse, A. (2013). Solute Transport in Soil. *Soil Processes and Current Trends in Quality Assessment*,33-86.

Water Oak. (n.d.). Retrieved from

<https://www.arboday.org/trees/treeguide/TreeDetail.cfm?ItemID=1085>

Waters, P. W. McFarland, and J. W. Lea, 1955, Geologic Framework of Gulf Coastal Plain of Texas, Bulletin, A.A.P.G. Vol . 39. NO. 9 (September, 1955). PP. 1821-1850.

Watkins, J. (2018) Mercury in Big Cypress Bayou and Caddo Lake watersheds in Marion and Harrison Counties Texas (unpublished master's thesis).

Stephen F. Austin State University, Nacogdoches, Texas.

Wendlandt, E. A., and Knebel, G. M., 1926, Lower Claiborne of East Texas, with Special Reference to Mount Sylvan Dome and Salt Movements: Am.

Assoc. Petroleum Geologists Bull., v. 13, p. 1347— 1375.

## APPENDIX (B) METHODOLOGY

## Methodology

Electrical resistivity data for this survey was collected using a SuperSting R8 WIFI RES/IP/SP produced by *Advanced Geosciences Inc.* All resistivity data was collected along three survey lines within Nacogdoches County, TX. The SuperSting R8 WIFI RES/IP/SP is an eight-channel resistivity meter capable of collecting eight individual readings simultaneously (AGI). All three lines were surveyed using a dipole-dipole array with 56 electrodes per line with at a one-meter electrode spacing. The one-meter electrode spacing was chosen due to the capability to examine the subsurface at depths below the suspected level of the local water table, as well as producing high resolution of the subsurface in which the solute plume's movement and migration pathways could be more accurately tracked.

### **Command File**

Command files created in *Advanced Geosciences Inc's.* Administrative software instructs the SuperSting R8 WIFI RES/IP/SP on how to perform the resistivity survey (**Figure B 1**). 2-D command files are manually manipulated by the user to fit the desired parameters of the survey. Once created on a P.C. the command file can be downloaded onto the instrument via data cable. The command file contains pertinent information such as number of electrodes in use, array type

and the option to set the max separation as well as max dipole based on the desired array. For this study 56 electrodes were utilized for each of the three survey lines in a dipole-dipole array configuration. The *Advanced Geosciences Inc.* instruction manual recommends using a max separation of 8 and a max dipole of 6 with a survey set to be performed as a dipole-dipole array (AGI, 2016).

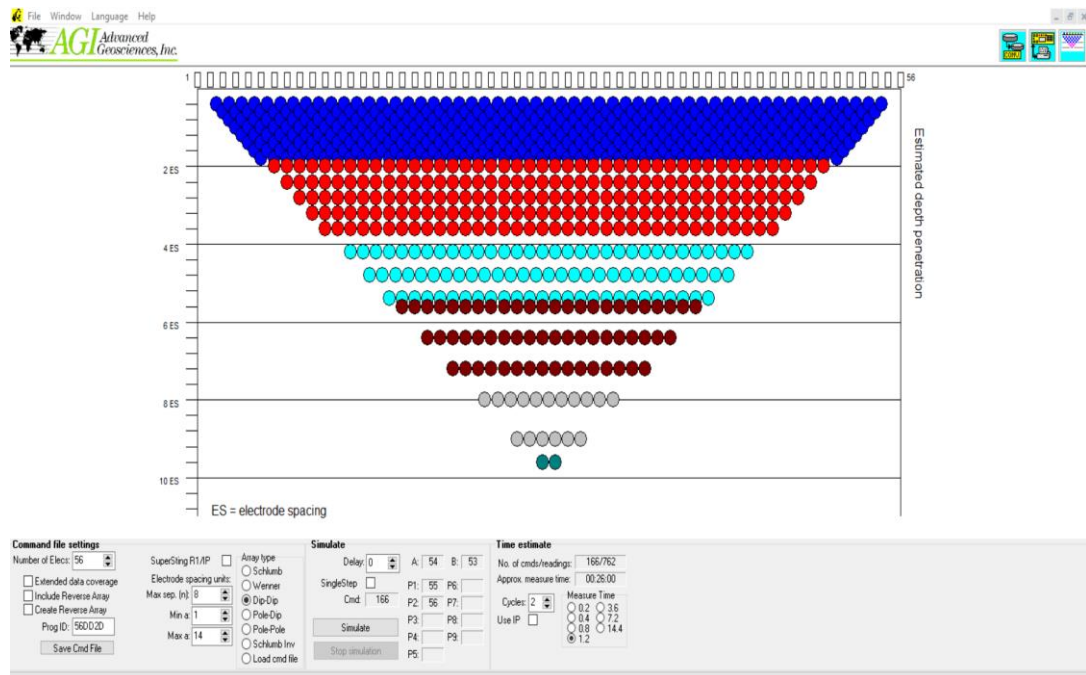


**Figure B 1.** Screen shot of the command file which is uploaded directly to the SuperSting R8 WIFI RES/IP/SP instrument. The purpose of the command file is to instruct the instrument on the parameters of the survey. All survey lines had the number of electrodes set to 56 and the array type set to a dipole-dipole array. All other parameters were set to default.

### ***Data Acquisition***

Survey lengths were determined based on the estimated depth of the groundwater system, 56 electrode long survey lines penetrated to a depth below the estimated ground water system while providing high resolution data. Survey lines were positioned around three preinstalled piezometers and measured using an open real measuring tape (***Figure B 2***). Once survey lines were measured, stainless steel stakes were hammered into the ground at one-meter intervals. Line 1 was located fourteen meters northwest of piezometer one, line two was located fourteen meters west and line three located fourteen meters north. All three lines intersected at their forty third electrode (***Figure B 3***).

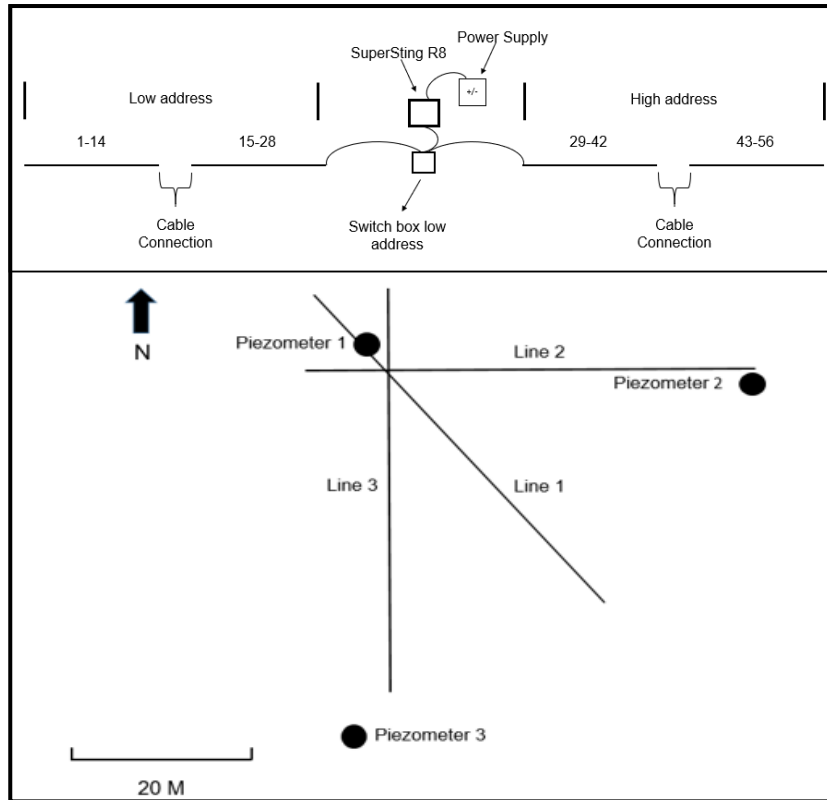


**Figure B 2.** (A) Diagram representing the arrangement of each survey line. The low address is composed of two cables (1-14;15-28) connected to the low address switchbox, while the high address is composed of two cables (29-42; 43-56) connected to switch box 1-56. The switch box is then connected to the SuperSting R8 WIFI RES/IP/SP which is powered by two marine batteries. (B) Represents the spacing of the three piezometers as well as the three survey lines.



**Figure B 3.** Image of the field setup with electrodes connected to the stakes along survey line one. The flags represent the stake locations for survey line two and survey line three. Seen in the forefront of the image is piezometer one.

### **Field Setup**

Each of the three 56-meter-long survey lines is composed of four sections of cable separated into a high and low address. The low address consists of cable 1, electrodes 1-14 and cable 2, electrodes 15-28. The high address consists of cables 3, electrodes 29-43 and cable 4, electrodes 44-56. The switch

located between the 28<sup>th</sup> and 29<sup>th</sup> electrode connects the low address to the high address. Once all the cables are connected the switchbox is then connected to the SuperSting R8 WIFI RES/IP/SP, powered by two 12 V deep cycle marine batteries (**Figure B 2**). Once the instrument setup was complete contact resistance tests were conducted to ensure proper contact between the electrode of the cable and the stakes as well as the stakes and the ground. Prior to any data acquisition the contact resistance for all 56 electrodes had to be under 5k ohms with a priority towards electrodes being under 2k ohms. Electrodes that showed a contact resistance higher than desired were wetted with a heavily diluted saline solution until the contact resistance is lowered below the 5k ohm desired range. After all electrodes were below 5k ohms the survey was then conducted. The SuperSting R8 WIFI RES/IP/SP individually measured each electrode starting at the low address and concluding at the high address. Approximate survey duration for all fifty-six electrodes was thirty-three minutes.

An infiltration pit was placed between the 49<sup>th</sup> and 50<sup>th</sup> electrode northwest of piezometer 1 (**Figure B 2**). Strategically positioned in that any lateral movement of the solute plume would be recognized by survey line 2 or 3. The infiltration pit was dug deep enough that the solute solution would not affect the root system of the grass growing nearby, to the dimensions of 1 meter in length, .75 meters in width and .33 meters in depth (**Figure B 4**).



**Figure B 4.** Infiltration pit dug between the 49<sup>th</sup> and 50<sup>th</sup> electrode along survey line one.

### ***Data Processing***

Electrical Resistivity data collected on the SuperSting R8 WIFI RES/IP/SP was uploaded to a PC in the field directly from the instrument using the AGI SuperSting Administrator software. The data was then stored on an external memory drive as an .stg file and processed in *EarthImager 2D* a product of Advanced Geosciences, Inc. Terrain corrections were applied to each of the

survey lines to accurately represent the elevation changes of the survey site. All data was inverted using the surface setting in the EarthImager software with the Robust Inversion method (**Figure B 5**). To ensure each inverted resistivity section was fully processed the max RMS error and error reduction percentage were unchecked and turned off (**Figure B 6**). Unique color and contour properties were created for this survey (**Figure B 7**). In adjusting the levels within the contour tab to different maximum ohm cutoffs the inverted lines would look smoother. Allowing for the solute plume to be picked out easier within the subsurface.

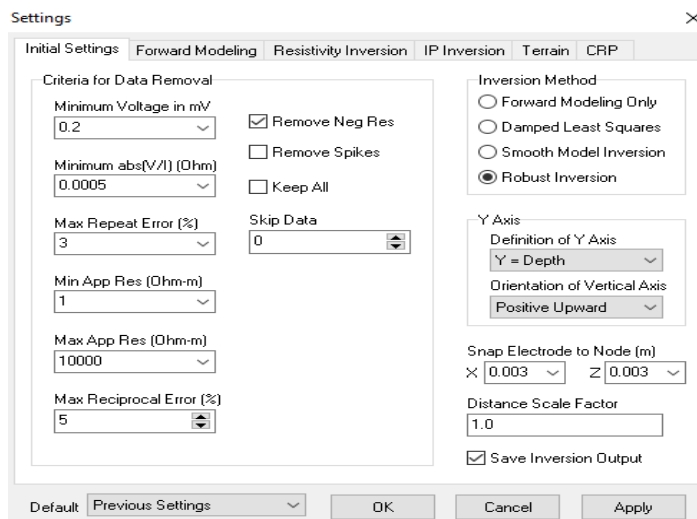


**Figure B 5.** Screenshot of the initial settings for all line survey lines. All settings are set to the default surface settings with the exception of the Robust Inversion Method. Default surface settings select a Smooth Model Inversion however, for this survey the Robust Inversion proved to provide a higher quality inversion section (Image was created in AGI's EarthImager 2D, 2016).

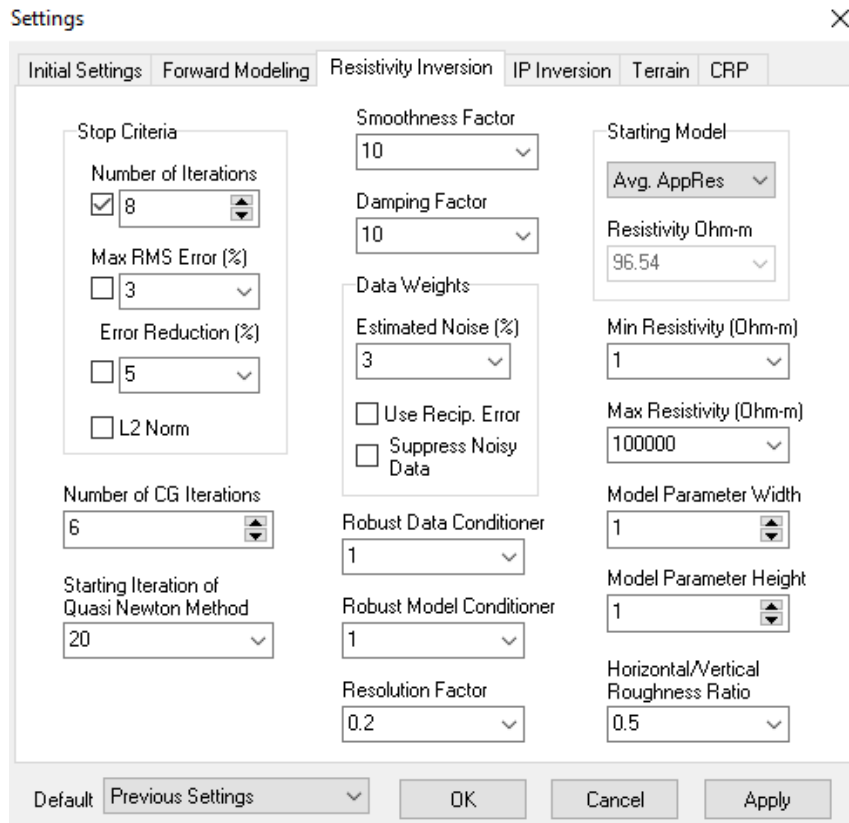


**Figure B 6.** Screenshot of the Resistivity Inversion settings for all survey lines. All settings are default surface settings with the exception of the Max RMS Error (%) and the Error Reduction (%) stop criteria being unselected. This allows for the inversions to be processed fully to their eighth iteration (Image was created in AGI's EarthImager 2D, 2016).

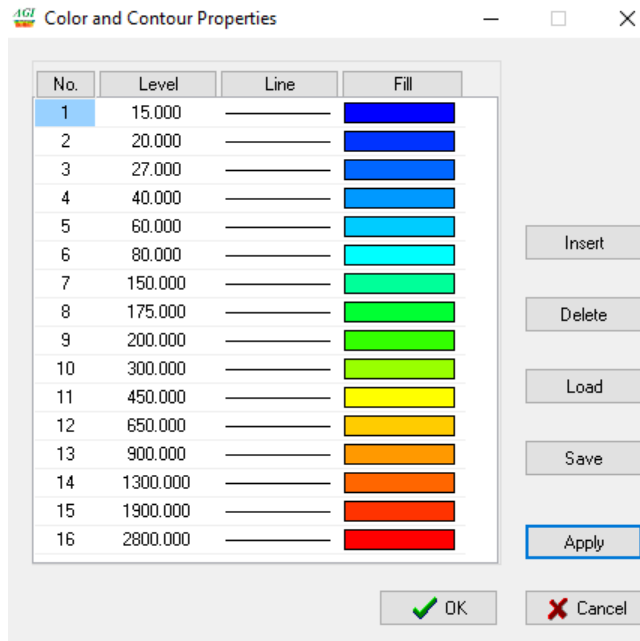


**Figure B 7.** Screenshot of the Color and Contour Properties used for all survey lines within this study. These properties are not default and were generated in order to show the highest contrast within the survey lines. The level tab represents the ohm meter cutoff at each of the sixteen numbers (Image was created in AGI’s EarthImager 2D, 2016).

### **Data Misfit**

Poorly fitted data points (outliers) can be removed within *EarthImager 2D* allowing for an improved resistivity model to be produced. Noisy data points are represented by a high root-mean squared (RMS) error. Poorly fitted data for this survey was removed manually through the utilizing of a *Data Misfit Histogram*, a

histogram available after the first inversion of the resistivity line has been completed (**Figure B 8**). Data was removed in small increments at a time ranging from one to three percent. No more than 20% of the total data was removed from a survey line. To ensure the accuracy of the inverted resistivity lines a data misfit cross plot was generated, plotting the measured resistivity data versus the apparent resistivity (**Figure B 9**). The data misfit cross plot just like the data misfit histogram is available after the first inversion of the resistivity line.

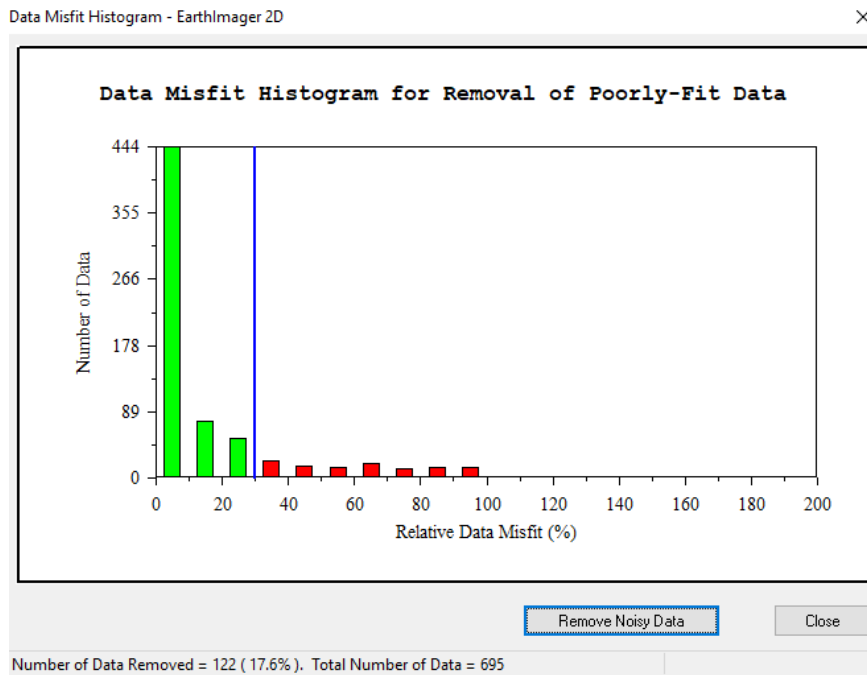


**Figure B 8.** Screenshot of the Data Misfit Histogram designed to remove poorly fitted (noisy data) from the survey lines. Data highlighted in green to the left of the blue line will be preserved while data highlighted in red to the right of the blue line will be deleted when the Remove Noisy Data button is selected. Data selection is made by moving the blue line on the histogram with the right and left arrow keys on the keyboard. The percentage of noisy data that will be removed at a given point is displayed in the bottom left hand corner (Image was created in AGI's EarthImager 2D, 2016).

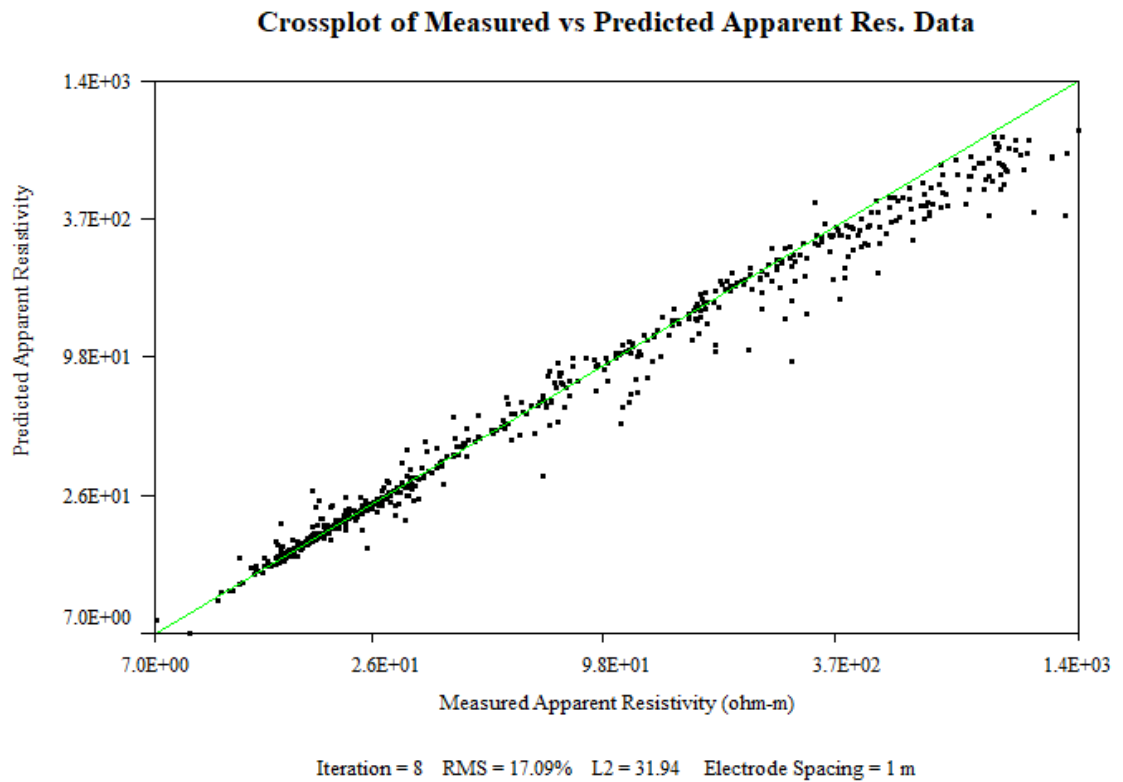
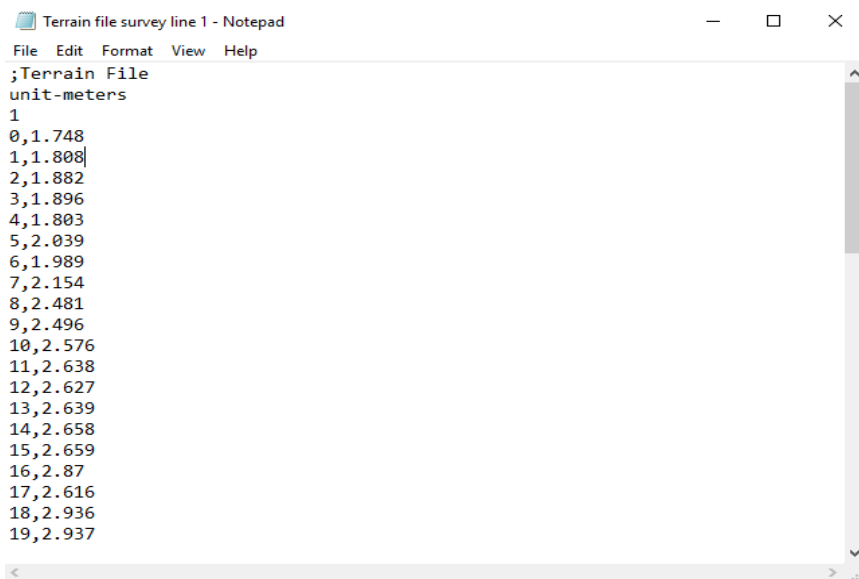


**Figure B 9.** Screenshot of the data misfit cross-plot. The x-axis is represented by the measured apparent resistivity, while the y-axis is represented by the predicted apparent resistivity (Image was created in AGI's EarthImager 2D, 2016).

## **Terrain Corrections**

In order to more accurately represent the electrical resistivity data and track the migration of the solute plume a terrain file was applied to survey line 1. Elevation data was acquired at each of the fifty-six electrodes using a laser distance measure in conjunction with leveling tools. The elevations found were then displayed within Notepad and converted to a terrain file (**Figure B 10**).



```
 Terrain file survey line 1 - Notepad
File Edit Format View Help
;Terrain File
unit-meters
1
0,1.748
1,1.808
2,1.882
3,1.896
4,1.803
5,2.039
6,1.989
7,2.154
8,2.481
9,2.496
10,2.576
11,2.638
12,2.627
13,2.639
14,2.658
15,2.659
16,2.87
17,2.616
18,2.936
19,2.937
```

**Figure B 10.** Terrain file used for survey line one. Elevation data was collected using a laser measuring tape as well as a leveling tool and then imported into Notepad. The elevation data is displayed to the right of the correlation electrode.

### ***Slug Test***

Slug tests were conducted on each of the three previously installed piezometers using the Solinst Levelogger. Three different measurements were conducted on each of the wells, data was recorded on the loggers. The Solinst Leveloggers were launched and positioned into the piezometers forty-five minutes prior to the addition of the first non-saline water sample in order to calibrate to the water pressure of each of the piezometers. The three-sample consisted of non-saline water in volumes of 0.5 L, 1.0 L and 2.0 L. Each Solinst Levelogger was left to recalibrate to normal for two hours after the addition of each water sample. The slug tests were conducted in order from the smallest volume to the largest to allow for equilibrium within the piezometers to be regained.

### ***Infiltration test***

Three infiltration tests were conducted along survey line 1. The tests were conducted adjacent to electrode 52, 28 and 4. Each infiltration test consisted of three infiltration rings as shown in **Figure B 11**, the average infiltration across the three rings was recorded for each test site. The infiltration rings were hammered into the ground using a steal plate and sledgehammer until the ring was buried five centimeters into the soil to ensure water did not seep out of the bottom. Infiltration rings were then filled with water and allowed fifteen minutes to adjust.

After the fifteen minutes the infiltration rings were refilled, and the water height was measured to begin the survey. The water level within the rings was measured at fifteen-minute intervals for one hour. At the completion of one hour, the infiltration rings were relocated to the next test site and the process was repeated.



**Figure B 11.** *Three infiltration rings used to conduct the infiltration test at three locations along survey line one. At each of the three locations, three infiltration rings were used and the average rate of infiltration among the three rings was calculated.*

## **Soil Sampling**

Three 1.5-meter-deep cores were collected and sampled from the same three locations along survey line one as the infiltration tests were conducted. The soil from the core was segregated at ten-centimeter intervals and bagged (**Figure B 12**). Once collected the soil samples transported to the laboratory for analyses. In addition, soil samples collected during the drilling of the piezometers were also analyzed.



**Figure B 12.** 1.5-meter auger used to collect the three soil cores along survey line one. The samples were collected in ten-centimeter increments and placed in zip lock bags.

## ***Soil Analysis***

Once in the laboratory, the still saturated soils were weighed out to between 100 and 200 grams and placed in a curing oven at 105°C and left to dry overnight. The soil samples were weighed daily until the samples had identical weights for three consecutive days. Once the drying was completed the unsaturated soil samples were crushed with a hammer and weighed and separated into fifty-gram portions. The fifty grams of soil sample was added to solution composed of fifteen milliliters of 10% sodium hexametaphosphate solution and left to settle for twenty-four hours. Sodium hexametaphosphate acts as a dispersing agent that separates clays within the soil samples. Post rest the solution was blended for ten minutes in which the grains become suspended. The mixed solution was then added to a graduated cylinder with 1000 milliliters tap water, at that time measurements were taken on each sample at forty seconds, two hours and twelve hours using a hydrometer (***Figure B 13***).

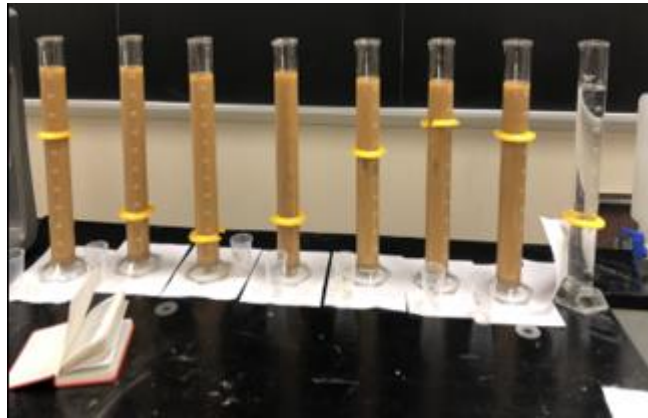


**Figure B 13.** Image showing the graduate cylinders used to conduct the hydrometer survey. Samples were surveyed in groups of seven with a test cylinder that contained the same 1000 mL of water and fifteen mL of sodium hexametaphosphate. Hydrometer recordings were conducted at three different time intervals.

### **Particle Size Analysis**

Calculations for the particle size analysis were conducted at ten-centimeter intervals across the three 1.5-meter-deep cored soil sections as well as the three cores obtained through the instillation of the piezometers. The eight hydrometers were placed in their perspective cylinders, seven with soil samples and one blank. Readings were taken from the meniscus of the hydrometers at the three specified time intervals: forty seconds, two hours and twelve hours. At the completion of the twelfth hour the soil samples were discarded, and the hydrometers were cleaned before beginning the next set of samples.

The first measurement of the hydrometers conducted at the forty second interval was used to calculate the percent of sand sized particles out of suspension. At this time the smaller clay and silt sized grains were still in suspension. The readings collected at the two-hour mark represent a partial settling of silt sized grains, not all grains classified as silt sized had yet fallen out of suspension and they would not do so until the twelve hours had elapsed. At the twelve-hour mark sand and silt sized grains had completely fallen out of suspension leaving only clay sized particles, again the hydrometer was measured at the meniscus. Equations were applied to the readings calculated at the forty second and twelve-hour mark generating the percentages of sand and clay, respectively. Then the clay and sand percentages were added together and subtracted from 100 to produce the percentage of silt. Corrections were applied to the resulting hydrometer readings in order to accurately calculate grain size percentages.

Three corrections were applied to each sample during the duration of the particle size analysis test, those corrections were: temperature correction, hydrometer correction and a double hydrometer correction. Eight hydrometers were used to conduct the test. Each hydrometer has slight variances due to the manufacturing process; these variances alter the readings gained from each particular hydrometer slightly. In order to accurately calculate the particle size of samples and normalize the hydrometers the two hydrometer corrections were

applied to each of the hydrometers. Each hydrometer was numbered during the duration of the test in order to accurately track the correction values associated with each of the eight hydrometers.

### ***Hydraulic Conductivity Calculations***

Using the particle size data collected from the Bouyoucos hydrometer test hydraulic conductivity was calculated for each ten-centimeter interval of soil core based on Shepherd (1990) in which the hydraulic conductivity is related to grain size. Grain size was represented using a grain size distribution chart (**Figure B 14**) in which values obtained from the Bouyoucos Hydrometer test were inputted and the distribution curve was exploited.

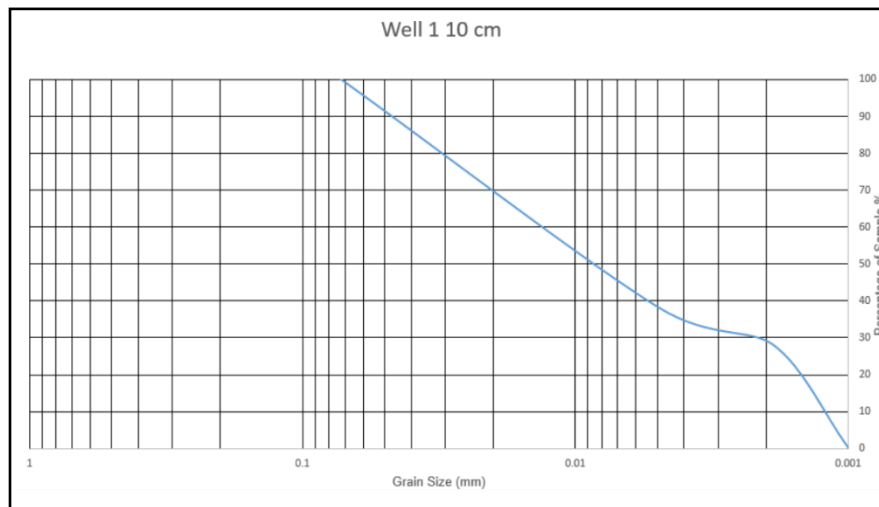


**Figure B 14.** Grain size distribution curve plotting grain size vs percentage sample for a ten-centimeter increment of soil core.

### ***Soil Descriptions***

Soil descriptions on each of the ten-centimeter increments of core as well as the additional samples collected from the instillation of the piezometers were conducted using the ribbon method in conjunction with the Munsell Soil-Color Charts. The color descriptions were accomplished by placing a small sample of dry soil onto a white sheet of paper and comparing the samples color to the colors within the Munsell book. The ribbon test was conducted using a handful of soil placed in the palm and wetted until it could form and hold shape. After the soil was wetted it was pinched between the thumb and forefinger producing a ribbon. The soil was pinched into the ribbon until it collapsed from its own weight. Once collapsed the ribbon was measured and the resulting length of ribbon produced describes the textural property of the soil.

### ***Sodium Adsorption on Clays***

Hydraulic conductivity values fluctuate depending on the percentage of clay expanding in association with sodium, called sodium adsorption. The clay expansion directly reduces the hydraulic conductivity of the soil and effected the migration of the solute plume. Calculations were conducted using the hydraulic conductivities obtained from the Bouyoucos Hydrometer method. These calculations produced a hydraulic conductivity accounting for maximum clay swelling and the reduction in porosity.

## REFERENCES

- AGI, 2014. Instruction manual for EarthImager 2D Version 2.4.2 Resistivity and IP Inversion Software: Austin, TX, Advanced Geosciences, Inc. 29-32p.
- AGI, 2016. Instruction manual for The SuperSting™ with Wi-Fi Automatic Resistivity and IP Systems: Austin, TX, Advanced Geosciences, Inc. 29-32p.
- Shepherd, R. G. (1990). "Correlations of Permeability and Grain Size". *Ground Water*, 28(1), 116-116.

## APPENDIX (C) RESULTS

Hydraulic Conductivity					
Sample (cm)	Hydraulic Conductivity (cm/s)	Sample (cm)	Hydraulic Conductivity (cm/s)	Sample (cm)	Hydraulic Conductivity (cm/s)
C1-10	1.56E-04	C2-10	1.26E-04	C3-10	2.62E-05
C1-20	9.95E-05	C2-20	1.69E-04	C3-20	7.22E-05
C1-30	3.00E-05	C2-30	9.98E-05	C3-30	1.22E-04
C1-40	4.76E-05	C2-40	9.86E-05	C3-40	1.30E-04
C1-50	6.00E-05	C2-50	2.42E-04	C3-50	1.24E-04
C1-60	6.26E-05	C2-60	1.93E-04	C3-60	1.05E-04
C1-70	5.24E-05	C2-70	2.67E-04	C3-70	1.11E-04
C1-80	1.74E-04	C2-80	1.11E-04	C3-80	1.33E-04
C1-90	1.64E-04	C2-90	1.95E-04	C3-90	1.52E-04
C1-100	6.33E-05	C2-100	2.29E-04	C3-100	1.30E-04
C1-110	1.31E-04	C2-110	4.87E-04	C3-110	1.15E-04
C1-120	1.13E-04	C2-120	3.12E-04	C3-120	1.14E-04
C1-130	3.81E-05	C2-130	2.11E-04	C3-130	2.27E-04
C1-140	1.08E-04	C2-140	2.32E-04	C3-140	1.41E-04
C1-150	2.12E-04	C2-150	3.03E-04	C3-150	1.52E-04
<b>Average (cm/s)</b>	1.01E-04		2.18E-04		1.24E-04

Figure C 1. Hydraulic conductivity across the three 1.5-meter-deep soil cores.

Soil Descriptions											
Sample (cm)	Color	Classification	Sample (cm)	Color	Classification	Sample (cm)	Color	Classification	Sample (cm)	Color	Classification
P1-121.9	Brownish Yellow (6/6)	Sandy Loam	P2-91.4	Strong Brown (5/6)	Silty Clay Loam	P3-121.9	Brownish Yellow (6/6)	Sandy Clay Loam			
P1-213.4	Brownish Yellow (6/6)	Sandy Loam	P2-182.9	Red (5/8)	Silty Clay Loam	P3-243.8	Strong Brown (4/6)	Silty Clay Loam			
P1-274.3	Reddish Brown (4/4)	Sandy Loam	P2-426.7	Yellowish Brown (5/6)	Silty Clay Loam	P3-365.7	Dark Yellowish Brown (4/4)	Silty Clay Loam			
P1-365.76	Reddish Brown (4/4)	Sandy Loam	P2-457.2	Dark Yellowish Brown (4/6)	Silty Clay	P3-426.6	Yellowish Brown (5/6)	Silty Clay Loam			
P1-487.68	Brownish Yellow (6/6)	Silt Clay Loam	P2-609.6	Olive Brown (4/3)	Sandy Loam	P3-487.6	Dark Yellowish Brown (4/4)	Silty Clay			
P1-609.6	Brownish Yellow (6/6)	Silty Clay	-	-	-	P3-518.1	Dark Yellowish Brown (4/4)	Sandy Clay			
P1-655.3	Brownish Yellow (6/6)	Silty Clay	-	-	-	-	-	-			
P1-670.6	Grayish Green (5/2)	Sandy Loam	-	-	-	-	-	-			

Figure C 2. Soil descriptions for the three cores obtained through the drilling of the piezometers. Soils are described based on color and grain size.

Soil Descriptions					
Sample (cm) Color	Classification	Sample (cm) Color	Classification	Sample (cm) Color	Classification
C1-10 Dark Brown (3/2)	Sandy Loam	C2-10 Brown (4/4)	Sandy Loam	C3-10 Dark Brown (3/3)	Loamy Sand
C1-20 Yellowish Brown (5/8)	Sandy Loam	C2-20 Dark Yellowish Brown (4/4)	Sandy Loam	C3-20 Dark Yellowish Brown (4/6)	Loamy Sand
C1-30 Yellowish Brown (5/8)	Sandy Clay Loam	C2-30 Dark Yellowish Brown (4/6)	Sandy Loam	C3-30 Reddish Yellow (6/6)	Sandy Loam
C1-40 Yellowish Brown (5/8)	Sandy Clay Loam	C2-40 Brownish Yellow (6/6)	Sandy Loam	C3-40 Dark Yellowish Brown (4/6)	Loam
C1-50 Yellowish Brown (5/8)	Sandy Clay Loam	C2-50 Yellowish Brown (5/6)	Sandy Loam	C3-50 Yellowish Brown (5/6)	Sandy Loam
C1-60 Yellowish Brown (5/8)	Sandy Clay Loam	C2-60 Strong Brown (4/6)	Sandy Loam	C3-60 Dark Yellowish Brown (4/4)	Loam
C1-70 Strong Brown (5/8)	Sandy Clay Loam	C2-70 Dark Yellowish Brown (4/6)	Sandy Loam	C3-70 Reddish Yellow (6/6)	Loam
C1-80 Yellowish Brown (5/6)	Sandy Clay Loam	C2-80 Yellowish Brown (5/6)	Loam	C3-80 Yellowish Brown (5/6)	Loam
C1-90 Yellowish Red (4/6)	Sandy Clay Loam	C2-90 Yellowish Brown (5/8)	Sandy Loam	C3-90 Yellowish Brown (5/6)	Loam
C1-100 Strong Brown (5/8)	Sandy Clay Loam	C2-100 Brownish Yellow (6/8)	Sandy Loam	C3-100 Yellowish Brown (5/6)	Loam
C1-110 Strong Brown (5/6)	Sandy Clay Loam	C2-110 Strong Brown (5/8)	Sandy Loam	C3-110 Brownish Yellow (6/8)	Loam
C1-120 Yellowish Red (5/6)	Sandy Clay	C2-120 Strong Brown (5/8)	Sandy Loam	C3-120 Yellowish Brown (5/6)	Loam
C1-130 Strong Brown (5/6)	Sandy Clay	C2-130 Yellowish Brown (5/6)	Sandy Loam	C3-130 Yellowish Brown (5/6)	Sandy Loam
C1-140 Yellowish Red (4/6)	Sandy Clay Loam	C2-140 Yellowish Brown (5/6)	Sandy Loam	C3-140 Yellowish Brown (5/6)	Loam
C1-150 Yellowish Red (4/6)	Sandy Clay Loam	C2-150 Brownish Yellow (6/8)	Sandy Loam	C3-150 Brownish Yellow (6/6)	Loam

Figure C 3. Soil descriptions for the three 1.5-meter-deep cores, soils are described based on color and grain size.

Infiltration Test									
Ring A	Location 1		Location 2		Location 3		Water Level (cm)	Water Level (cm)	Water Level (cm)
	Time (minutes)	Water Level (cm)	Time (minutes)	Water Level (cm)	Time (minutes)	Water Level (cm)			
	0	10.9	0	10	0	9			
	15	10.7	15	9.8	15	8.3			
	30	10.2	30	9.7	30	7.5			
	45	10	45	9.5	45	6.5			
	60	9.8	60	9.2	60	6.2			
Ring B	Time (minutes)	Water Level (cm)	Time (minutes)	Water Level (cm)	Time (minutes)	Water Level (cm)			
	0	10.7	0	10.9	0	9.1			
	15	10.5	15	10.8	15	8.9			
	30	10.1	30	10.3	30	8.2			
	45	9.8	45	10	45	7.4			
	60	9.6	60	9.9	60	7.3			
Ring C	Time (minutes)	Water Level (cm)	Time (minutes)	Water Level (cm)	Time (minutes)	Water Level (cm)			
	0	11	0	10	0	8.3			
	15	10.9	15	9.7	15	7.9			
	30	10.8	30	9.3	30	7.4			
	45	10.6	45	9	45	6.5			
	60	10.5	60	8.9	60	5.9			
Average Rate of Infiltration (cm/s)		3.43E-04		3.52E-04		6.48E-04			

Figure C 4. Infiltration tests conducted on 02/01/2019. Three rings were sampled at each location along the survey line: electrode 4, 28, 47. The results of the three rings were then averaged to give an infiltration rate at each given position along the survey line.

Slug Test	
Piezometer #1	
0.5 Liters	1.27E-02 cm/s
1 Liter	2.53E-02 cm/s
2 Liters	2.53E-02 cm/s
Average	2.11E-02 cm/s
Piezometer #2	
0.5 Liters	8.45E-03 cm/s
1 Liter	8.45E-03 cm/s
2 Liters	1.27E-02 cm/s
Average	9.85E-03 cm/s
Piezometer #3	
0.5 Liters	1.27E-02 cm/s
1 Liter	2.53E-02 cm/s
2 Liters	1.27E-02 cm/s
Average	1.69E-02 cm/s

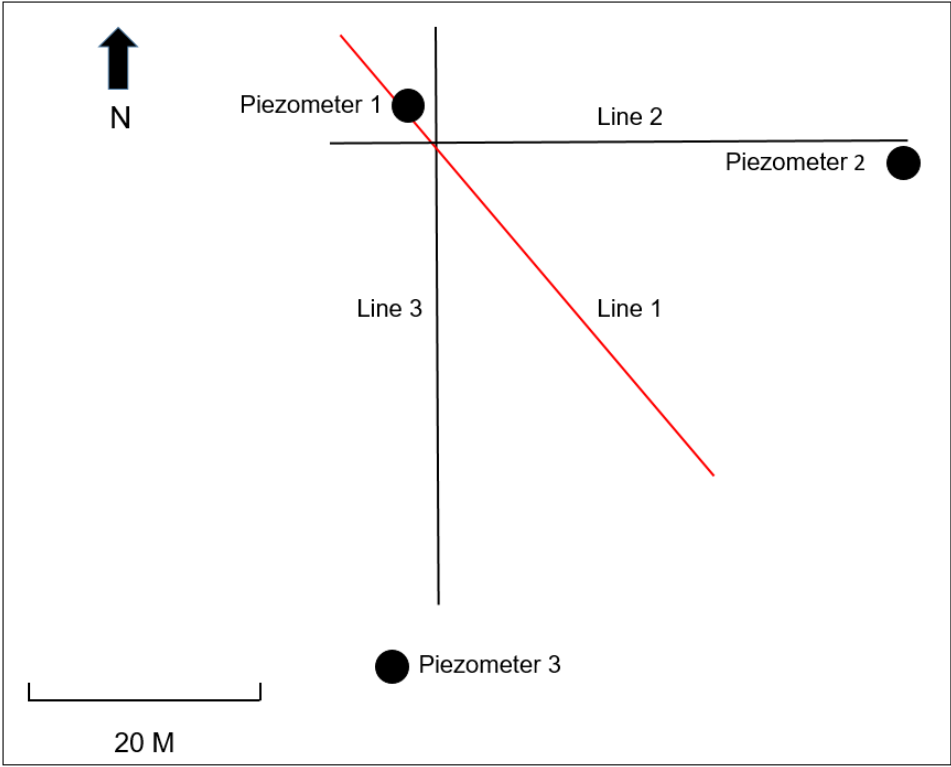
Figure C 5. Results of the slug tests conducted on each of the three piezometers.

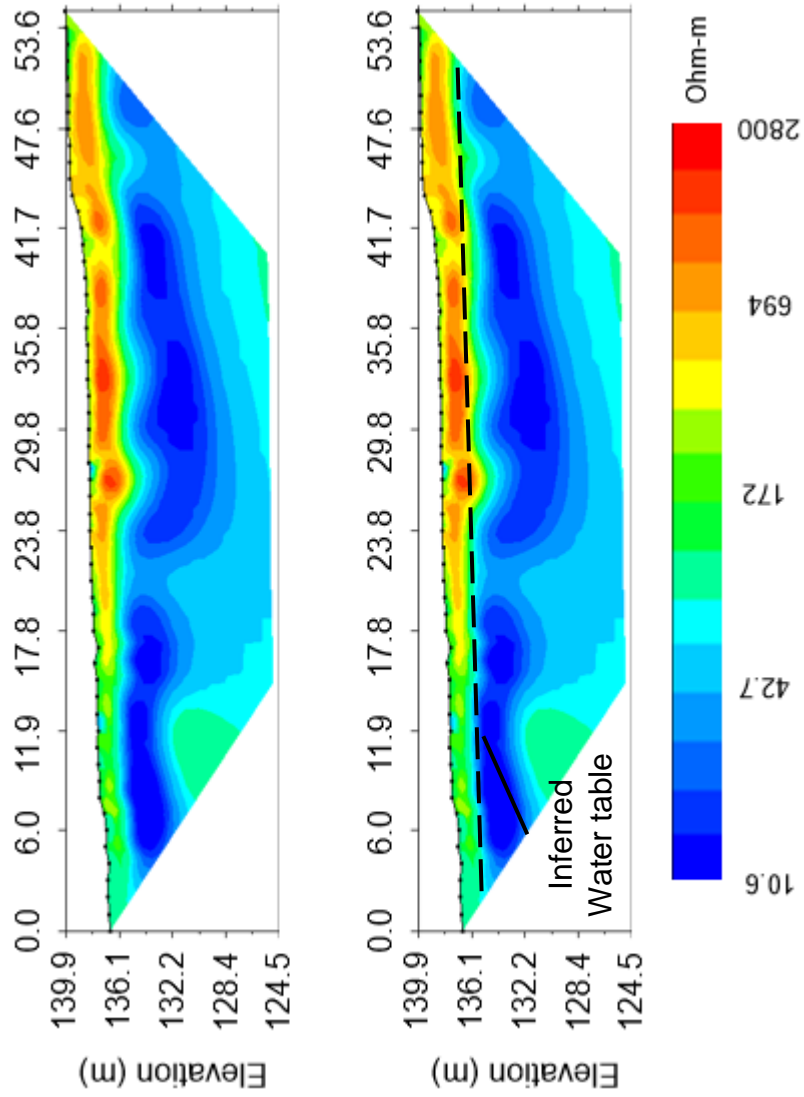
Soil Analysis: Hydrometer Method (Percentage)											
Sample (cm)	% Sand	% Silt	% Clay	Sample (cm)	% Sand	% Silt	% Clay	Sample (cm)	% Sand	% Silt	% Clay
P1-121.9	56.52	21.74	21.74	P2-91.4	58.11	21.94	19.95	P3-121.9	54.07	27.96	17.97
P1-213.4	62.00	18.00	20.00	P2-182.9	46.25	17.92	35.84	P3-243.8	49.80	22.09	28.11
P1-274.3	51.96	18.01	30.02	P2-426.7	24.44	21.87	53.69	P3-365.7	28.12	27.96	43.93
P1-365.76	36.61	17.83	45.56	P2-457.2	45.83	22.07	32.10	P3-426.6	46.35	25.83	27.82
P1-487.68	26.06	19.98	53.96	P2-609.6	66.00	26.00	8.00	P3-487.6	62.02	21.99	15.99
P1-609.6	38.55	27.75	33.70	-	-	-	-	P3-518.1	64.66	17.67	17.67
P1-655.3	63.94	22.04	14.02	-	-	-	-	-	-	-	-
P1-670.6	73.97	16.02	10.01	-	-	-	-	-	-	-	-

Figure C 6. Results demonstrating the fine grained percentages of piezometer cores.

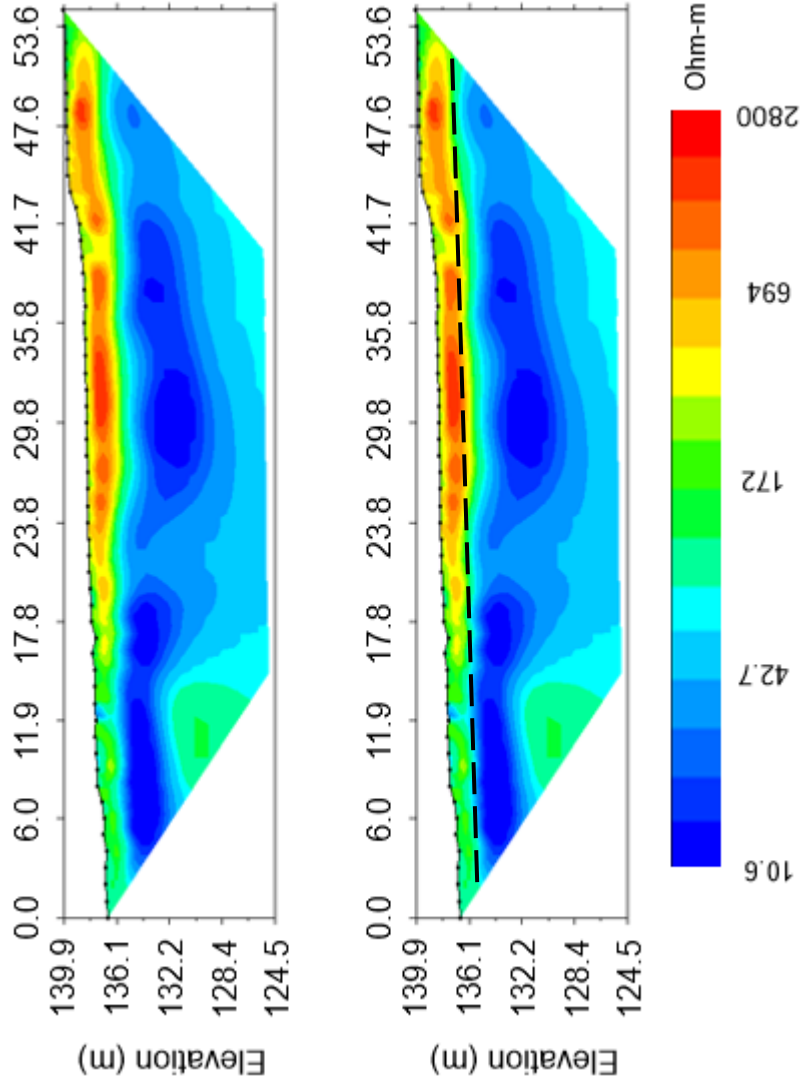
Soil Analysis: Hydrometer Method (Percentage)											
Sample (cm)	% Sand	% Silt	% Clay	Sample (cm)	% Sand	% Silt	% Clay	Sample (cm)	% Sand	% Silt	% Clay
C1-10	63.72	22.17	14.11	C2-10	68.42	25.66	5.92	C3-10	78.33	19.70	1.97
C1-20	57.79	24.12	18.09	C2-20	62.63	25.57	11.80	C3-20	82.07	15.94	1.99
C1-30	44.20	21.92	33.88	C2-30	58.75	27.50	13.75	C3-30	69.95	20.03	10.02
C1-40	49.59	20.17	30.25	C2-40	58.28	27.82	13.91	C3-40	49.82	28.10	22.08
C1-50	50.26	21.89	27.86	C2-50	59.86	22.08	18.07	C3-50	54.15	27.91	17.94
C1-60	50.65	19.74	29.61	C2-60	56.59	25.65	17.76	C3-60	48.80	27.57	23.63
C1-70	50.04	21.98	27.98	C2-70	58.72	21.62	19.66	C3-70	46.65	27.66	25.69
C1-80	58.63	13.79	27.58	C2-80	52.25	29.84	17.91	C3-80	52.54	27.68	19.77
C1-90	57.89	12.03	30.08	C2-90	55.98	24.01	20.01	C3-90	54.35	25.80	19.85
C1-100	50.85	19.66	29.49	C2-100	56.22	23.88	19.90	C3-100	51.92	28.04	20.03
C1-110	54.82	15.71	29.46	C2-110	61.58	18.20	20.22	C3-110	52.57	27.67	19.76
C1-120	52.72	11.82	35.46	C2-120	57.98	22.01	20.01	C3-120	49.81	28.11	22.08
C1-130	46.06	17.98	35.96	C2-130	56.71	23.61	19.68	C3-130	65.89	18.06	16.05
C1-140	52.82	13.76	33.42	C2-140	58.09	23.95	17.96	C3-140	48.47	29.73	21.80
C1-150	61.90	10.03	28.07	C2-150	58.78	21.59	19.63	C3-150	46.90	25.57	27.53

Figure C 7. Results demonstrating the fine grained percentages of three 1.5-meter-deep soil cores.



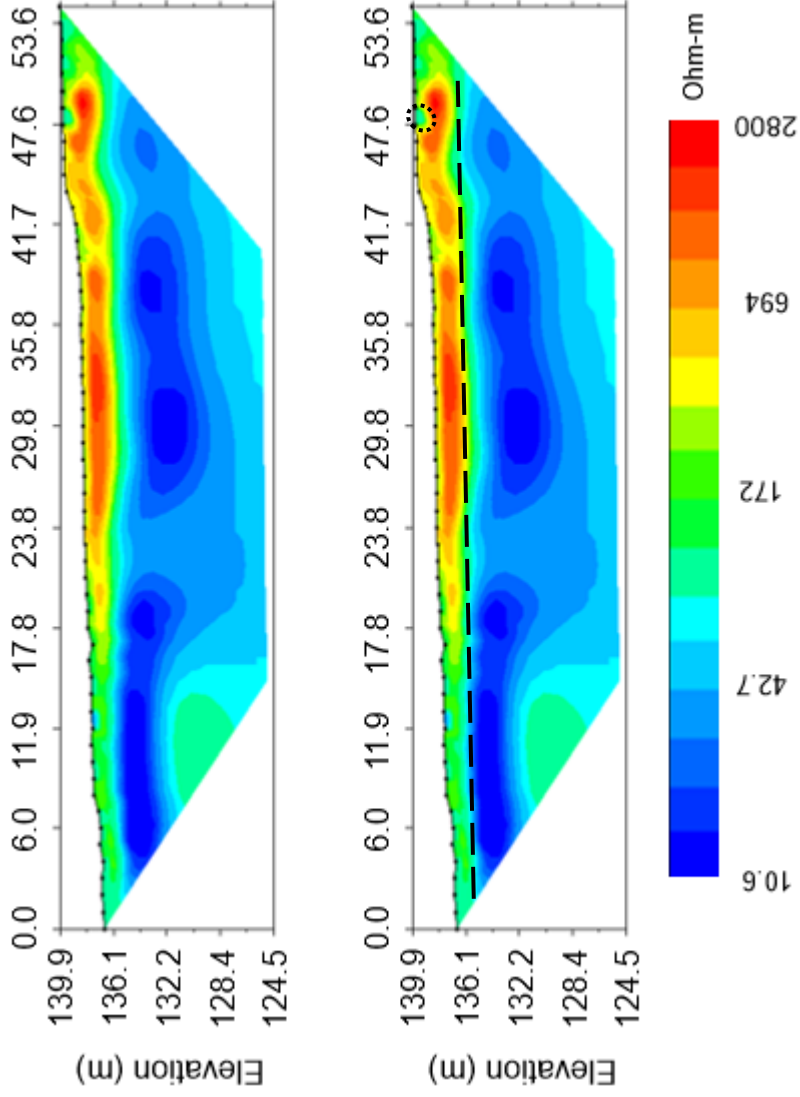


**Figure C 8.** Survey line 1. 56 electrodes spaced one-meter apart in a dipole-dipole array configuration. Surveyed 7/20/2018



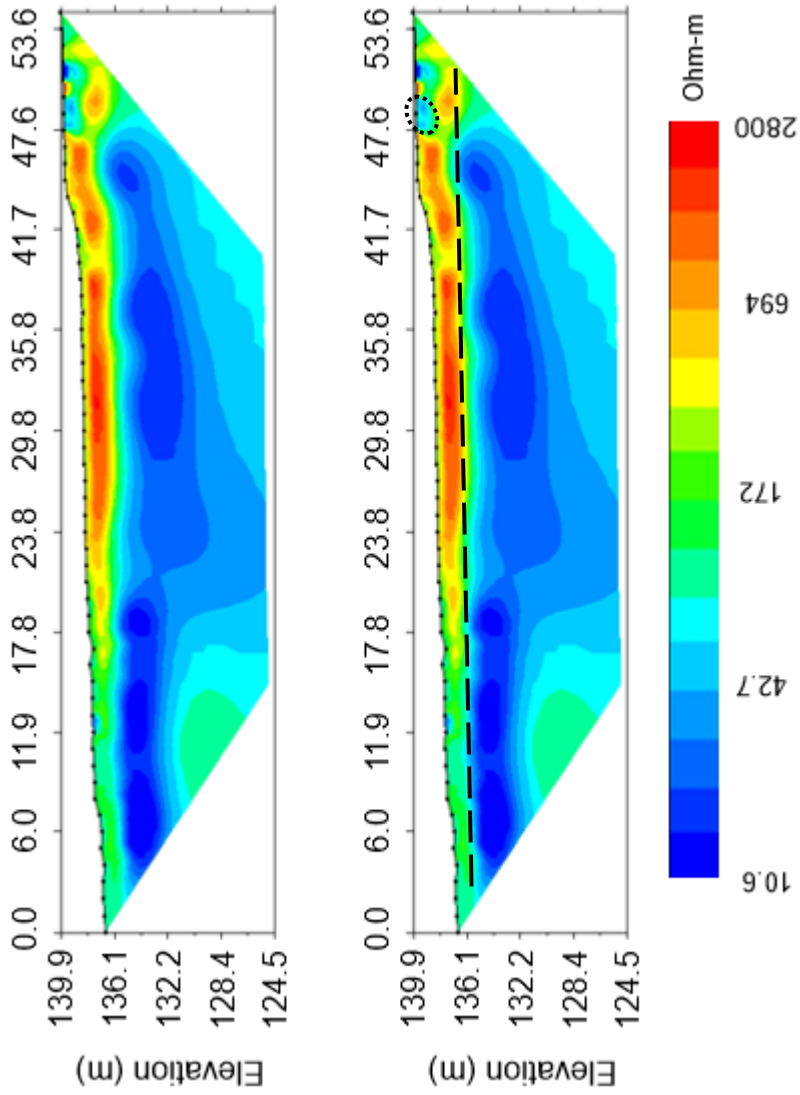
**Figure C 9.** Survey line 1. 56 electrodes spaced one-meter apart in a dipole-dipole array configuration. Surveyed 7/22/2018

**Inverted Resistivity Section Iteration=8 RMS=11.78% L2=15.02  
Electrode Spacing 1m**



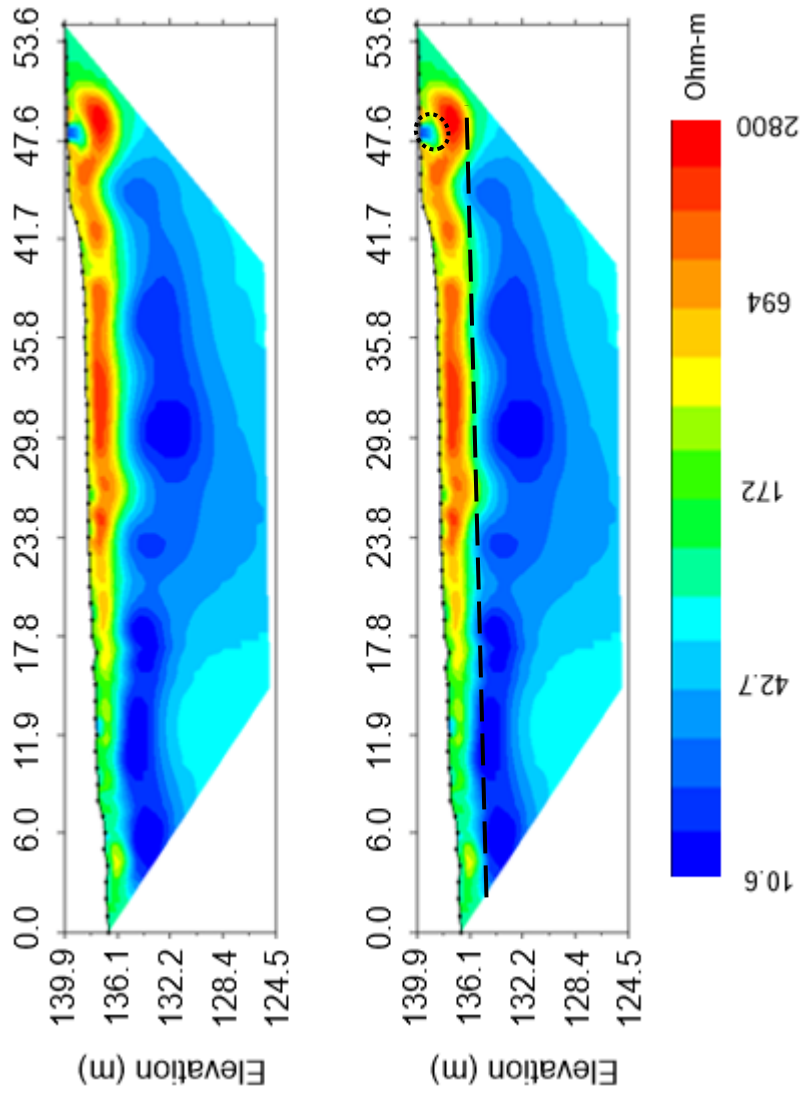
**Figure C 10.** Survey line 1. 56 electrodes spaced one-meter apart in a dipole-dipole array configuration. Surveyed 7/24/2018

**Inverted Resistivity Section Iteration=8 RMS=9.69% L2=10.04  
Electrode Spacing 1m**



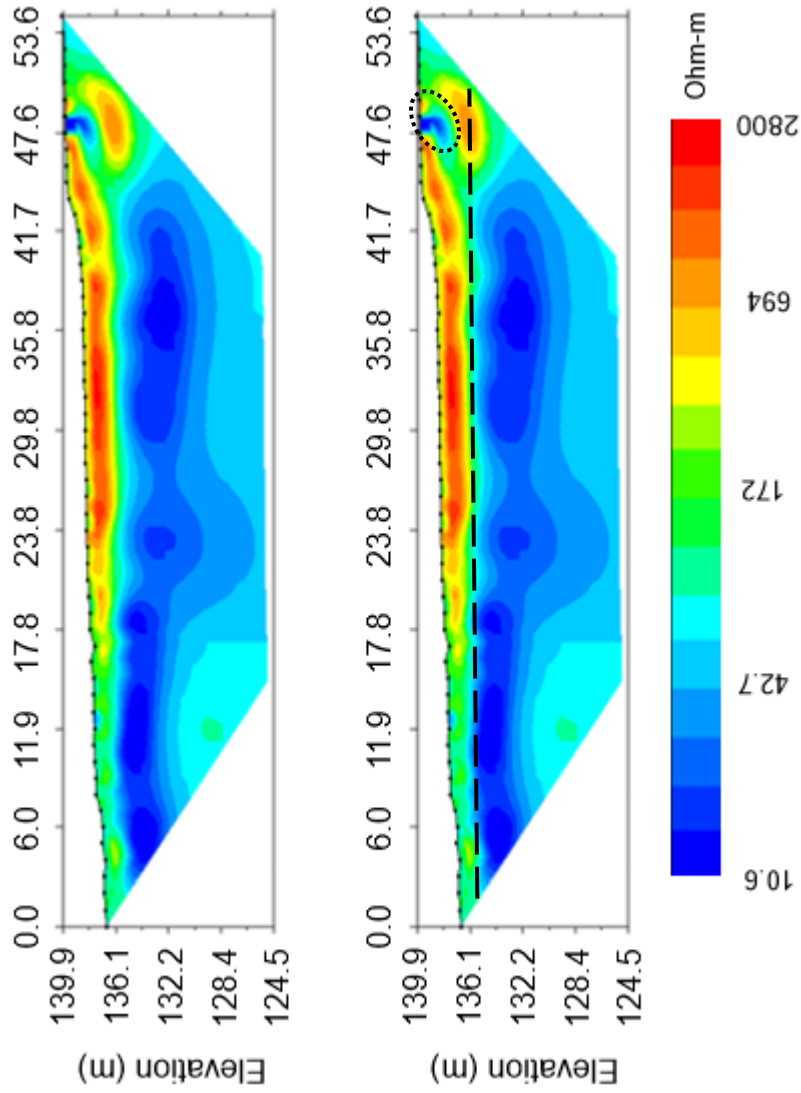
**Figure C 11.** Survey line 1. 56 electrodes spaced one-meter apart in a dipole-dipole array configuration. Surveyed 7/26/2018

**Inverted Resistivity Section Iteration=8 RMS=7.49% L2=5.98  
Electrode Spacing 1m**

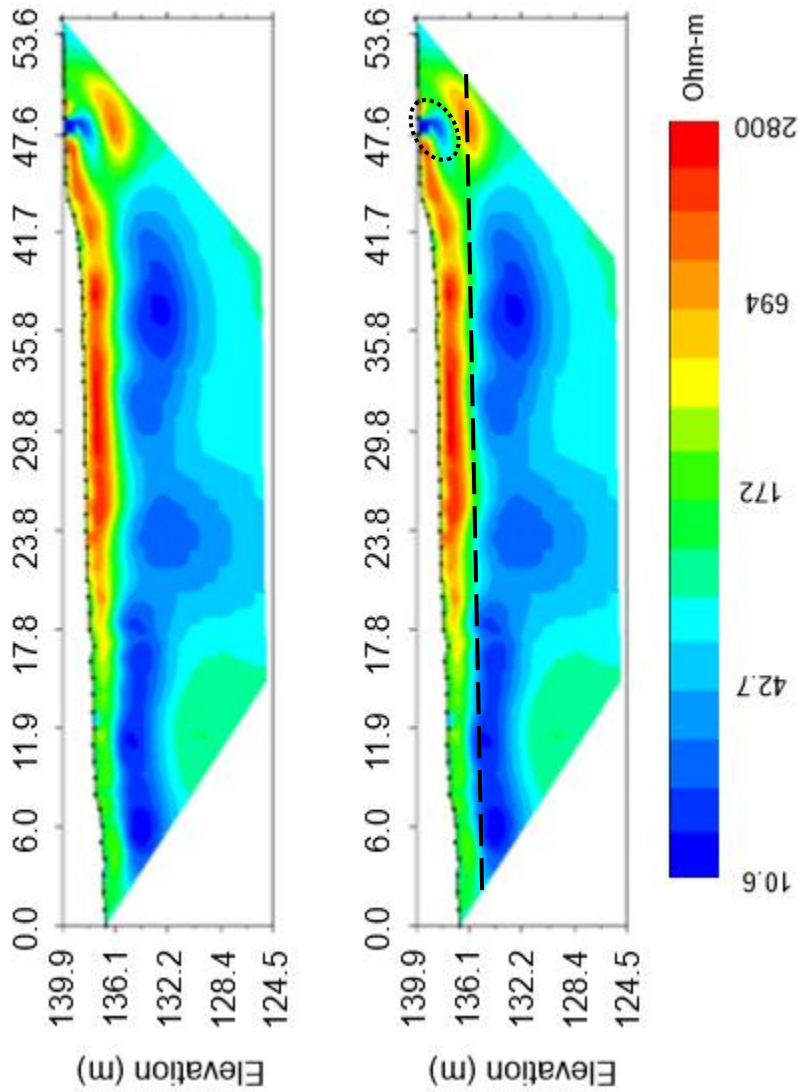


**Figure C 12.** Survey line 1. 56 electrodes spaced one-meter apart in a dipole-dipole array configuration. Surveyed 7/28/2018

**Inverted Resistivity Section Iteration=8 RMS=9.42% L2=9.52  
Electrode Spacing 1m**

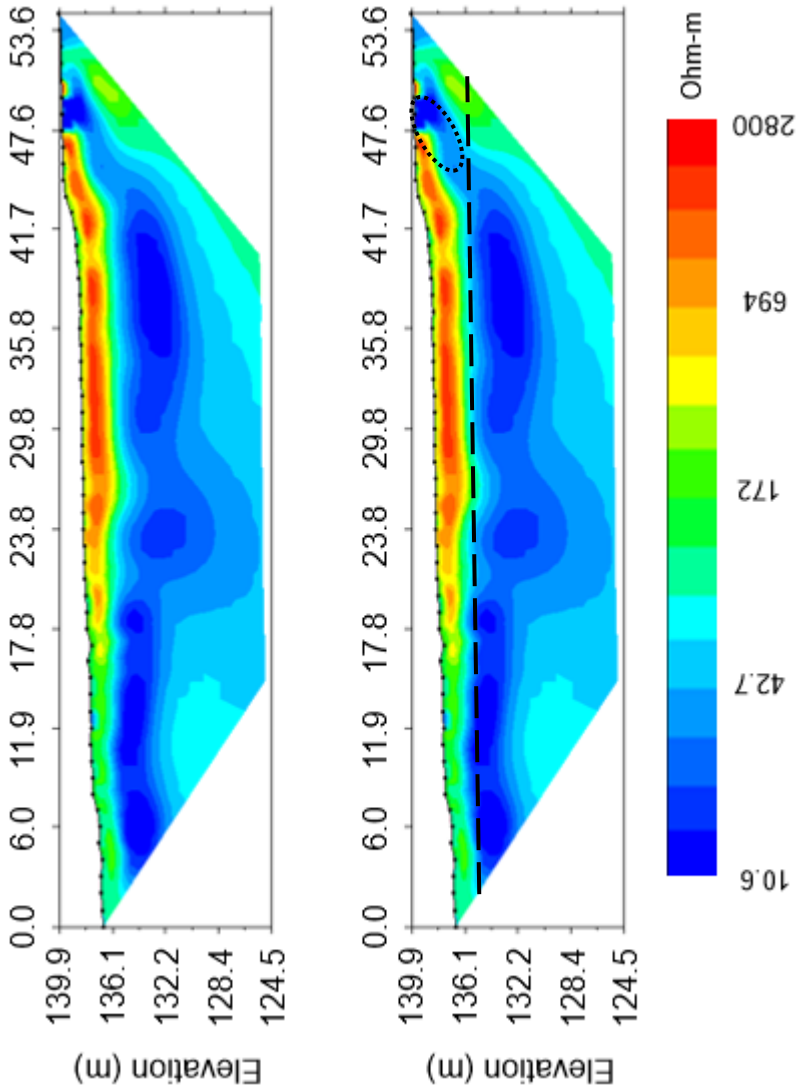


**Figure C 13.** Survey line 1. 56 electrodes spaced one-meter apart in a dipole-dipole array configuration. Surveyed 7/30/2018  
**Inverted Resistivity Section Iteration=8 RMS=15.43% L2=25.67  
 Electrode Spacing 1m**

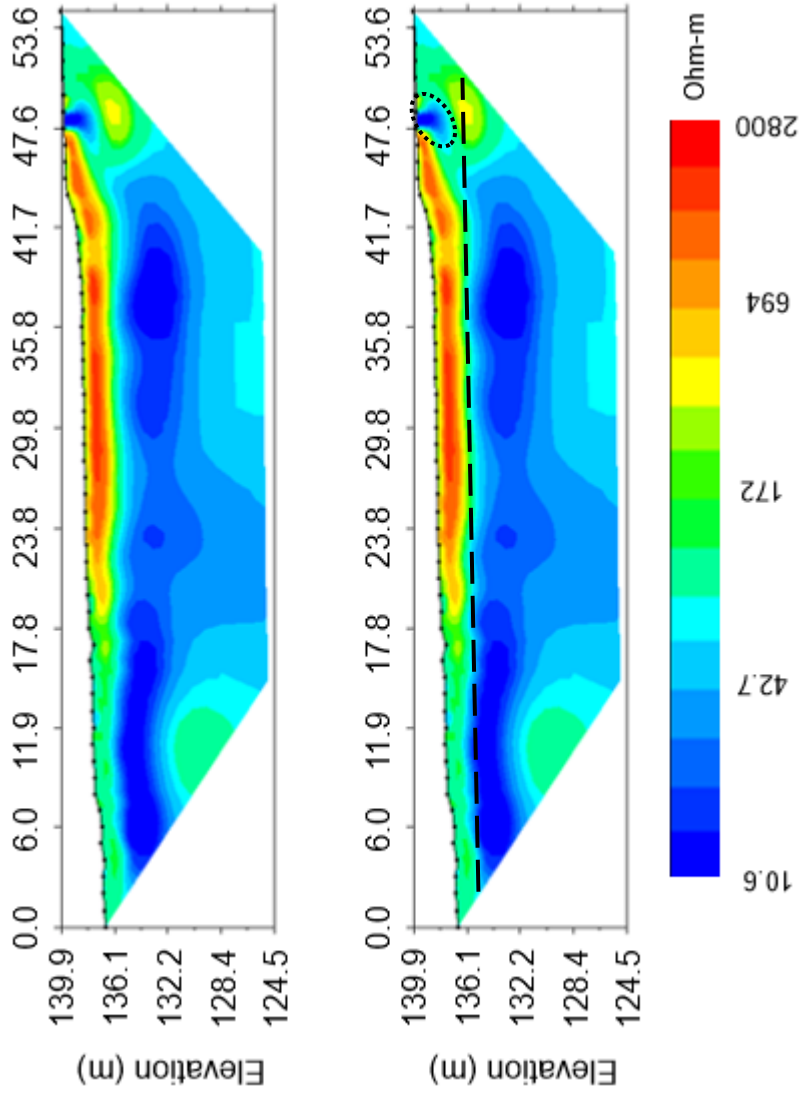


**Figure C 14.** Survey line 1. 56 electrodes spaced one-meter apart in a dipole-dipole array configuration. Surveyed 8/01/2018

**Inverted Resistivity Section Iteration=8 RMS=15.17% L2=24.78  
Electrode Spacing 1m**

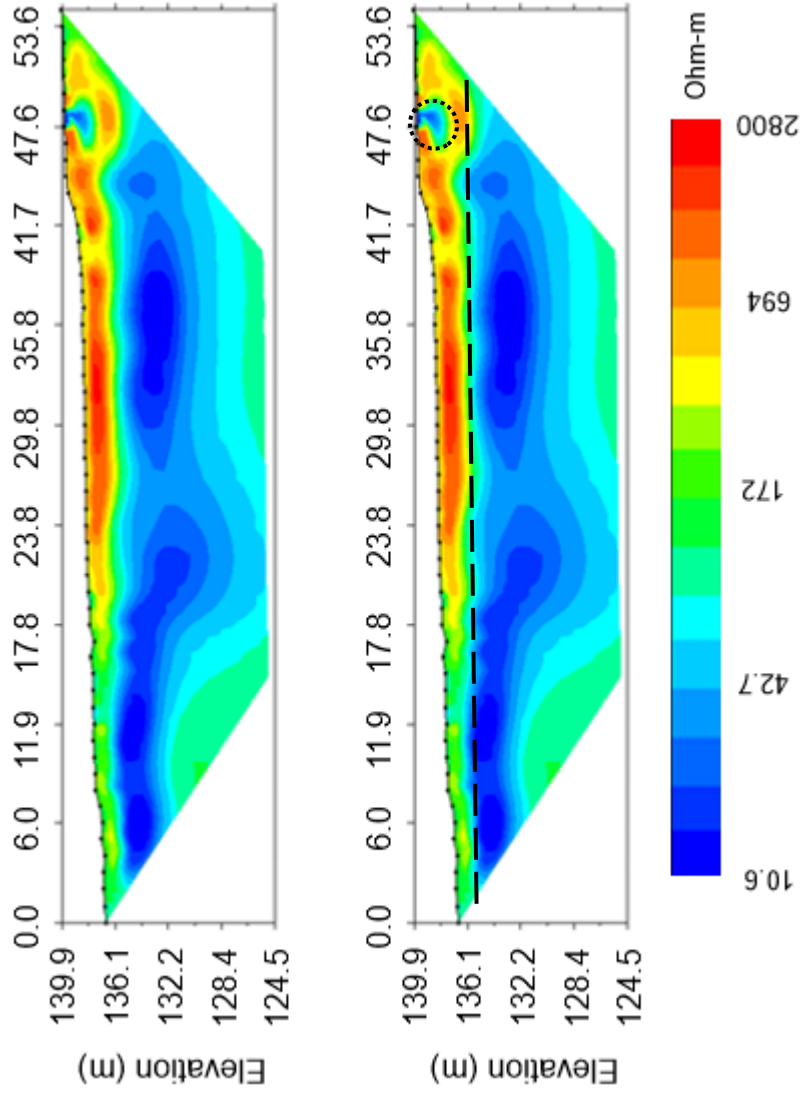


**Figure C 15.** Survey line 1. 56 electrodes spaced one-meter apart in a dipole-dipole array configuration. Surveyed 8/03/2018  
**Inverted Resistivity Section Iteration=8 RMS=16.27% L2=27.49  
 Electrode Spacing 1m**

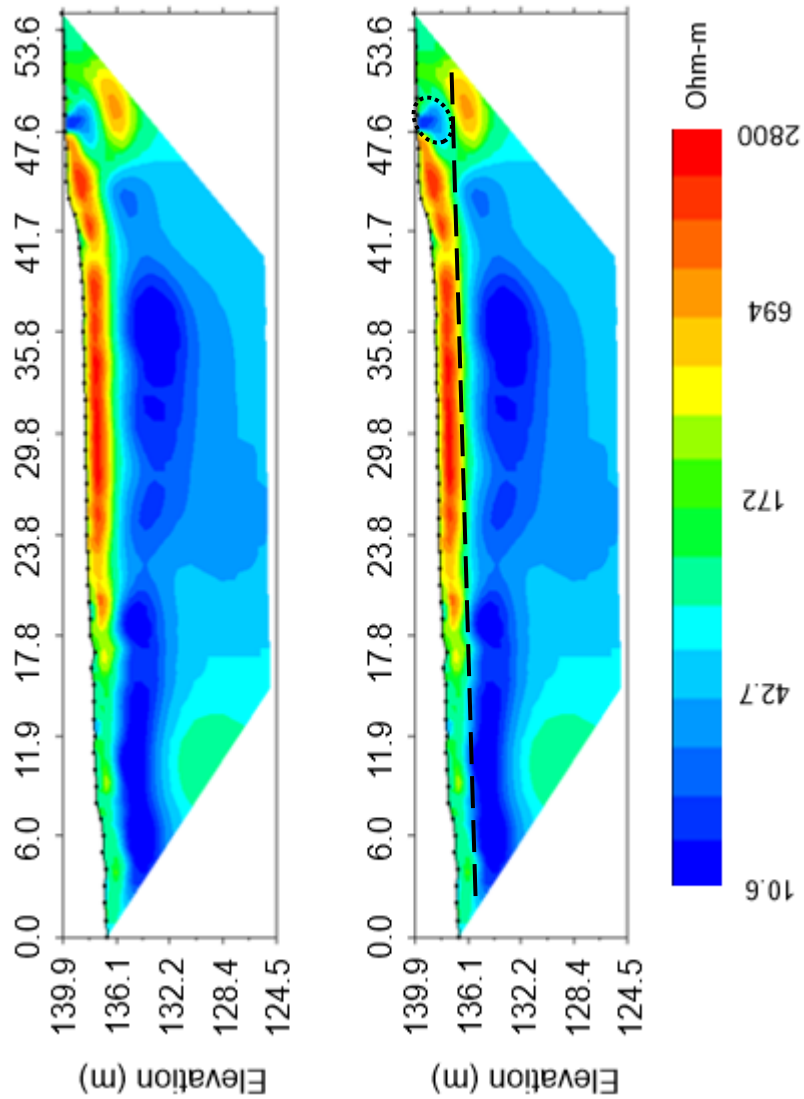


**Figure C 16.** Survey line 1. 56 electrodes spaced one-meter apart in a dipole-dipole array configuration. Surveyed 8/10/2018

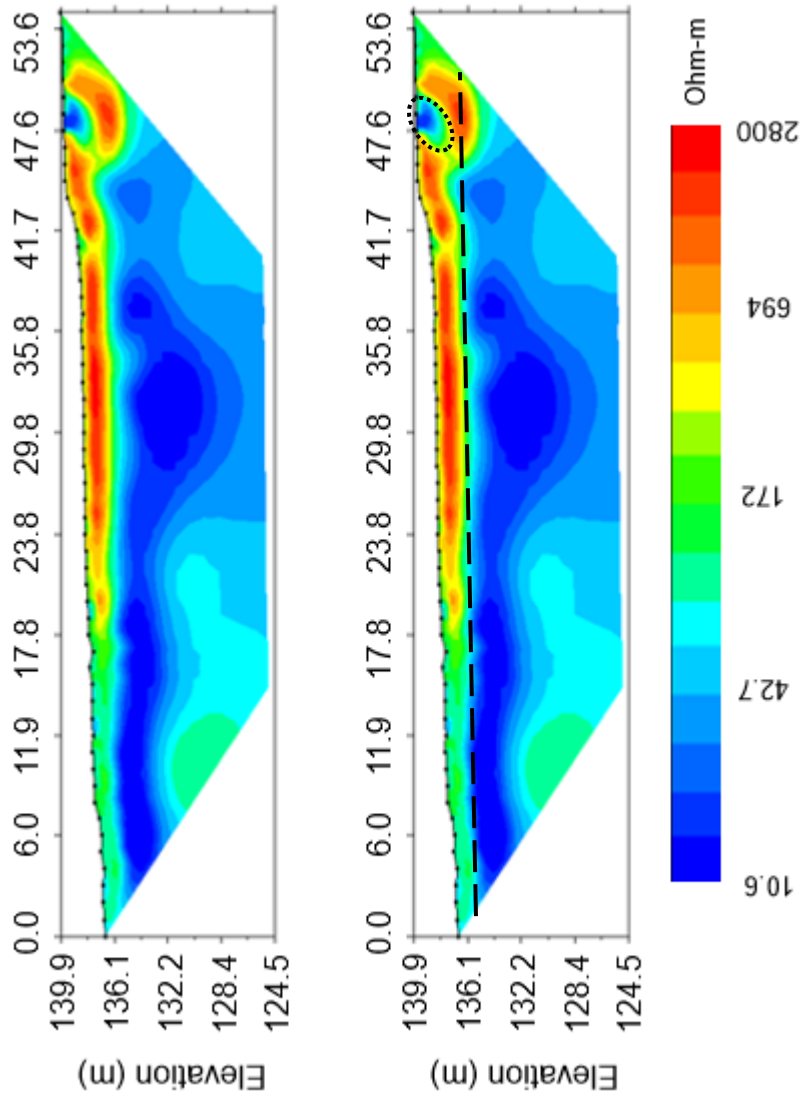
**Inverted Resistivity Section Iteration=8 RMS=14.63% L2=23.60  
Electrode Spacing 1m**



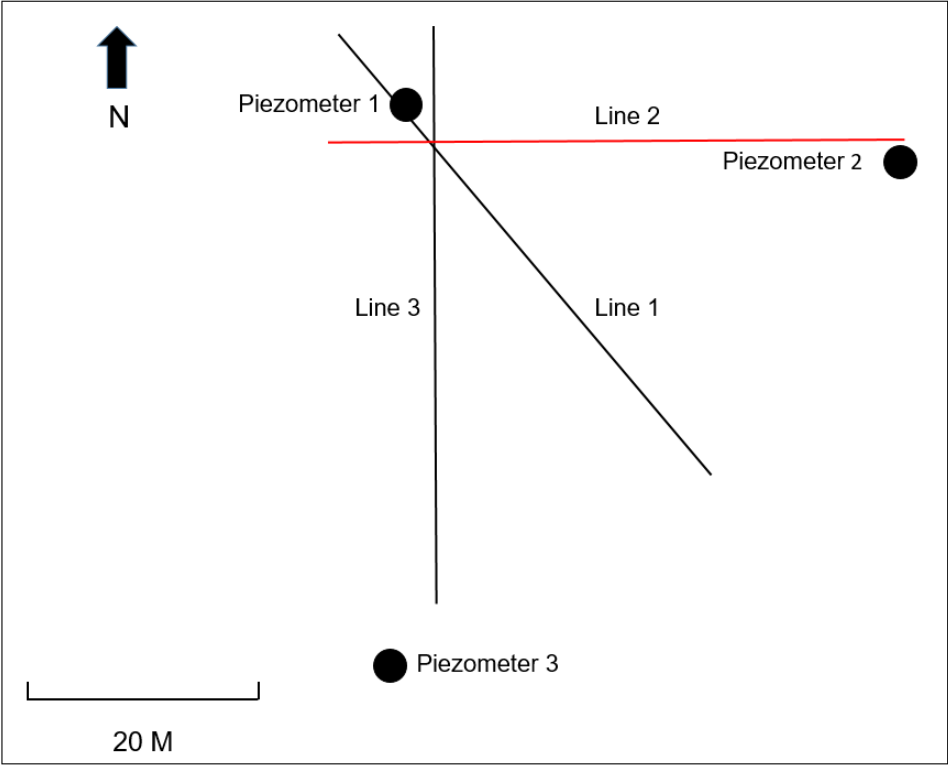
**Figure C 17.** Survey line 1. 56 electrodes spaced one-meter apart in a dipole-dipole array configuration. Surveyed 8/17/2018  
**Inverted Resistivity Section Iteration=8 RMS=17.67% L2=34.26  
 Electrode Spacing 1m**

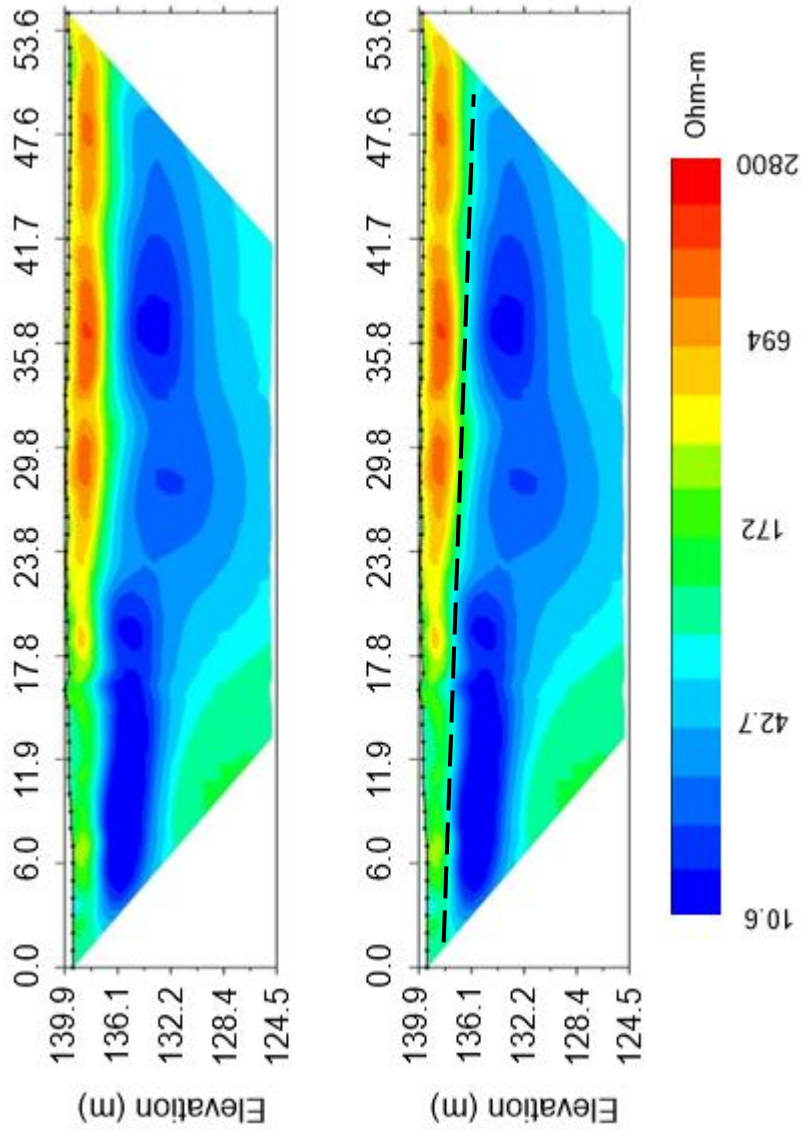


**Figure C 18.** Survey line 1. 56 electrodes spaced one-meter apart in a dipole-dipole array configuration. Surveyed 8/24/2018  
**Inverted Resistivity Section Iteration=8 RMS=14.17% L2=21.55  
 Electrode Spacing 1m**



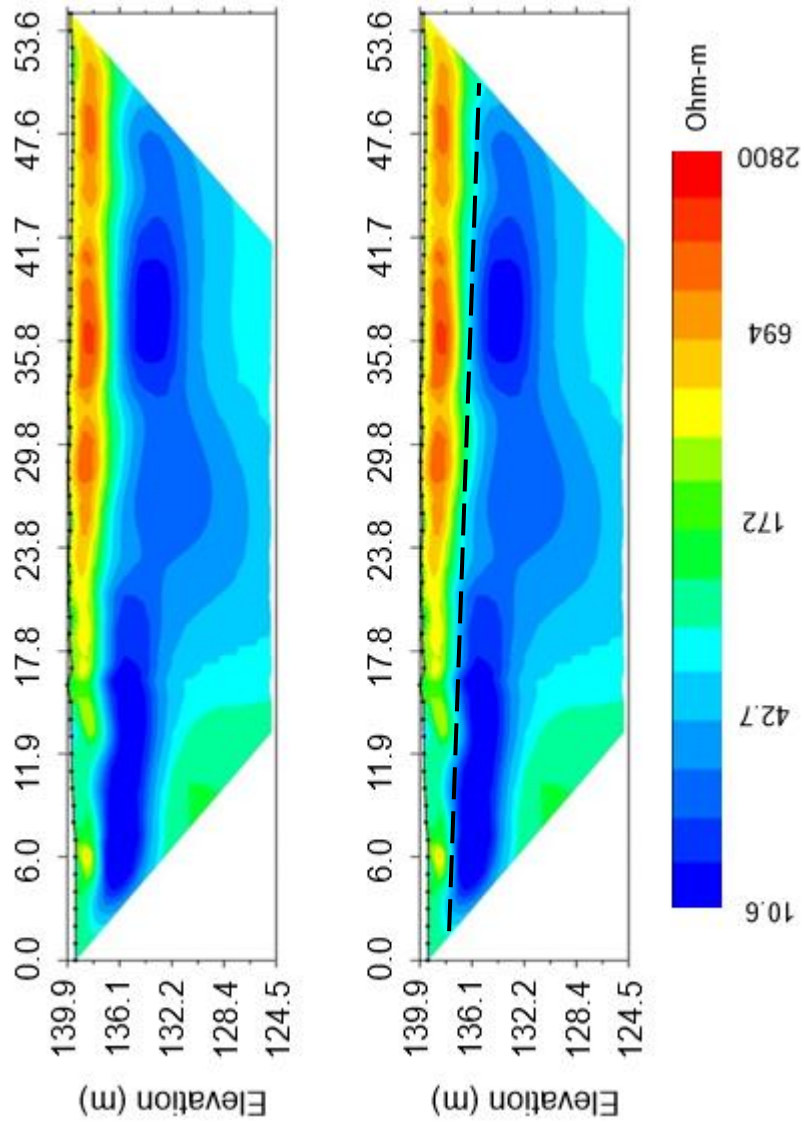
**Figure C 19.** Survey line 1. 56 electrodes spaced one-meter apart in a dipole-dipole array configuration. Surveyed 8/30/2018  
**Inverted Resistivity Section Iteration=8 RMS=12.30% L2=16.63  
 Electrode Spacing 1m**





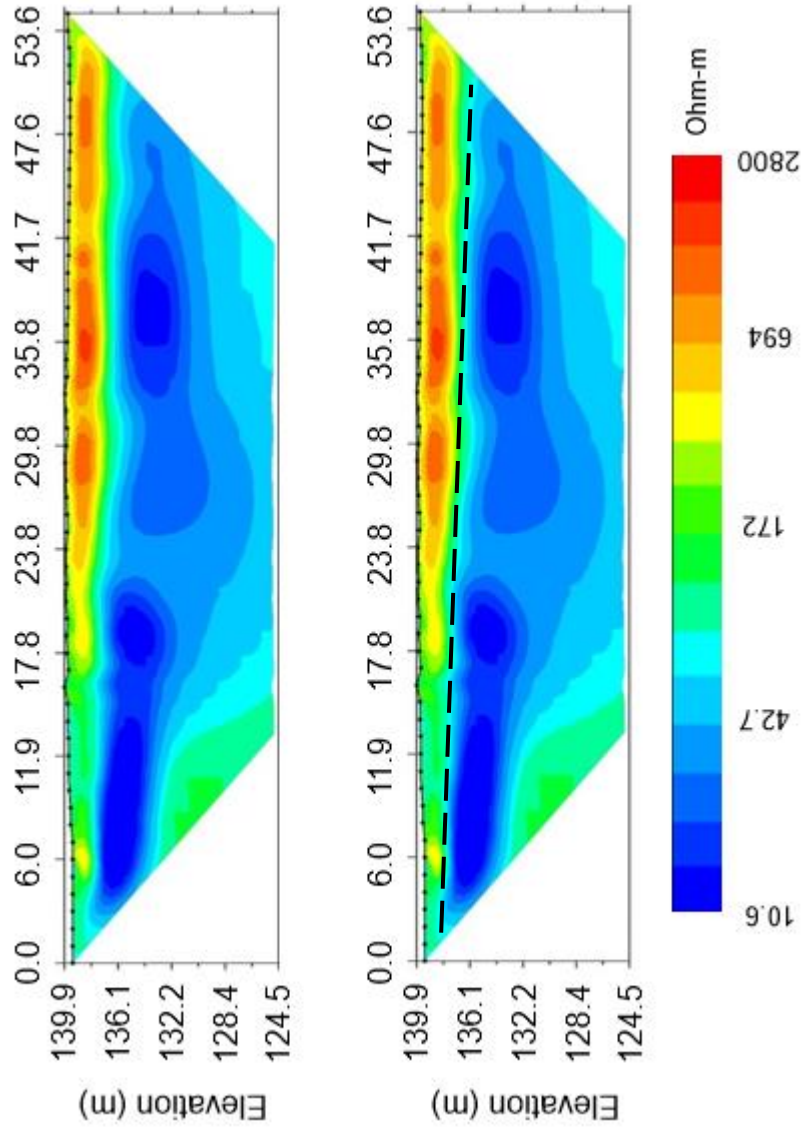
**Figure C 20.** Survey line 2. 56 electrodes spaced one-meter apart in a dipole-dipole array configuration. Surveyed 7/20/2018

**Inverted Resistivity Section Iteration=8 RMS=6.18% L2=4.18  
Electrode Spacing 1m**



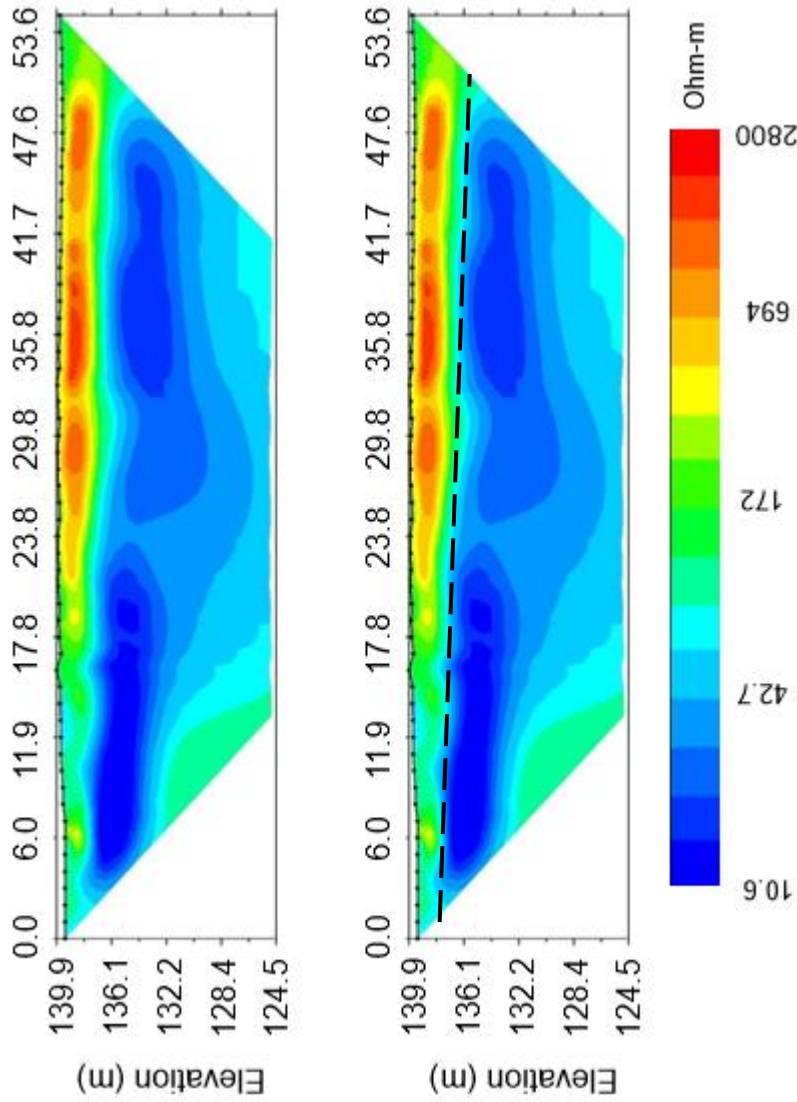
**Figure C 21.** Survey line 2. 56 electrodes spaced one-meter apart in a dipole-dipole array configuration. Surveyed 7/22/2018

**Inverted Resistivity Section Iteration=8 RMS=6.58% L2=4.72  
Electrode Spacing 1m**



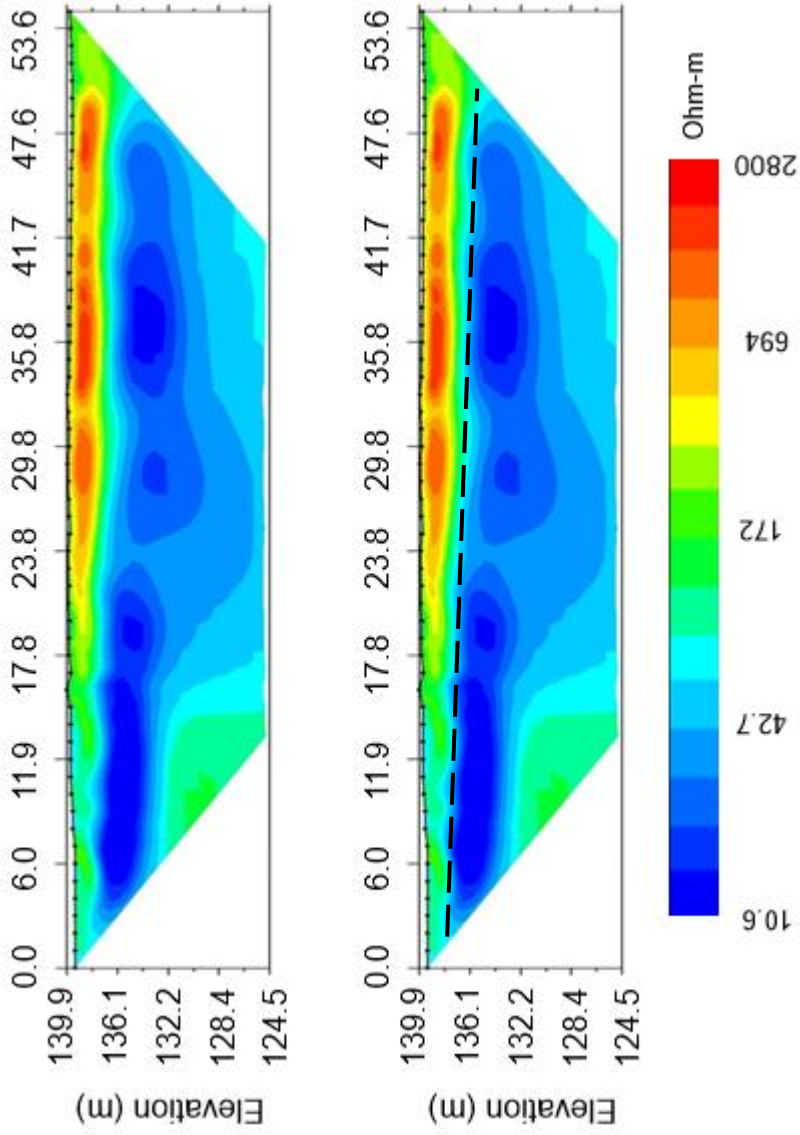
**Figure C 22.** Survey line 2. 56 electrodes spaced one-meter apart in a dipole-dipole array configuration. Surveyed 7/24/2018

**Inverted Resistivity Section Iteration=8 RMS=5.49% L2=3.25  
Electrode Spacing 1m**

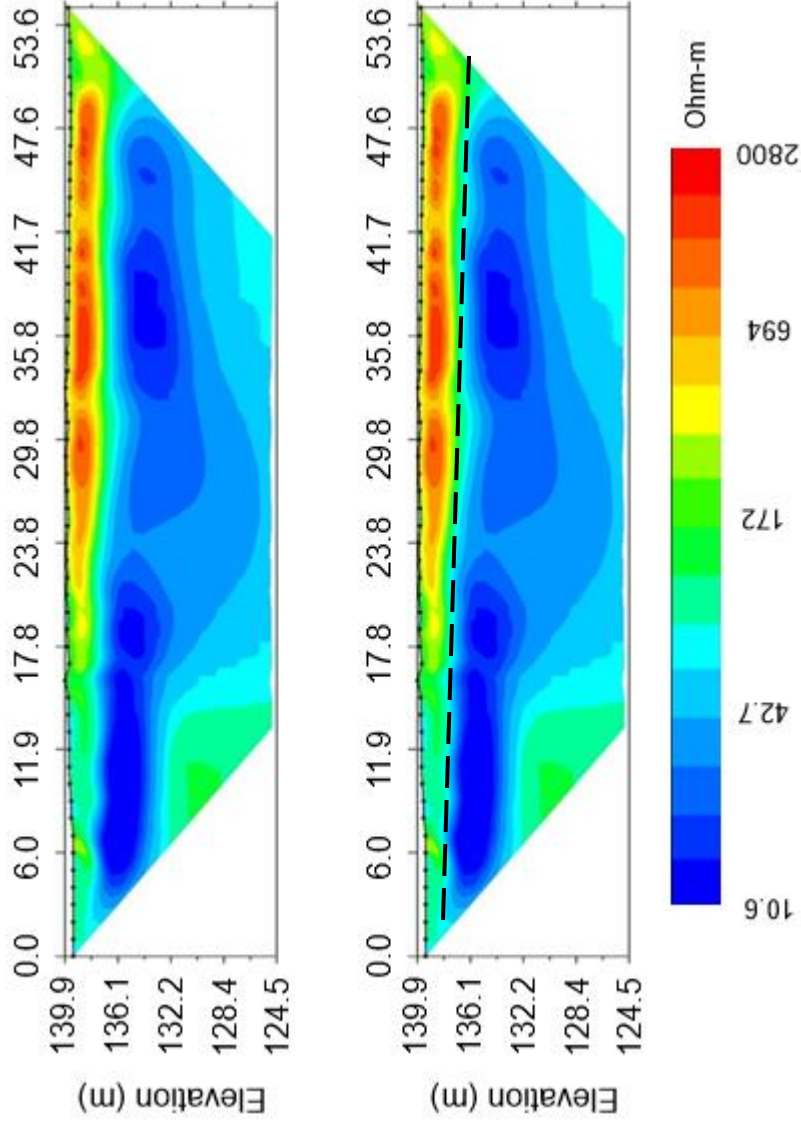


**Figure C 23.** Survey line 2. 56 electrodes spaced one-meter apart in a dipole-dipole array configuration. Surveyed 7/26/2018

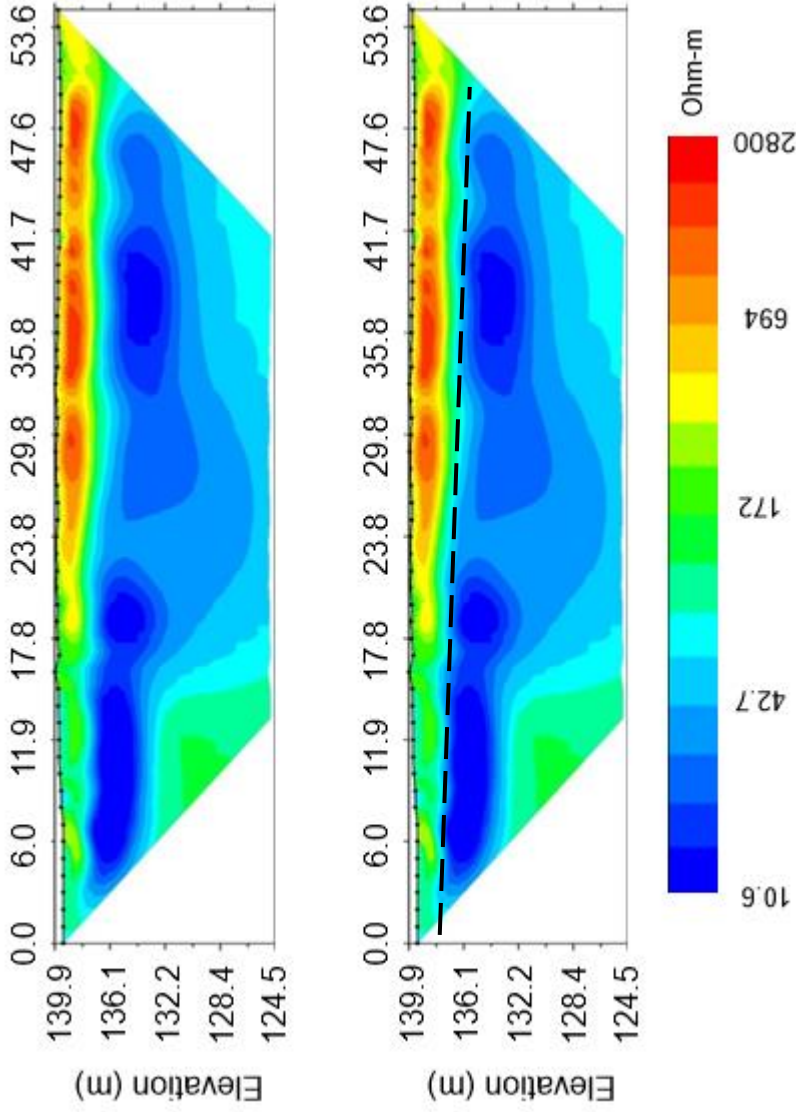
**Inverted Resistivity Section Iteration=8 RMS=7.84% L2=6.77  
Electrode Spacing 1m**



**Figure C 24.** Survey line 2. 56 electrodes spaced one-meter apart in a dipole-dipole array configuration. Surveyed 7/30/2018  
**Inverted Resistivity Section Iteration=8 RMS=9.53% L2=9.97  
 Electrode Spacing 1m**

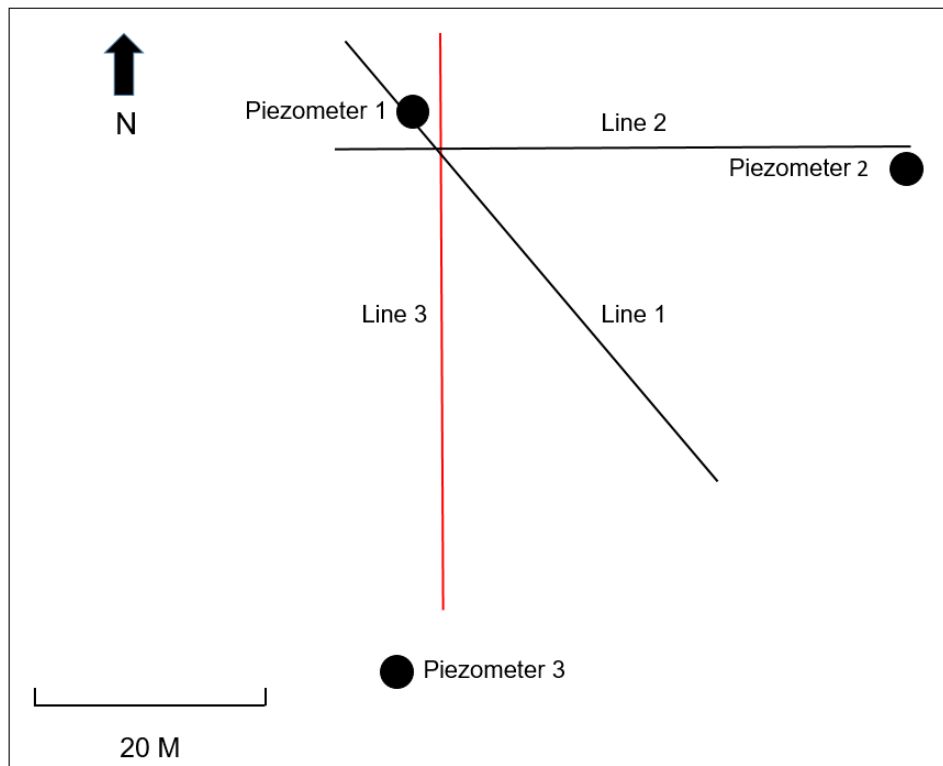


**Figure C 25.** Survey line 2. 56 electrodes spaced one-meter apart in a dipole-dipole array configuration. Surveyed 8/01/2018  
**Inverted Resistivity Section Iteration=8 RMS=9.70% L2=10.37  
 Electrode Spacing 1m**



**Figure C 26.** Survey line 2. 56 electrodes spaced one-meter apart in a dipole-dipole array configuration. Surveyed 8/03/2018

**Inverted Resistivity Section Iteration=8 RMS=9.05% L2=9.00  
Electrode Spacing 1m**



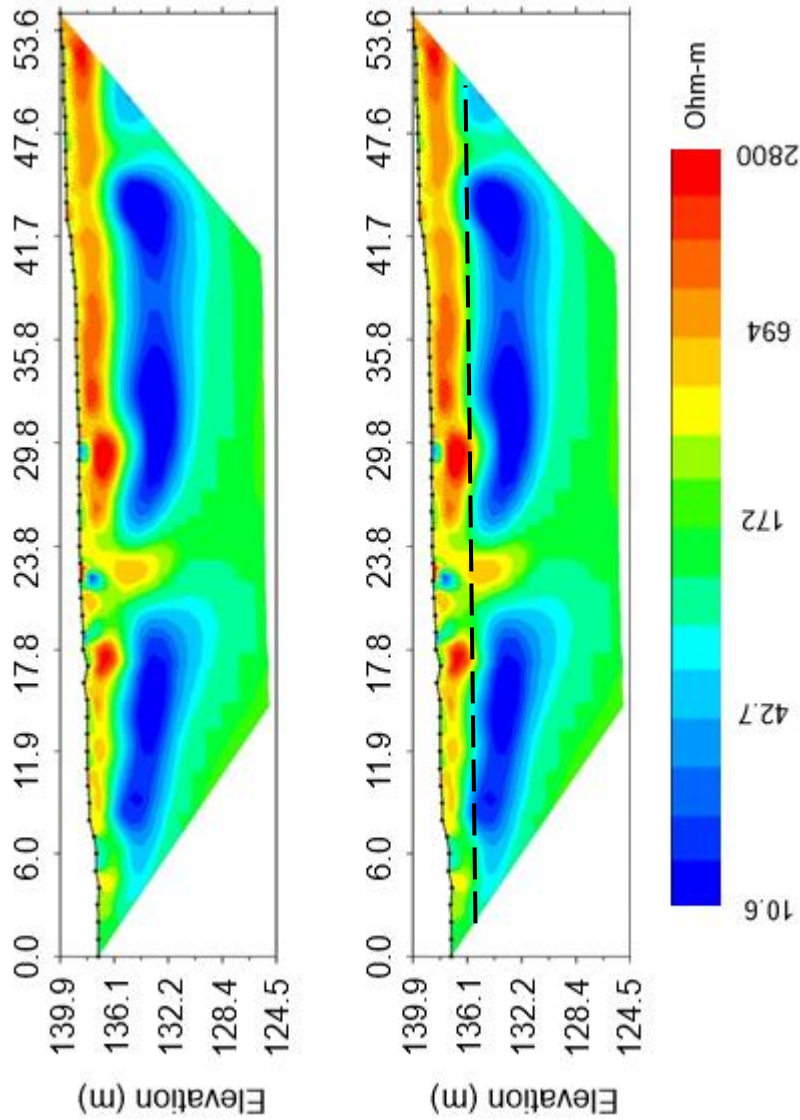


**Figure C 27.** Survey line 3. 56 electrodes spaced one-meter apart in a dipole-dipole array configuration. Surveyed 7/20/2018  
**Inverted Resistivity Section Iteration=8 RMS=31.28% L2=107.43  
 Electrode Spacing 1m**

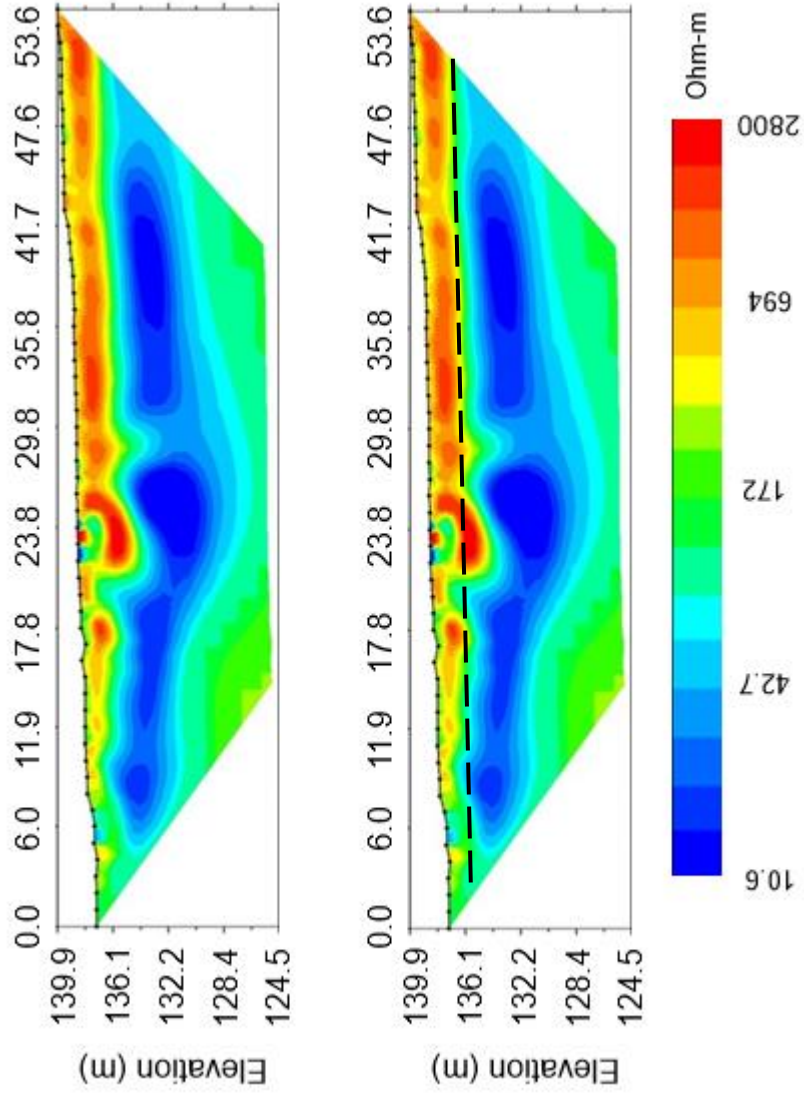


**Figure C 28.** Survey line 3.56 electrodes spaced one-meter apart in a dipole-dipole array configuration. Surveyed 7/22/2018

***Inverted Resistivity Section Iteration=8 RMS=28.40% L2=86.33  
Electrode Spacing 1m***

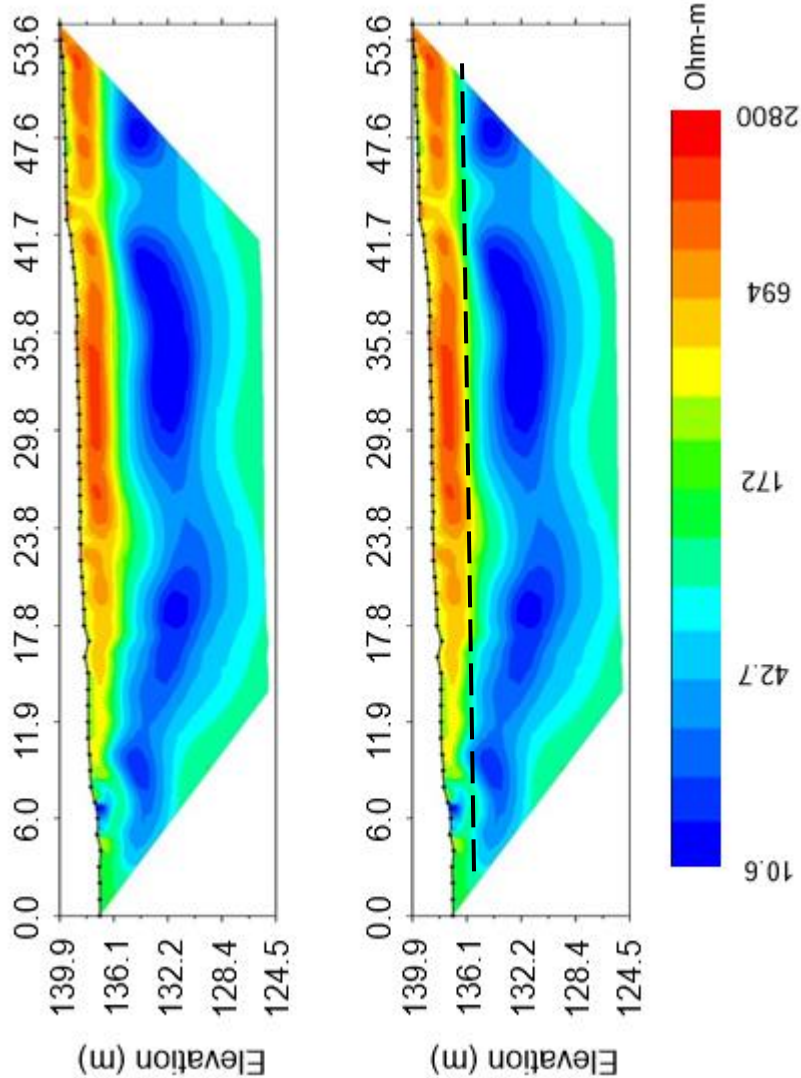


**Figure C 29.** Survey line 3. 56 electrodes spaced one-meter apart in a dipole-dipole array configuration. Surveyed 7/24/2018

**Inverted Resistivity Section Iteration=8 RMS=13.42% L2=19.52  
Electrode Spacing 1m**

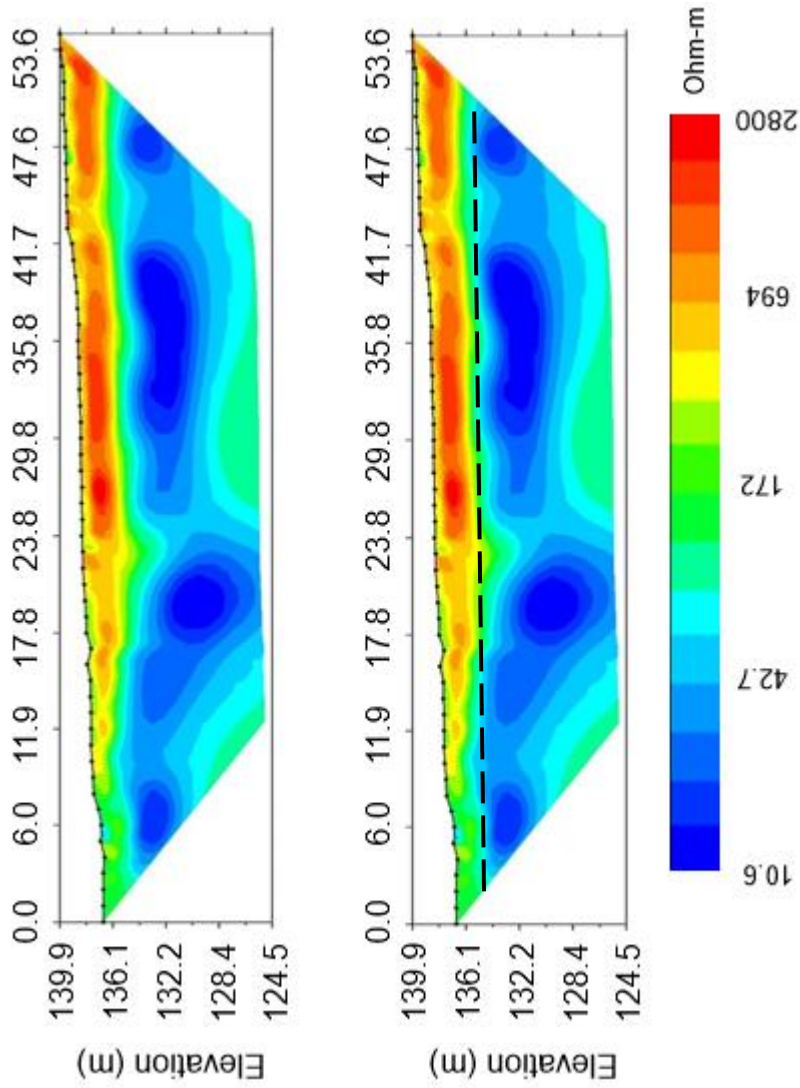


**Figure C 30.** Survey line 3. 56 electrodes spaced one-meter apart in a dipole-dipole array configuration. Surveyed 7/26/2018  
**Inverted Resistivity Section Iteration=8 RMS=14.22% L2=21.94  
 Electrode Spacing 1m**

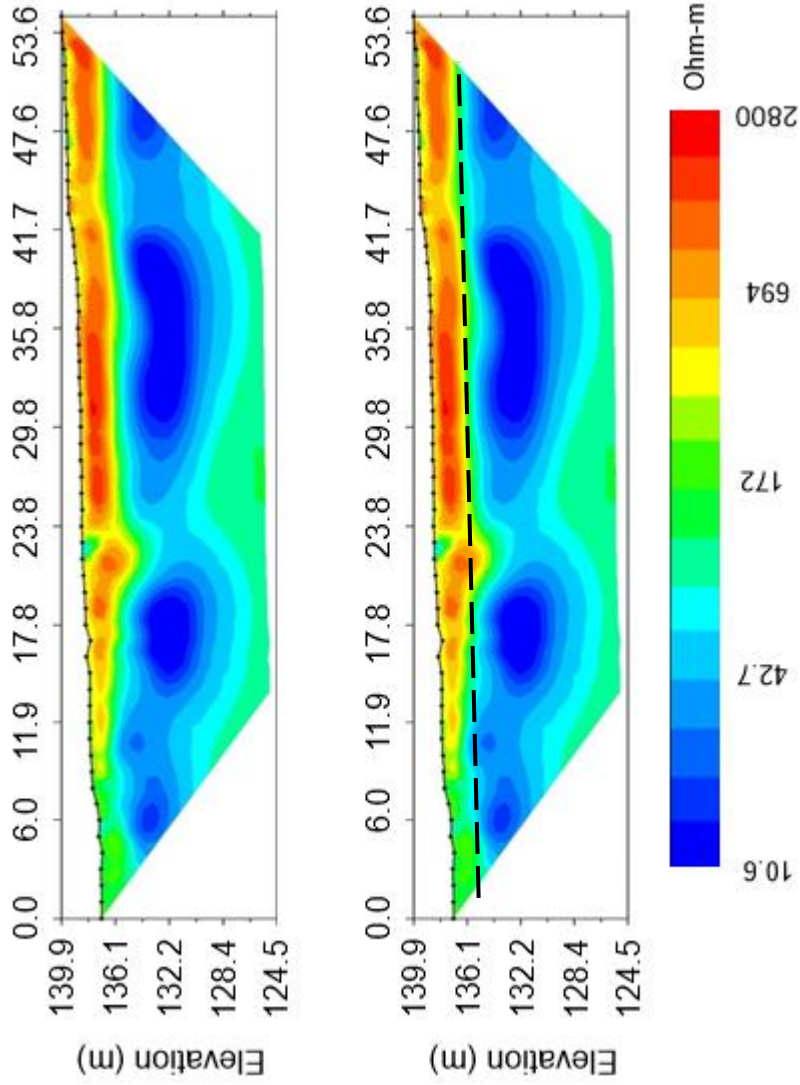


**Figure C 31.** Survey line 3. 56 electrodes spaced one-meter apart in a dipole-dipole array configuration. Surveyed 7/28/2018

**Inverted Resistivity Section Iteration=8 RMS=14.21% L2=21.87  
Electrode Spacing 1m**

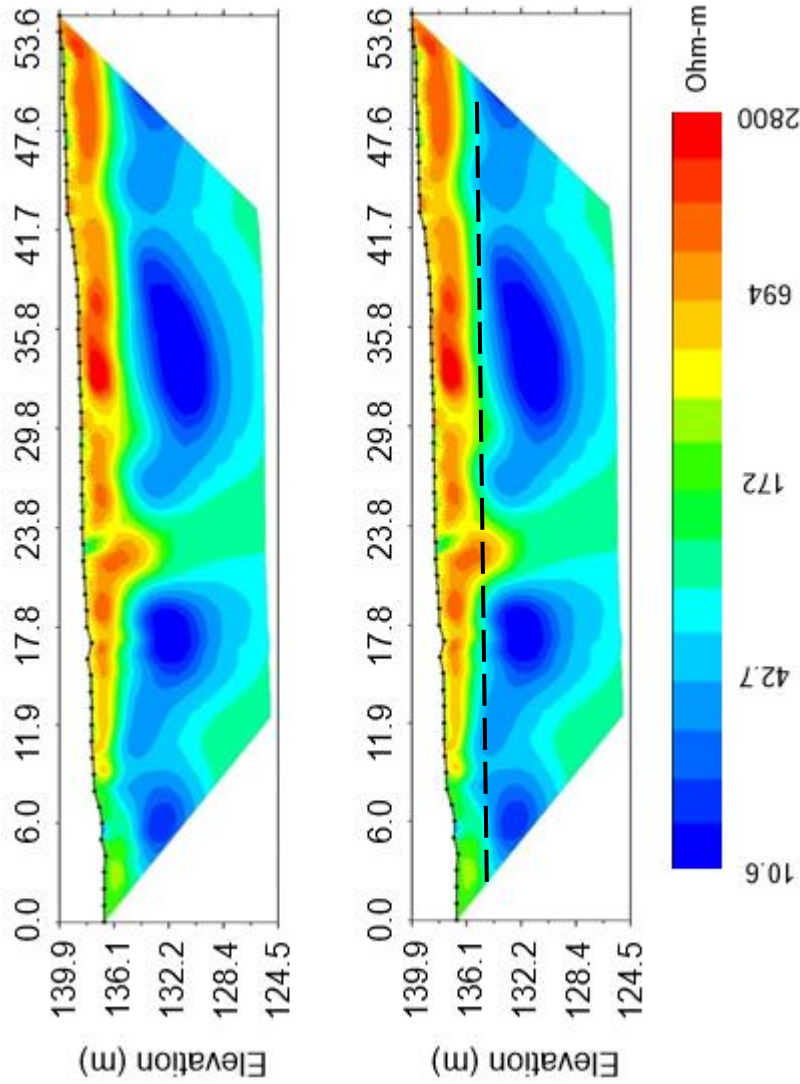


**Figure C 32.** Survey line 3. 56 electrodes spaced one-meter apart in a dipole-dipole array configuration. Surveyed 7/30/2018  
**Inverted Resistivity Section Iteration=8 RMS=21.66% L2=51.13  
 Electrode Spacing 1m**

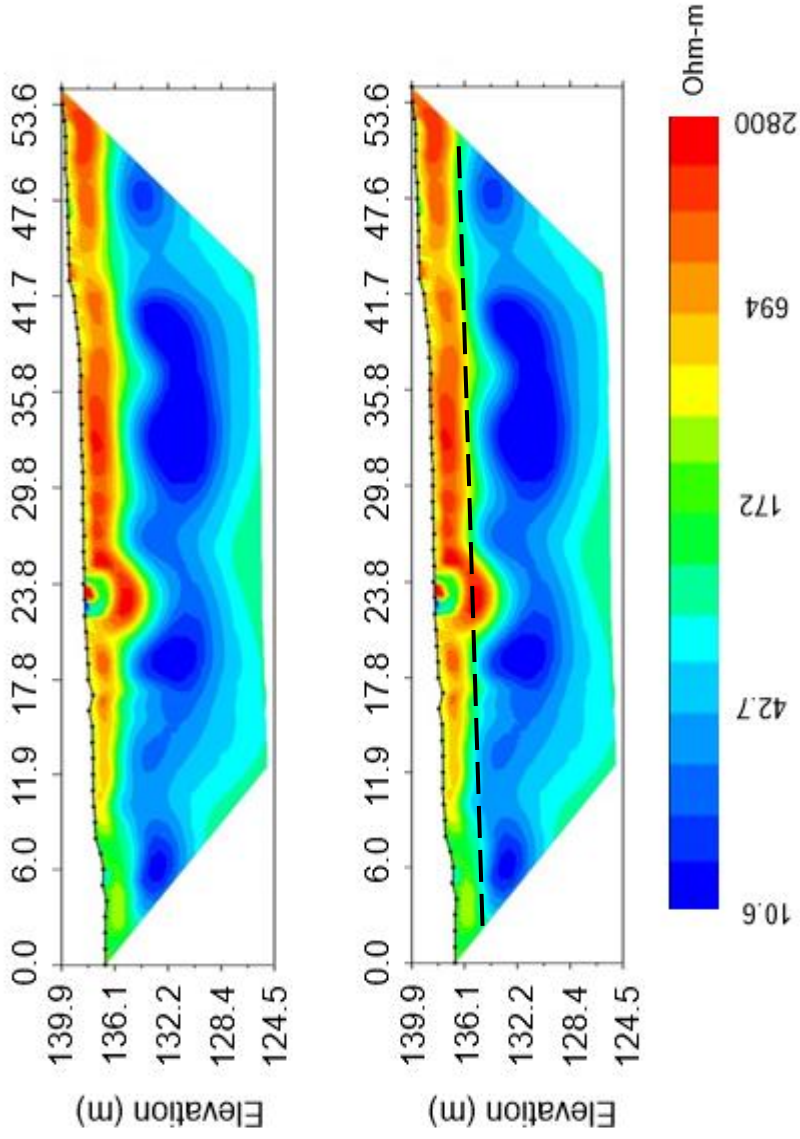


**Figure C 33.** Survey line 3. 56 electrodes spaced one-meter apart in a dipole-dipole array configuration. Surveyed 8/01/2018

**Inverted Resistivity Section Iteration=8 RMS=13.73% L2=20.65  
Electrode Spacing 1m**

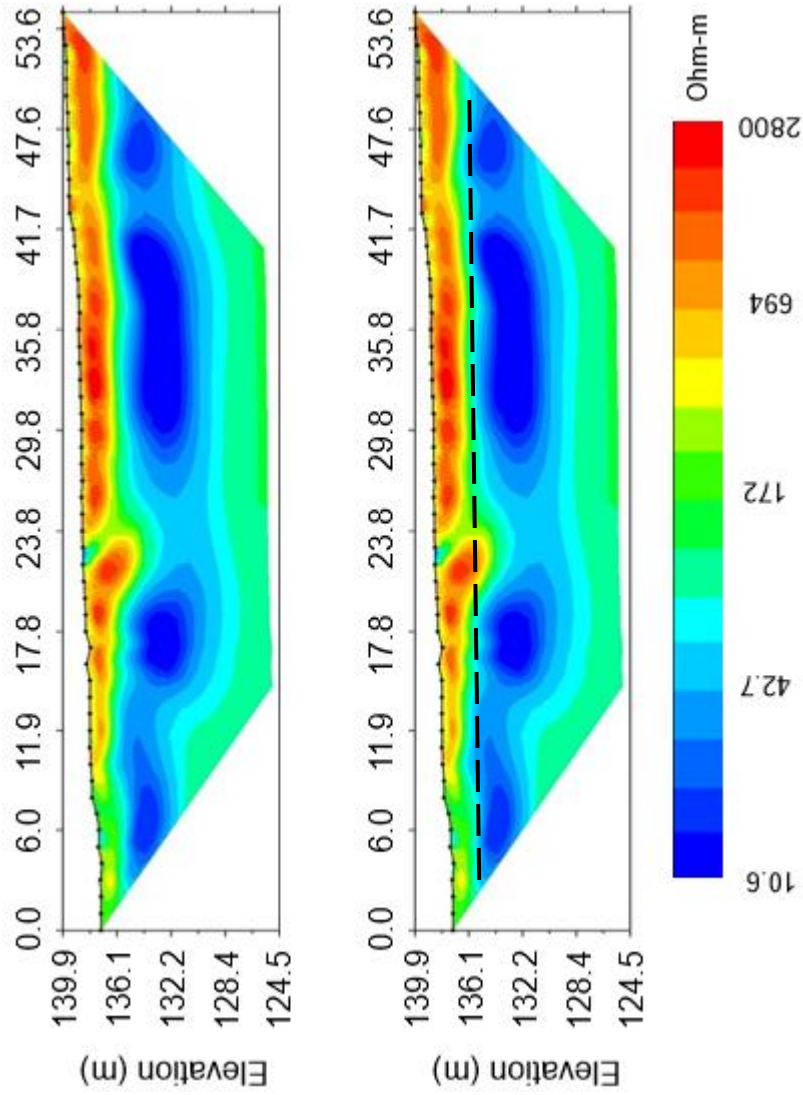


**Figure C 34.** Survey line 3. 56 electrodes spaced one-meter apart in a dipole-dipole array configuration. Surveyed 8/03/2018

**Inverted Resistivity Section Iteration=8 RMS=20.23% L2=44.01  
Electrode Spacing 1m**

## Vita

Tyler A. Tandy graduated from Fort Worth Christian School in Fort Worth, Texas in the year of 2013. He received his bachelors in Geology from Oklahoma State University in 2017. Tyler Tandy was admitted to the graduate school of Stephen F. Austin State University and received a degree of Master of Science in Geology in December 2019.

Permanent Address: 5500 Perkins Road, APT:2221

Baton Rouge, Louisiana 70808

Style manual designation: Gulf Coast Association of Geological Societies

This thesis was typed by Tyler A. Tandy